DIPARTIMENTO DI INGEGNERIA CIVILE, EDILE E AMBIENTALE - I C E A
DEPARTMENT OF CIVIL, ENVIRONMENTAL AND ARCHITECTURAL ENGINEERING

Via F. Marzolo, 9 - I 35131 Padova
tel +39 049 8275424 fax +39 049 8275446

C.F 80006480281 - P.IVA 007 42430283

RESEARCH REPORT

X-BRACKET

A HIGH-DUCTILITY AND DISSIPATIVE CONNECTION FOR EARTHQUAKE-RESISTANT CROSS-LAMINATED TIMBER STRUCTURES

Research Supervisor: Ph.D. Eng. Roberto Scotta

Research Assistants: Ph.D. Eng. Luca Marchi
Ph.D. Eng. Davide Trutalli
Ph.D. Eng. Luca Pozza

February 2019

Table of contents

Abstract

Cross-laminated timber is a construction material with significant potential to realize multi-storey earthquake-resistant buildings, exploiting the lightness of timber and the high in-plane strength and stiffness of the shear-wall panels, conferred by cross lamination of massive boards. In such buildings, connections play a vital role to assure an optimal seismic performance. However, traditional connections, i.e., angle brackets and hold-downs, have well-known drawbacks: low dissipative capacity due cyclic deformation of fasteners with consequent wood embedment and possible brittle failures due to uncertainty of actual strength of fasteners and relative overstrength factors. The current diffusion of tall cross-laminated timber buildings in high-seismicity areas requires the development of new strategies to increase ductility and dissipative capacities and to improve the reliability of the ductile parts of the structure. Both these purposes can be achieved with the adoption of new connections with optimized cyclic behaviour and localization of deformation in a steel element, preventing damage to the timber panel. A new connection for cross-laminated timber structures named “X-bracket” has been designed and tested at the University of Padova; it works both in tension and shear and can be used as panel-to-panel or panel-to-foundation joint. The special “X” shape is optimized to assure high stiffness and diffused yielding of material, resulting in extraordinarily high ductility and dissipative capacities. Furthermore, the possibility of producing multiple elements from cutting of a mild steel plate with minimal waste of material assures low production costs. This Report presents main details of the X-bracket and summarizes the research activities from the design to the experimental validation, discussing results from numerical simulations and laboratory tests. Installation, anchoring to the panel and possibility of replacement after a strong earthquake are also addressed and supported by additional tests, to verify the reliable response and controlled overstrength of the X-bracket, in compliance with capacity design.

PATENT APPLICATION:

DEVICE FOR COUPLING WALLS AND STRUCTURE COMPRISING SUCH DEVICE

Applicant: UNIVERSITA' DEGLI STUDI DI PADOVA

Inventors: SCOTTA, Roberto; POZZA, Luca; TRUTALLI, Davide; MARCHI, Luca

Pub. No.: ITUB20152555; Publication Date: 2017-01-28

Pub. No.: WO2017017563; Publication Date: 2017-02-02

Pub. No.: US20180216337; Publication Date: 2018-08-02

1. INTRODUCTION

Cross-laminated timber (CLT) is a new constructive technology suitable for realizing multi-storey earthquake-resistant buildings, as demonstrated by recent full-scale shake-table tests of three-storey buildings (Ceccotti 2008, Flatscher and Schickhofer 2015) and a seven-storey building (Ceccotti et al. 2013). The buildings withstood strong earthquakes with limited damages concentrated in connection elements, which played a critical role in achieving the necessary stiffness, strength and ductility of the structure.

Traditional connections for CLT buildings, known as angle brackets and hold-downs, are manufactured to prevent the horizontal sliding or vertical rocking of the wall panels respectively: they are made of punched and cold-formed thin steel plates fastened to the panel generally with ring shank nails or screws. Their derivation is from light-frame system, which is a technology that assures good dissipative properties given by small-diameter fasteners that diffusively connect bracing panels to the timber frame, allowing the wall to deform in shear. Such type of deformation may be also achieved with massive timber shear walls, which make use of strategies alternative to glue to confer in-plane shear stiffness to the panel (Pozza et al. 2015). On the contrary, CLT panels are elastic and almost rigid in their plane, being cross-wise layers reciprocally glued; therefore, energy dissipation must localize only in fasteners connecting hold-downs and angle brackets to the panel and in screwed or nailed vertical joints connecting panels among them. The use of such types of connections in CLT structure leads to well-known drawbacks: low dissipative capacity due cyclic deformation of fasteners with consequent wood embedment and possible brittle failures of the steel plates due to uncertainty of actual strength of fasteners and relative overstrength factors. The direct result of the low ductility and dissipative capacities is a prudential structural design with low behaviour factors (EN1998, 2013) and consequent very high seismic forces concentrated in hold-downs and angle brackets, which require the use of many fasteners per connection, increasing the risk of brittle failures. A possible strategy to improve the seismic performance of such buildings is the fragmentation of the façades into narrow modular panels, vertically jointed by means of ductile fasteners, instead of the use of monolithic CLT panels (Pozza and Scotta 2015, Pozza et al. 2016, Pozza and Trutalli 2017, Trutalli and Pozza 2018).

The use of special steel connections with optimized hysteretic behaviour can overcome both the aforementioned drawbacks of traditional connections, independently from the dimensions and arrangements of CLT panels. These connections exploit the ductility and dissipative capacity of steel, reducing or completely avoiding wood embedment. The low scattering of strength properties and the well-predictable yielding and peak forces, reduce the overstrength factor, improving the reliability of the ductile parts of the structure, in compliance with capacity design (Scotta et al. 2017).

1.1 Innovative connections for CLT buildings

Innovative earthquake-resistant connections for CLT buildings are based on the concept of localizing the dissipative and ductility capacities of the structure to special devices, designed to exploit the hysteretic behaviour of steel or friction and to limit the pinching effect, provided that the anchoring to CLT panel be designed with sufficient overstrength to limit its elastic deformations. This means that, as opposed to angle brackets and hold-downs, the fastening of the device to the panel must be over-resistant. Innovative connection systems are also being developed in the perspective of low-damage structures, able to withstand subsequent seismic events by applying minor interventions, provided that connections be accessible.

Various types of innovative connections for CLT buildings are available, which differ in the type and shape of the device and in the technology used to restrain shear-walls.

1. Dissipative devices coupled with post-tensioned shear walls were originally designed for multi-storey precast concrete buildings (Priestley et al. 1999). The favourable results led to the development of steel connection devices capable of high relative displacements, maintaining a rather unaltered energy dissipation capacity (Henry et al. 2010). In New Zealand, UFP connector, originally developed by Kelly et al. (1972), exploits a simple U-shape device realized from bending of a thick steel plate. This device has been applied to CLT as high-performance panel-to-panel vertical joint (Baird et al. 2014) to dissipate energy exploiting the rocking behaviour of slender panels restrained at the base by post-tensioned cables (PRES-LAM system, Palermo et al. 2006). Fuse-type buckling-restrained dissipaters have also been used at the base of the panels (Kramer et al. 2016, Sarti et al. 2016).
2. The University of Salerno (Latour and Rizzano 2015) designed and tested brackets with hourglass shape (named XL-stubs) that concentrate energy dissipation in the flange plate, in substitution of traditional hold-downs.
3. More recently, Schmidt and Blass (2017) presented a study on a steel plate combined with special laminated veneer lumber (LVL) inserts to realize dissipative panel-to-panel joints for CLT shear walls.
4. The use of slip-friction devices for CLT shear walls has been investigated by Loo et al. (2014): a high-performance hold-down was designed and tested, which exploits 12-mm thick steel plates connected with bolts that slip through slotted holes. Specifically designed shear keys placed at the panel base prevent possible slip of the panel and consequent shear loading to the dissipative devices.
5. Hashemi et al. (2017) developed the Resilient Slip Friction (RSF) joint, in which the components are formed and arranged in a way that friction can occur avoiding relative residual displacements, without the use of post-tensioned tendons.
6. Polastri et al. (2017) presented a connection suitable for precast CLT structures, which incorporates self-tapping wood screws, LVL inserts and a high strength steel device. This system aims to improve the seismic performance of CLT structures and to reduce meanwhile the on-site installation costs.
7. The connection presented in this Report, named “X-bracket”, has been developed at the University of Padova. Various advantages make this device an efficient earthquake-resistant connection for CLT structures and a valid alternative to traditional connections and aforementioned devices. It works both in tension and shear and can be used as panel-to-panel and/or panel-to-foundation joint. The special “X” shape is optimized to assure high stiffness and diffused yielding of material, resulting in extraordinarily high ductility and dissipative capacities. Furthermore, its two-dimensional shape and the possibility of producing multiple elements from cutting of a mild steel plate with minimal waste of material assure low production costs.

This Report presents main details of the X-bracket and summarizes the research activities from the design to the experimental validation, discussing results from numerical simulations and laboratory tests. The installation and anchoring to the panel are also addressed and supported by additional tests, to verify the reliable response and controlled overstrength of the X-bracket.

1.2 Capacity design

Experimental evidences have demonstrated that uncertainty in applying the capacity design to traditional connections in CLT structures leads to frequent events of brittle failures (Gavric et al. 2013), which can compromise the stability of the entire structure. This derives from the high scattering of the peak strength of fasteners and the uncertainty in its analytical prediction. The consequence is that the actual peak strength of fasteners might exceed the strength of brittle components designed with insufficient overstrength, with subsequent brittle failure of the entire connection. On the contrary, the use of innovative connections, characterized by low scattering of strength properties and well-predictable yielding and peak forces, makes capacity design more reliable. In this case, the underestimation of the actual strength of fasteners (i.e., the brittle component of innovative connections) is on the safe side in the application of capacity design.

The capacity design approach was originally developed for RC structures (Paulay and Priestley 1992). Its extension to timber and specifically to CLT structures has been formally defined (Jorissen and Fragiacomo 2011, Fragiacomo et al. 2011, Sustersic et al. 2011, Scotta et al. 2017) and applied to fasteners and traditional connections (Gavric et al. 2013, Gavric et al. 2015a, Gavric et al. 2015b, Izzi et al. 2016, Ottenhaus et al. 2018) and to innovative connections (Scotta et al. 2017). Capacity design requires the definition of reliable overstrength factors γ_{Rd}, which are not provided in the current version of Eurocode 8 (2013) for timber structures. A proposal for revision of Chapter 8 of Eurocode 8 (2013) is available in literature (Follesa et al. 2015, Follesa et al. 2016), where a γ_{Rd} equal to 1.3 for the CLT building technology with traditional connections and the formulations for its application in the capacity design are proposed.

Fig. 1 shows a conceptual model according to Jorissen and Fragiacomo (2011) of the capacity design of the weakest brittle component of the connection system, starting from the strength properties of the ductile element. This approach is based on the scattering of the peak strength of the ductile part and the analytical procedures applied to evaluate such strength (i.e., rules according to Code). The main parameters in Fig. 1 are:

d_y	Yielding displacement;
d_{peak}	Displacement corresponding to peak strength;
F_{code}^{-}	Characteristic load-bearing capacity estimated according to Code;
F_{peak}^{-}	5th percentile of the maximum strength obtained by tests;
F_{peak}^{mean}	Mean value of the maximum strength obtained by tests;
F_{peak}^{+}	95th percentile of the maximum strength obtained by tests;
F_{y}^{-}	5th percentile of the yielding strength obtained by tests;
F_{y}^{mean}	Mean value of the yielding strength obtained by tests;
F_{y}^{+}	95th percentile of the yielding strength obtained by tests;
γ_{Rd}	Overstrength factor;
γ_{an}	Analytical overstrength ($F_{peak}^{-} = \gamma_{an}\, F_{code}^{-}$);
γ_{sc}	Scattering of peak strength ($F_{peak}^{+} = \gamma_{sc}\, F_{peak}^{-}$).

Subscripts B and D identify brittle and ductile element respectively.

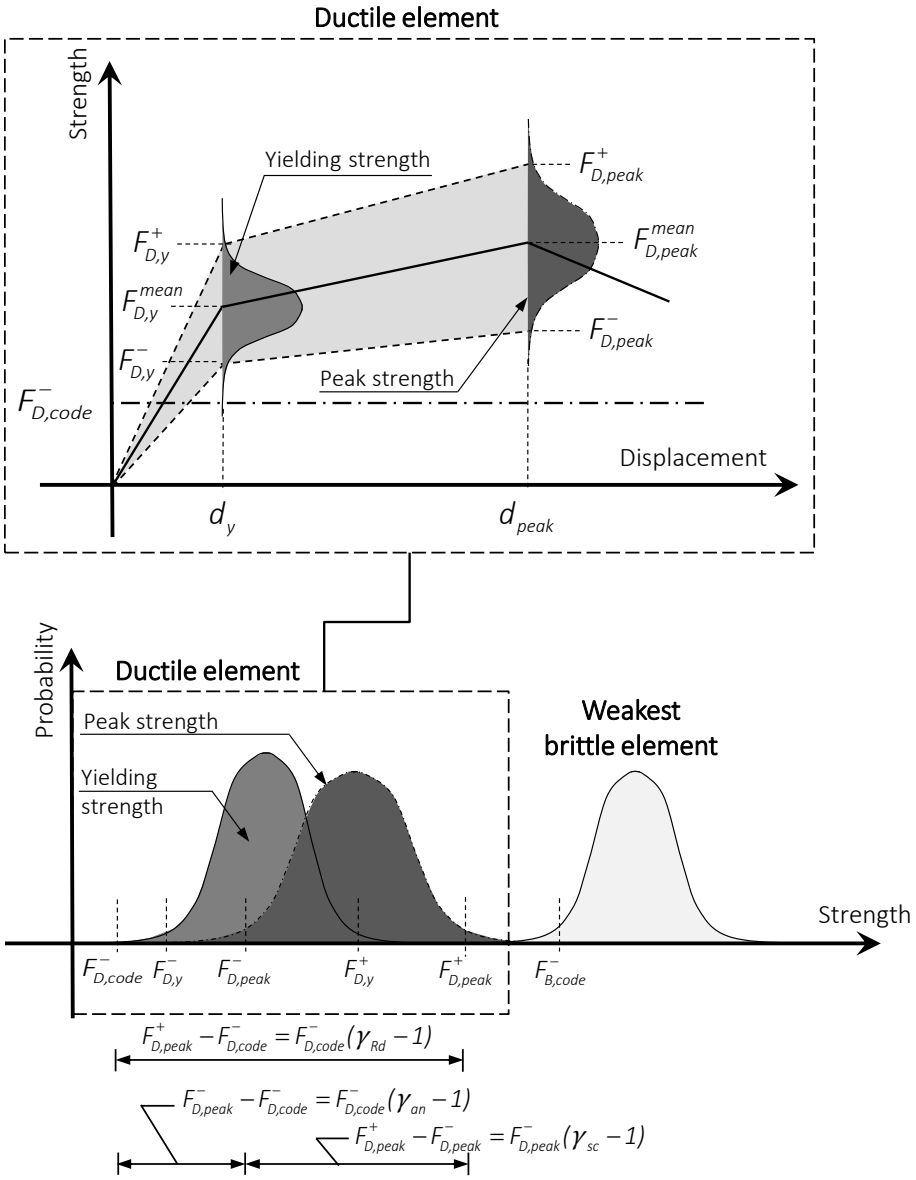

Fig. 1. Conceptual model of capacity design applied to a ductile connection (Scotta et al. 2017)

The capacity design consists in fulfilling Inequality (1), i.e., the brittle parts of the system must assure a characteristic load-bearing capacity higher or equal to the 95th-percentile peak strength of the ductile part, which is expressed as the product of the overstrength factor γ_{Rd} and the Code strength $F^{-}_{D,\,code}$:

$$F^{-}_{B,\,code} \geq F^{+}_{D,peak} = \gamma_{Rd} \cdot F^{-}_{D,\,code} \tag{1}$$

Hence, the overstrength factor γ_{Rd} can be defined directly as a unique term, according to Equation (2), or can be split into two parts as in Equation (3):

$$\gamma_{Rd} = F^{+}_{D,\,peak} / F^{-}_{D,\,code} \tag{2}$$

$$\gamma_{Rd} = \gamma_{sc} \cdot \gamma_{an} = F^{+}_{D,\,peak} / F^{-}_{D,\,peak} \cdot F^{-}_{D,\,peak} / F^{-}_{D,\,code} \tag{3}$$

The described conceptual model is based on the hypothesis that a set of experimental tests (at least three) is available to characterize the statistical distribution of the peak strength of the ductile component and then to compute directly $F^{+}_{D,\,peak}$. However, this experimental characterization is generally not available, and $F^{+}_{D,\,peak}$ is normally unknown by practitioners. Therefore, γ_{Rd} must be code-dependent being strictly correlated to the analytical method used to compute $F^{-}_{D,\,code}$, which is the only value available to practitioners. This aspect is of utmost importance for connections in timber structures, and specifically CLT, for which $F^{-}_{D,\,code}$ is currently not univocally defined, depending on the chosen values of parameters in the calculation model. For instance, for a dowel-type fastener, $F^{-}_{D,\,code}$ is normally computed according to Eurocode 5 (2014), applying the Johansen's Theory (1949), but the resulting load-bearing capacity is not univocal, depending on the chosen values of parameters in the analytical formulations and on the special rules provided by product approvals. Therefore, γ_{Rd} values are affected not only by the statistical variability of the strength of the ductile element (γ_{sc}) but also by the analytical method to estimate its characteristic strength, according to a particular Code (γ_{an}). Therefore, it is fundamental that γ_{Rd} values proposed in a Code be consistent with the analytical methods and parameters available in the same Code.

An exhaustive experimental research about steel-to-timber joints with ring shank nails for CLT is available in (Izzi et al. 2016). According to these tests and depending on the chosen parameters to compute $F^{-}_{D,\,code}$ and on the angle of the force to the face lamination of the panel, the obtained γ_{Rd} values are in the range between about 1.6 and 2.6, thus demonstrating the strict correlation between γ_{Rd} and the analytical models and parameters to compute $F^{-}_{D,\,code}$. These values may be used to apply the capacity design to traditional connections for CLT, as hold-downs and angle brackets, for which ring shank nails represent the ductile component. The steel plate and the anchoring to foundation or floor can be therefore designed applying the conceptual model described here with γ_{Rd} proposed by Izzi et al. (2016).

The adoption of innovative connections developed to localise yielding in steel parts, and therefore with well-defined and predictable yielding and peak strength, undoubtedly would result in a more reliable application of the capacity design. No formulas are normally available to evaluate the load-bearing capacity of such connections. According to Eurocode 3 (2014), in steel structures $F^{-}_{D,\,code}$ is normally assumed coincident with nominal $F^{-}_{D,\,y}$: this assumption can be extended to innovative connections and γ_{Rd} can be obtained directly as ratio between $F^{+}_{D,\,peak}$ and $F^{-}_{D,\,y}$, according to Equation 2.

2. DETAILS AND PROPERTIES OF THE X-BRACKET

The X-bracket has been designed and tested at the University of Padova. It is the result of a four-year research, which aimed to develop a connection element suitable to improve the seismic performance of CLT buildings at different levels, hereafter listed. The resulting device, characterized by a "X" shape, is made by cutting of a mild steel plate, resulting in several brackets with four fixing points (16-mm diameter holes) necessary for the anchoring to the timber panel or to the foundation.

Fig. 2 shows some examples of arrangement of the X-bracket as panel-to-foundation joint (Fig. 2a,b) or panel-to-panel joint (Fig. 2c,d), both in external or concealed utilizations, and some anchoring strategies to limit the wood embedment. More details are given in the following Sections.

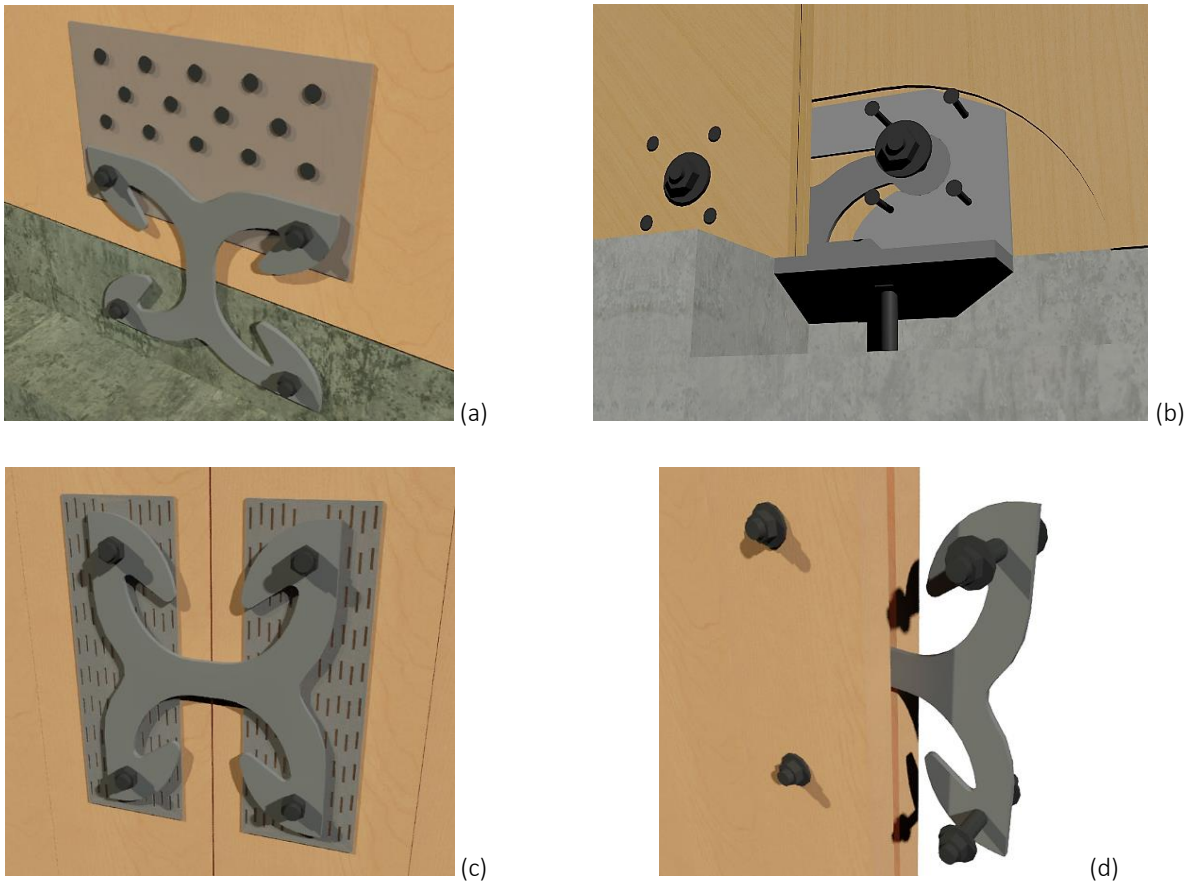

Fig. 2. Examples of possible arrangements of the X-bracket and possible strategies to guarantee a rigid anchoring to the panel: (a) Panel-to-foundation external joint; (b) Panel-to-foundation concealed joint; (c) Panel-to-panel external joint; (d) Panel-to-panel concealed joint

Main advantages of the X-bracket, given by its special shape, by the properties of structural steel and by the anchoring system to the CLT panel, are:

- An optimized mechanical behaviour to assure diffused yielding of material, resulting in extraordinarily high ductility and dissipative capacities;
- An optimized mechanical behaviour to assure high stiffness, which is favourable to avoid damages to non-structural components in case of static lateral loads or low-intensity earthquakes, and to guarantee, in case of strong earthquakes, that the dissipation be activated for small yielding displacements;
- The possibility of realizing a rigid anchoring to the panel with simple additional elements, which avoid or limit the wood embedment near bolts and the consequent “pinching” behaviour, allowing the connection system to exploit entirely the dissipative properties of the X-bracket;
- Mechanical characteristics can be easily adapted by changing dimensions and/or thickness and/or steel grade;
- The possibility of working as panel-to-foundation, panel-to-panel and inter-storey floor-wall joint, fulfilling in this way all functions of traditional connections with a unique type of connector, allocating ductility and dissipative properties in all the joints of the building;

- The use of a unique type of device to work in tension and/or shear, with well-defined strength and displacement domains;
- The reliability of the mechanical response to seismic loading, thanks to the deformation of a steel element and a rigid anchoring to timber, as opposed to traditional connections, whose response is governed by the interaction between fasteners and timber, with consequent greater uncertainty in the response;
- A more accessible and reliable capacity design, thanks to low scattering of mechanical properties and well-defined peak and yielding strength, resulting in low and controlled overstrength factors, easily estimable by means of a limited number of tests;
- The possibility of an easy replacement in the same position after strong earthquakes (if accessible), working as a fuse element and avoiding damages to CLT panel;
- The possibility of installing a couple of brackets externally to the panel to facilitate the replacement or a concealed bracket within the panel for aesthetic reasons or to guarantee the protection against fire (see Section 2.1);
- Very low production cost (*~2÷4€ per bracket)* thanks to its two-dimensional and simple shape, optimized to minimize waste of material (see Section 2.1);
- Fast installation (*~5min per bracket*) (see Section 2.2).

2.1 OPTIONS

Two options are available, optimized for external or concealed installation. Fig. 3 shows standard X-brackets and Fig. 4 and Fig. 5 alternative or special usages. Dimensions are relative to latest specimens tested in laboratory, for which a complete mechanical characterization is available in this Report.

X-bracket type 1 (Fig. 3a) is optimized to work as external bracket. Its shape is suitable to minimize waste of material from cutting of a mild steel plate (Fig. 6a). It can be used as panel-to-panel, panel-to-foundation and floor-wall joint. The anchoring to CLT can be realized by means of a screwed thin steel plate placed between the bracket and the panel with two holes in correspondence to the fixing points of the bracket. This allows X-bracket type 1 to be replaced after a strong earthquake in the same position, without removing the screwed steel plate.

X-bracket type 2 (Fig. 3b) is optimized to work as concealed connection within a groove in the panel edge. Its shape has been studied to work with complementary plates obtained directly in the cutting operations (Fig. 6b), which can be fixed to the panel with double shear plane self-drilling dowels as typical concealed beam hangers, assuring high strength and stiffness of the anchoring system. In this way, a cylindrical hinge at each fixing point is guaranteed allowing bending deformation of flanges and rotation around the calibrated bolts. This option is suitable to realize panel-to-panel joints for aesthetic reasons or to guarantee the protection against fire. A special usage of X-bracket type 2 as panel-to-foundation concealed connection (Fig. 4) can be obtained using half a bracket welded to a rectangular steel plate, which can be fixed to foundation by means of concrete anchors. The usage of X-bracket type 2 as external bracket is anyway possible (Fig. 5), with or without the use of the complementary plates.

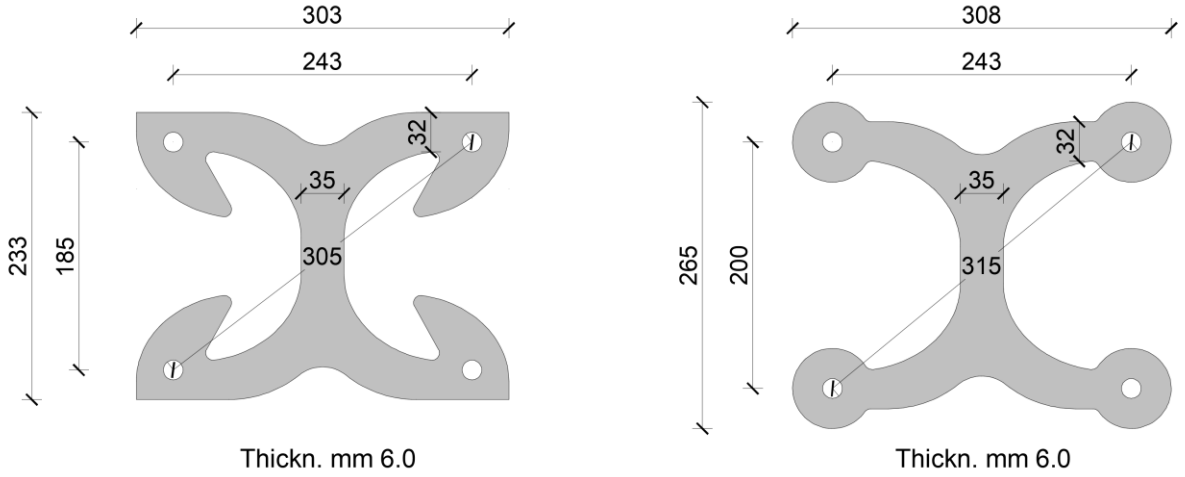

(a) (b)

Fig. 3. Standard usages of the X-bracket: (a) Type 1 as external application; (b) Type 2 as concealed application. Dimensions refer to the latest specimens tested in laboratory. Units: mm

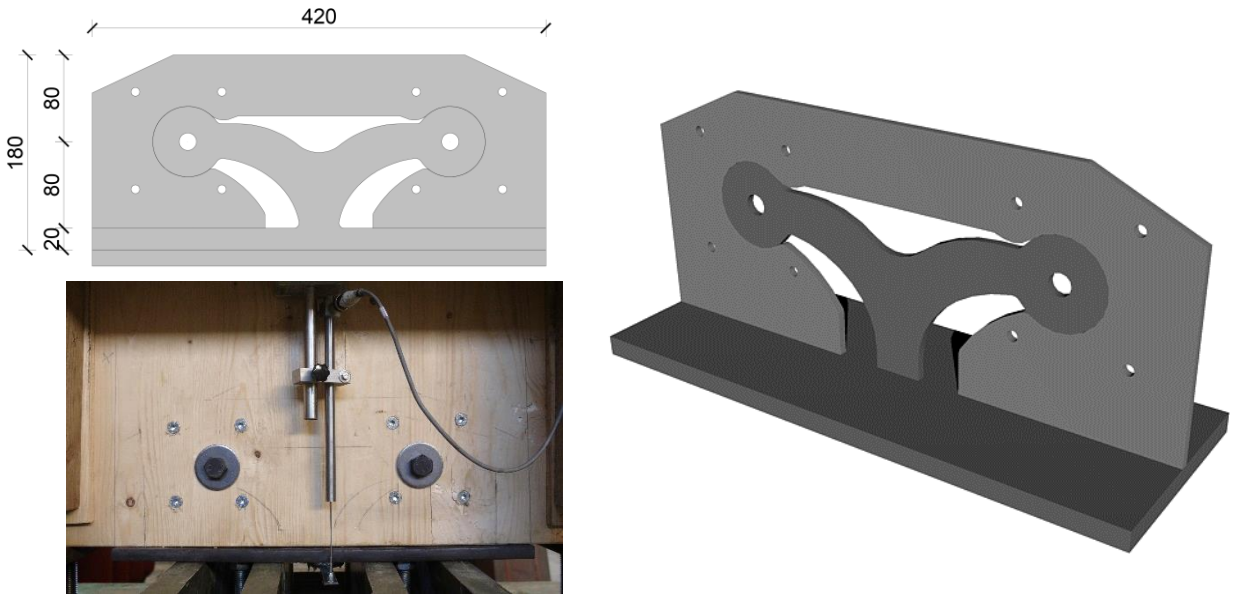

Fig. 4. Special usage of the X-bracket type 2 as panel-to-foundation concealed connection

Fig. 5. Alternative usage of the X-bracket type 2 as external connection

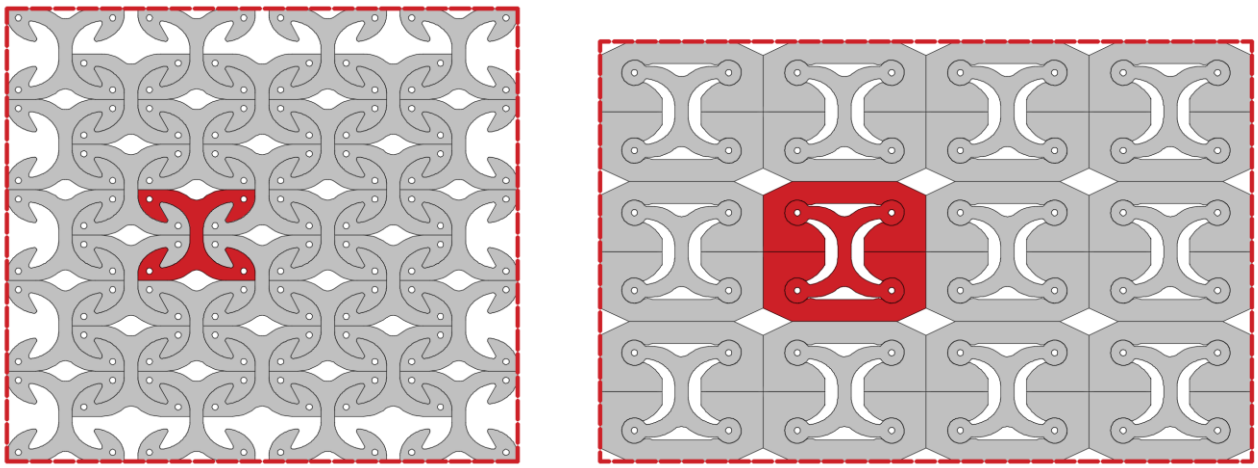

(a) (b)

Fig. 6. Production of X-bracket: (a) Type 1; (b) Type 2

2.2 INSTALLATION

A very fast installation is guaranteed since only four calibrated bolts are needed to connect one X-bracket to CLT or to foundation. Bolts are inserted into holes predrilled in panels. X-bracket type 1 must be used in a pair at both sides of the panel. A foundation curb or bottom rail is always needed. Alternative solutions are available to avoid wood embedment, both in external and concealed utilizations.

2.2.1 External X-bracket

Some possible anchoring systems of the external X-bracket are here listed.

- Use of a screwed thin steel plate between the bracket and the panel (Fig. 7). Analytical calculations based on the conceptual model of capacity design described in Section 1.2 and experimental tests[*] demonstrated that fourteen 8x100mm self-tapping partially threaded screws per bracket are sufficient to guarantee a rigid anchoring with negligible decrease of strength and dissipative capacity of the entire connection system with respect to the intrinsic capacities of a bracket (Scotta et al. 2017) (*[*]X-bracket realized with dimensions in Fig. 3a and S450 steel grade according to EN 10025-2)*.
- Use of punched metal plates (Blass et al. 2000) (see Fig. 2c).
- Use of special elements to increase the wood embedment strength near calibrated bolts. This strategy does not require the addition of steel plates or fasteners with the exception of the four calibrated bolts per bracket, which are always needed (see Fig. 2d and Fig. 5).

Fig. 7. Anchoring of external X-bracket type 1 to CLT with a screwed plate

2.2.2 Concealed X-bracket

Some possible anchoring systems of the concealed X-bracket type 2 are here listed.

- Use of complementary plates fastened to the panel with self-drilling dowels (Fig. 8 and Fig. 9). Analytical calculations based on the conceptual model of capacity design described in Section 1.2 and experimental tests[**] demonstrated that four 7x90mm self-drilling dowels per bolt are sufficient to guarantee a rigid anchoring (*[**]X-bracket realized with dimensions in Fig. 3b and Fig. 4and S355 steel grade according to EN 10025-2).*
- Use of special elements to increase the wood embedment strength near calibrated bolts. This strategy does not require the addition of steel plates or fasteners (see Fig. 2d and Fig. 10).

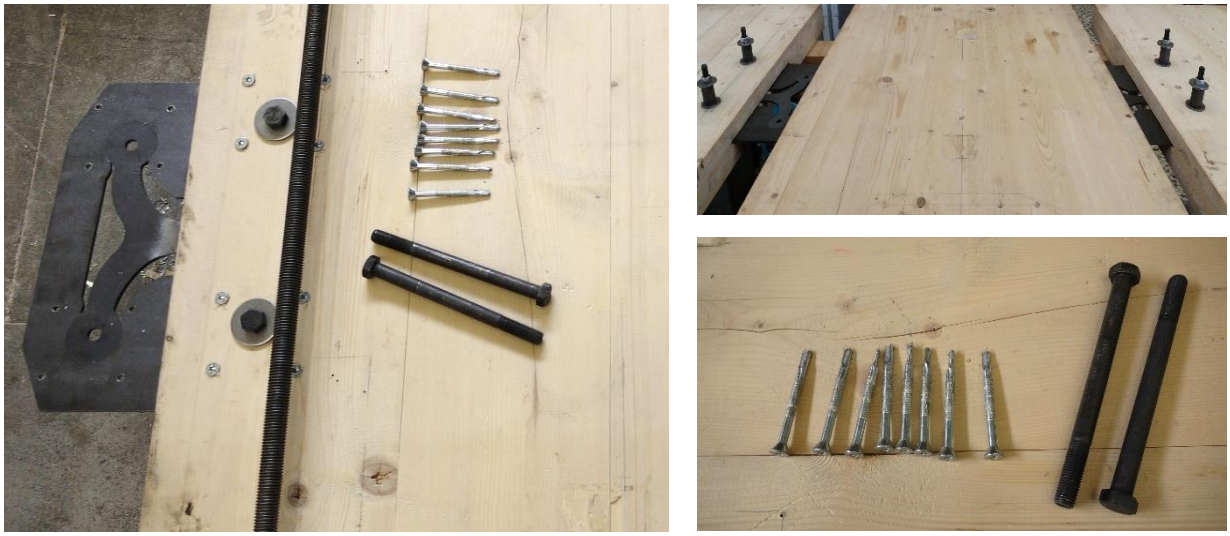

Fig. 8. Anchoring of concealed X-bracket type 2 to CLT with self-drilling dowels (panel-to-panel joint)

Fig. 9. Anchoring of concealed X-bracket type 2 to CLT with self-drilling dowels (panel-to-foundation joint)

Fig. 10. Anchoring of concealed X-bracket type 2 to CLT with special elements without the use of complementary plates or additional fasteners (panel-to-foundation joint)

3. MECHANICAL CHARACTERIZATION

The mechanical behaviour of the X-bracket has been characterized by means of numerical simulations with detailed Finite Element (FE) models and experimental tests performed in the Mechanical Laboratory of Construction and Materials of Department ICEA of the University of Padova. In this Section, main results from simulations and tests are reported and discussed. The complete mechanical characterization is available in Appendix A, which reports results from each performed test. Before presenting main results relative to X-bracket type 1 and type 2, preliminary tests and simulations of the first prototype are also briefly summarized (see also Scotta et al. (2015); Scotta et al. (2016); Marchi et al. (2016).

3.1 FIRST PROTOTYPE

3.1.1 Preliminary simulations

A three-dimensional (3D) FE model of the X-bracket using solid elements was implemented into ANSYS Workbench to design the optimal shape and dimensions of the first prototype. Main geometrical parameters chosen as variables in the model are evidenced with letters in Fig. 11. An elastic-plastic constitutive law combined with a Von-Mises yield criterion and a kinematic hardening model was adopted to simulate steel cyclic behaviour. The non-linear geometrical analysis option was activated to account for possible buckling phenomenon for high displacements. A total of about 80 combinations of parameters were examined. Each combination consisted in a pure tension and pure shear pushover and/or cyclic-loading analysis. The parametric analyses were helpful, as modifying length and thickness of vertical and horizontal arms allowed to calibrate strength in shear and tension and displacement capacity. Additionally, the variation of stiffness and strength was permitted by changing the internal curvature radius. The dimensions of the final shape listed in Fig. 11 resulted in an optimization of strength, stiffness and ductility and in assuring similar performances in tension and shear. The high ductility in shear is mainly assured by the plastic deformation of the vertical web, whereas in tension by the bending deformation of the horizontal arms. Fig. 12 shows the deformation at maximum imposed displacements, in tension and shear loading. The grey contour shows plastic regions, in which the yielding stress has been exceeded.

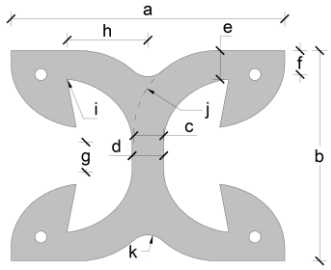

Parameters (units)	Dimensions	Parameters (units)	Dimensions
a (mm)	303.0	g (mm)	33.0
b (mm)	233.0	h (mm)	89.0
c (mm)	33.0	i (mm)	1.0
d (mm)	35.0	j (mm)	91.5
e (mm)	31.5	k (mm)	23.5
f (mm)	26.5	Thickness (mm)	6.0

Fig. 11. Dimensions of the first prototype as output of the parametric analysis

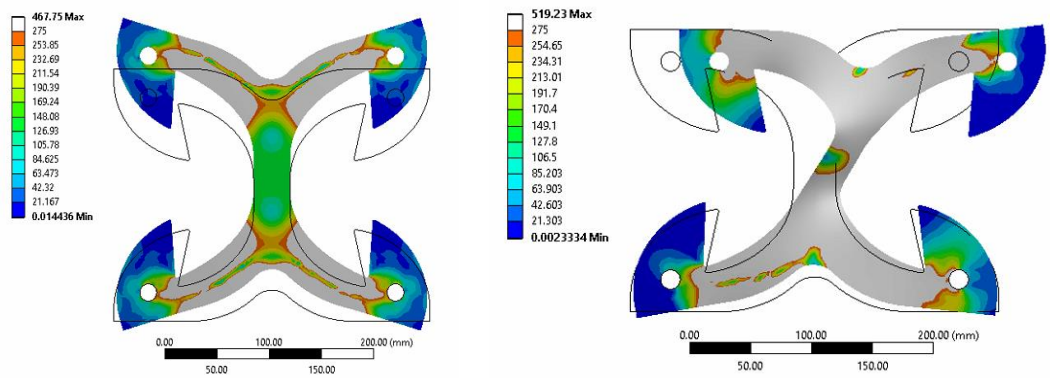

(a) (b)

Fig. 12. Numerical model of the first prototype: equivalent von Mises stress contour on deformed geometry of X-brackets. (a) Tension loading; (b) Shear loading. Plastic regions in grey colour (Scotta et al. 2016)

3.1.2 Preliminary tests

After the numerical design and optimization, preliminary experimental tests of the first prototype were carried out to obtain the actual cyclic behaviour and to compare results with numerical predictions. Three tests were performed in pure tension and three in pure shear loading, according to the quasi-static cyclic loading protocol in displacement control recommended by EN 12512 (2006). The cyclic procedure was stopped after reaching a relative displacement of 30 mm; then the specimens were loaded monotonically until failure. A couple of X-brackets was fixed externally on both sides of a rigid steel frame without blocking possible buckling; therefore, a total of twelve X-brackets were tested. Two specific setups were designed for tension and shear tests (Fig. 13). With reference to the setup for tension tests (Fig. 13a), the two lower fixing points of the X-brackets were connected to a rectangular 20mm thick steel plate, rigidly fixed to the portal. The two upper fixing points were connected to another rectangular 20mm thick plate fixed to the hydraulic actuator with rotational hinge. The pure shear loading was obtained with an unbraced 15mm thick steel truss, in which the X-brackets worked as cross-bracing elements (see Fig. 13b); the whole assembly was positioned in a rotated configuration, in order to keep the loading direction as close as possible to the virtual diagonal line. Polytetrafluoroethylene (Teflon - PTFE) sheets were interposed between contact surfaces to minimize friction.

During tests, displacements were measured by a Linear Variable Differential Transducer (LVDT) per side of the supporting steel frame. For tension tests, the LVDTs measured directly the relative displacement Δy of the two rigid plates (see Fig. 13a). The shear displacements Δx were obtained projecting the virtual diagonal deformation (see Fig. 13b) to the lateral direction of the X-bracket; the progressive rotation of the steel frame was considered in the evaluation of the shear component of the applied force. It is worth noting that this preliminary experimental phase was useful also to test the setup and the measuring system, in order to make possible improvements for the following experimental campaign of the final versions of X-bracket.

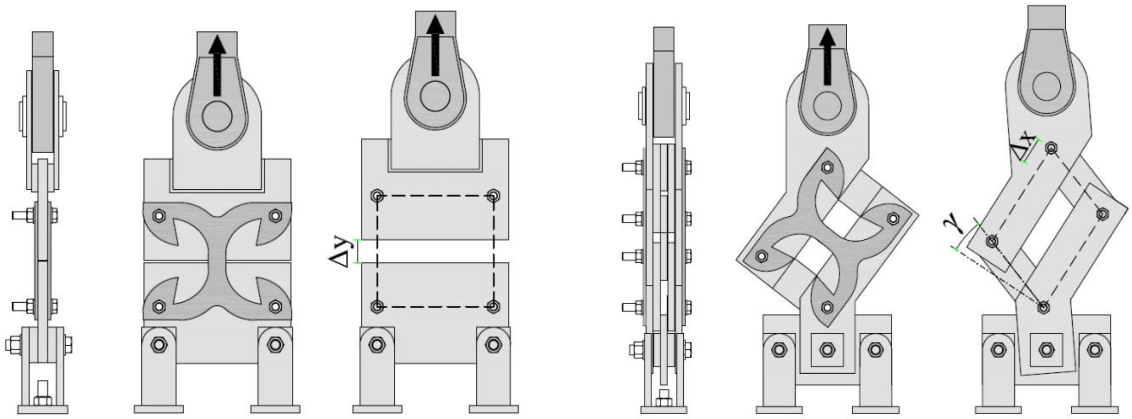

(a) (b)

Fig. 13. Test setups: (a) Rigid frame for tension tests; (b) Unbraced steel truss for shear tests (Scotta et al. 2016)

Fig. 14 plots the results of tests in comparison with numerical prediction (the numerical model was calibrated according to mean steel parameters derived from tensile tests of the material according to EN ISO 6892-1 (2016). Force refers to one bracket. With reference to the curves of the specimens loaded in shear, the projection of forces and displacements to the lateral direction of the X-bracket are shown, to present the results in terms of lateral force and lateral displacements. Results for tension loading (Fig. 14a) show that during the 30 mm cycles the reloading stiffness decreased gradually due to buckling. For the same reason, the maximum compression force measured during unloading was lower than the tension one, but still maintained a wide hysteresis area and, consequently, an appropriate dissipative capacity. The numerical model tolerably underestimated unloading stiffness. With reference to the shear loading results (Fig. 14b), the experimental hysteresis cycles are perfectly centred on the origin of the axes, thus demonstrating the suitability of the setup configuration. The experimental cyclic shear tests were stopped at about ±15 mm due to the limitations of the test setup. Then, X-brackets were deformed monotonically up to 50, 58 and 80mm in Tests 1, 2 and 3, respectively. In general, no noticeable strength degradation was observed in the experimental tests. Numerical simulations of cyclic shear tests were extended up to ±30 mm. In the range ±15 mm, the numerical results are in good agreement with the experiments, even if the numerical predictions slightly over-estimate shear force at higher displacements. Moreover, flexural-torsional buckling of the X-brackets, started at ±15 mm cycles, was correctly simulated, Fig. 15.

Fig. 16 shows the tested specimens subjected to very large displacement (35 mm in tension test, 50 mm in shear test). The main evidence is that the X-brackets are able to experience large plastic deformations before failure, in both loading configurations. Specimens failed at very large displacements due to stress concentration in fillet “i” (Fig. 11). Based on these preliminary results, the ductility of X-brackets was further improved with a proper modification of this detail. Moreover, test setups and measuring systems were optimized for the test campaigns of the final versions to permit tests to continue in cyclic loading up to failure of the specimens.

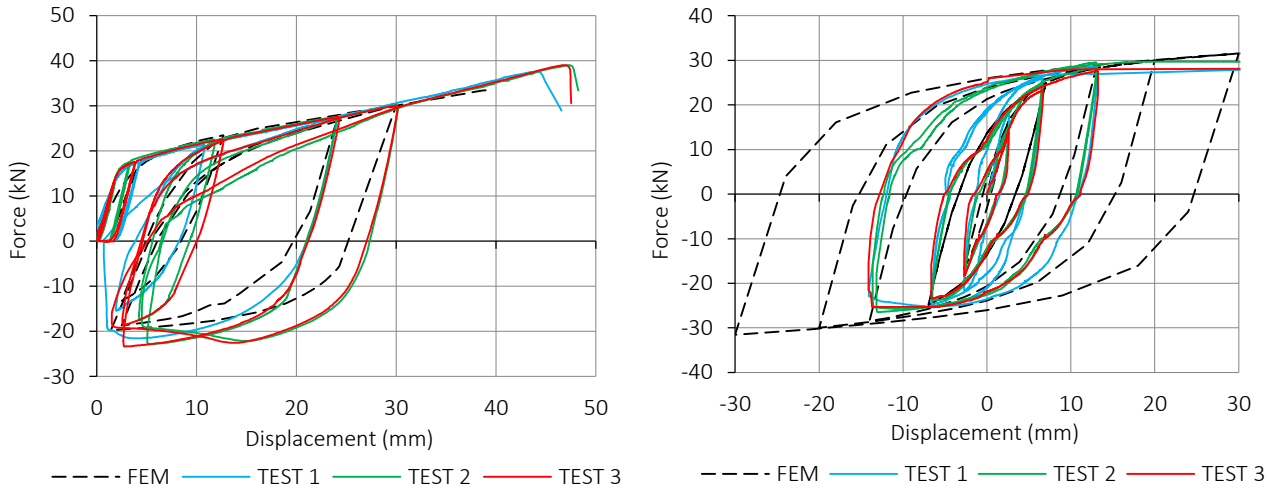

Fig. 14. Experimental and numerical results of one bracket. (a) Tension tests; (b) Shear tests (Scotta et al. 2016)

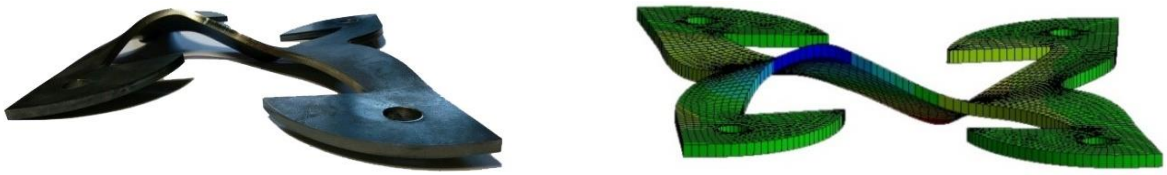

Fig. 15. Plate buckling under shear loading. (a) Experimental evidence; (b) Numerical prediction (Scotta et al. 2016)

Fig. 16. Deformed specimens. (a) Tension test; (b) Shear test (Scotta et al. 2016)

The cyclic tests were analysed, fitting the envelope curve with the analytical formulation proposed by Foschi and Bonac (1977). Then, method (a) of EN 12512 (2006) was chosen for both tension and shear tests, in order to obtain the best linear fitting of the envelope curve. Moreover, also the equivalent elastic–plastic energy (EEEP) method (Foliente 1996) was used to analyse the results of the shear tests, because of the almost elastic perfectly plastic behaviour. From the bi-linear curves, it was possible to obtain: elastic and post-elastic stiffness (k_{el}, k_{pl}), yielding point (d_y, F_y), ultimate displacement d_u, peak strength F_{max} and ductility μ. Finally, according to Eurocode 8 (2013) it was possible to classify the connection into the appropriate ductility class, i.e., low (L), medium (M) or high (H). Table 1 and Table 2 list the obtained results referring to a single bracket, i.e., strength and stiffness represent the mean result between the couple of X-brackets contemporarily tested. Therefore, average values, standard deviations (SD) and 5th and 95th characteristic values (k^-, k^+), were computed considering a sample of six brackets. Results show that the proposed connection is characterized by a high initial stiffness and adequate strength for both tension and shear loads. However, the most valuable result is the very high ductility obtained and the limited pinching effect. High values of ductility are the consequences of a combination of large displacement capacity d_u, similar or greater than traditional connections, and an early yielding condition d_y. Ductility for the shear configuration was computed assuming d_u equal to 50 mm, although in Test 3, failure of the specimen occurred for a displacement equal to 80 mm, whereas Tests 1 and 2 were stopped before failure.

Table 1 - Tension tests: main mechanical parameters (Scotta et al. 2016)

Parameters (units)	Test 1	Test 2	Test 3	Mean	SD	k^-	k^+
F_y (kN)	17.55	18.37	17.99	17.97	0.36	17.18	18.76
d_y (mm)	1.89	2.01	1.98	1.96	0.06	1.83	2.09
F_{max} (kN)	37.18	37.84	38.25	37.76	0.48	36.70	38.81
d_u (mm)	44.30	47.30	47.00	46.20	1.48	-	-
k_{el} (kN/mm)	9.31	9.12	9.08	9.17	0.11	8.94	9.40
k_{pl} (kN/mm)	0.46	0.43	0.45	0.45	0.01	0.42	0.48
μ (d_u) (-)	23.49	23.49	23.72	23.57	0.12	23.30	-
Ductility Class	H	H	H	-	-	-	-

Table 2 - Shear tests: main mechanical parameters (Scotta et al. 2016)

Parameters	Test 1		Test 2		Test 3		Mean		SD		k^-		k^+	
(units)	EN	EEEP	EN	EEEP	EN	EEEP	EN	EEEP	EN	EEEP	EN	EEEP	EN	EEEP
F_y (kN)	26.71	27.41	29.41	28.88	28.14	27.83	28.09	28.04	1.21	0.68	25.46	26.56	30.71	29.52
d_y (mm)	2.38	2.60	4.00	4.45	4.02	4.53	3.46	3.86	0.84	0.98	1.63	1.73	5.30	5.99
F_{max} (kN)	29.00	27.41	29.70	28.88	28.40	27.83	29.03	28.04	0.58	0.68	27.76	26.56	30.30	29.52
d_u (mm)	50.00*	50.00*	58.00*	58.00*	80.00	80.00	-	-	-	-	-	-	-	-
k_{el} (kN/mm)	11.24	10.55	7.36	6.49	7.00	6.14	8.53	7.73	2.10	2.19	3.95	2.95	13.12	12.50
k_{pl} (kN/mm)	0.05	0.00	0.01	0.00	0.00	0.00	-	-	-	-	-	-	-	-
μ (d_u=50mm)	21.04	19.24	12.51	11.24	12.44	11.03	-	-	-	-	-	-	-	-
Ductility Class	H	H	H	H	H	H	-	-	-	-	-	-	-	-

* Tests 1 and 2 were stopped before the ultimate displacement

3.2 EXTERNAL X-BRACKET TYPE 1

X-bracket type 1 (see Section 2) is an enhanced version of the first prototype. According to results of preliminary tests, minimal shape adjustments were performed, increasing fillet radius "*i*" in Fig. 11 and modifying hole spacing. A 6-mm thick steel plate, with strength corresponding to a S450 steel grade according to EN 10025-2 (2004), was chosen to realize the specimens for the experimental campaign. Dimensions of the specimens are in Fig. 3a.

3.2.1 Simulations

A 3D FE model of the X-bracket type 1 was performed to predict the actual behaviour in tension or shear and then to derive the full shear-tension strength and displacement domain (Marchi et al. 2017). The FE model was developed in ANSYS Workbench, using high-order SOLID185 elements, meshed with a mesh size between 2-5 mm, Fig. 17. Cylindrical hinges placed at the four fixing points (i.e., holes where bolts are inserted) allowed horizontal arms to rotate. The geometrical nonlinearity was activated to account for possible Eulerian buckling (Fig. 17b) and lateral-torsional buckling (Fig. 17d) for large deformations. A compression-only surface placed on the back side of the bracket forced the possible out-of-plane buckling only towards the opposite side, to simulate the presence of the CLT panel.

An elastic-plastic constitutive law combined with a Von Mises yield criterion and a kinematic hardening model was adopted to simulate steel cyclic behaviour. The mechanical properties of steel were extrapolated from monotonic tensile tests on specimens according to EN ISO 6892-1 (2016) and applied to the model through a multilinear true stress-*vs.*-strain curve. Elastic and hardening moduli of S450JR steel were set to 210000 and 957 MPa, respectively, whereas yielding stress and ultimate true stress were set to 450 MPa and 700 MPa, respectively.

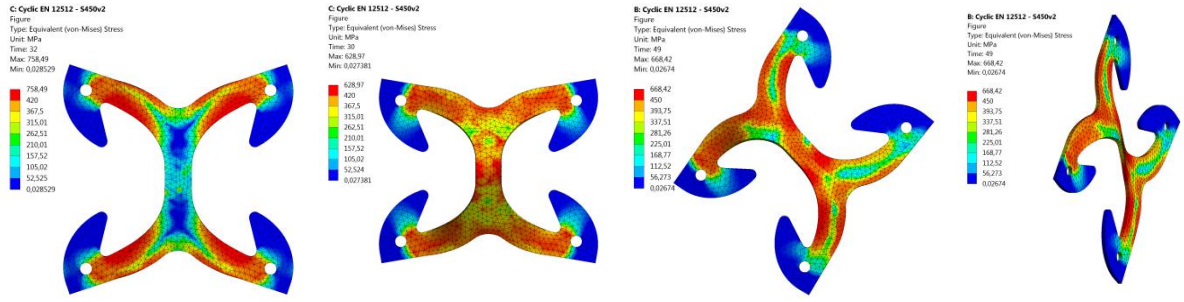

(a) (b) (c) (d)

Fig. 17. Mesh of X-bracket type 1 and contour of the Von Mises stress from cyclic-loading simulations: (a) Loading in tension; (b) Unloading in tension and Eulerian buckling; (c) Loading in shear, front view; (d) Loading in shear and lateral torsional buckling, side view

For this type of bracket, additional displacement-driven non-linear static analyses were performed, varying the angle α of the resulting force between pure shear condition (α = 0°) and pure tension condition (α = 90°). Obtained force-*vs.*-displacement curves (Fig. 18) have same stiffness in the initial elastic phase, and deviate when entering the plastic phase. The resulting displacement and strength domains, applying ten combinations of tension and shear forces are shown in Fig. 19. First yielding conditions were evaluated after decomposition of the applied force to the tension and shear components FHD and FSH respectively. Failure conditions were

set at the achievement of the ultimate steel strain. A conservative analytic ultimate displacement domain was defined according to Equation (4), as shown with dashed line in Fig. 19a.

$$\sqrt{d_x^2+d_y^2} \leq 38mm \tag{4}$$

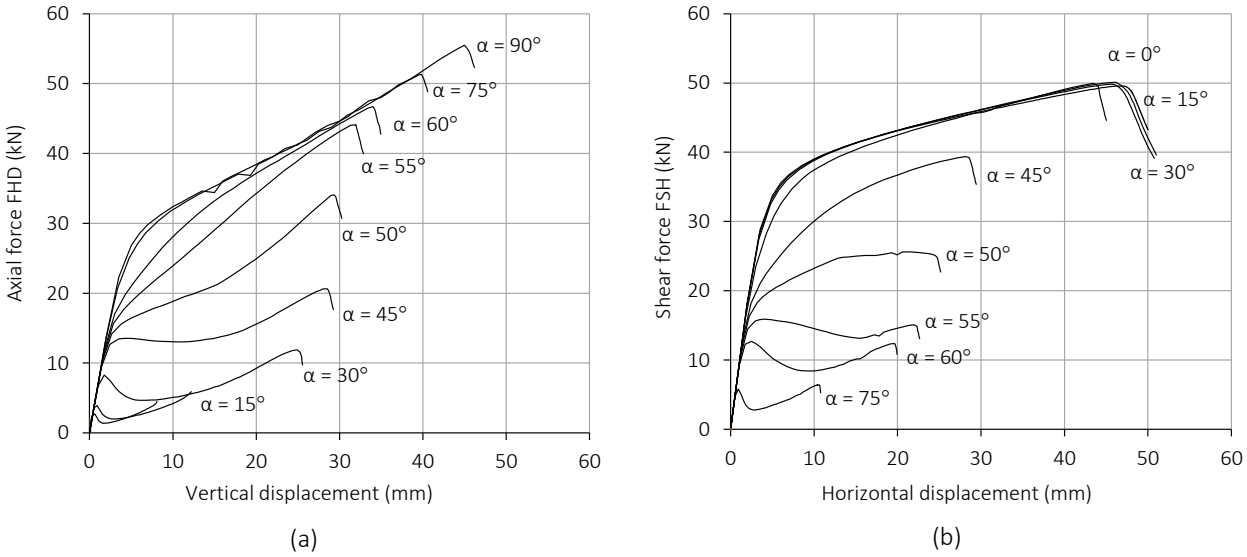

Fig. 18. Monotonic curves varying the angle of the applied force: (a) Vertical component FHD; (b) Shear component FSH

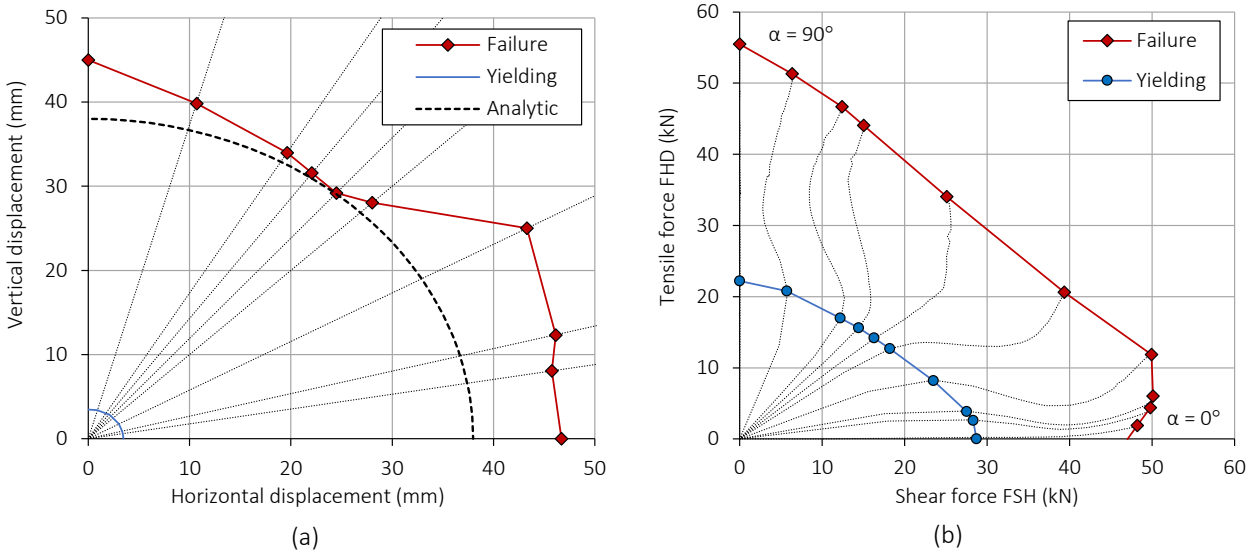

Fig. 19. Coupling domains obtained from the imposed angles of the applied forces: (a) Displacement domain; (b) Strength domain

3.2.2 Tests

Six mechanical tests (three in tension and three in shear) were performed according to the quasi-static cyclic-loading protocol of EN 12512 (2006), imposing a yielding displacement $d_{y,est}$ equal to 4mm. The same symmetric test procedure of the preliminary tests was followed, by anchoring a couple of X-brackets to a rigid steel frame, with M16 8.8-class steel bolts (Fig. 20). Therefore, six brackets were tested in tension and six in shear. Fig. 21 shows photos of the setup and measurement system and positions, with some improvements with respect to preliminary tests.

Test results are plotted in Fig. 22 and Fig. 23 in terms of force-displacement curve for all the tests. Strength refers to a single X-bracket. With reference to the curves of the specimens loaded in shear, the projection of forces and displacements to the local axis x (see Fig. 20) are shown, to present the results in terms of lateral force and lateral displacements of one bracket.

Results show that X-bracket type 1 is characterized by very high ductility resulting from a combination of high elastic stiffness and high displacement capacity. In tension tests, failure occurred due to large amount of plastic deformations of the vertical web, which is subjected to Eulerian buckling during the unloading phase and consequent strength degradation during the reloading (Fig. 24). This phenomenon starts from the 24mm cycles, whereas up to this deformation, no instability or strength degradation occurred. Moreover, for the subsequent 32, 40 and 48mm cycles, the hysteretic response was still very acceptable and all the three repeated cycles were successfully completed. Also for shear tests, failure was located in the vertical web, which is subjected to repeated load inversions and consequent flexural-torsional buckling (Fig. 25) for large deformations (i.e., ±16mm cycles in Fig. 23). However, also for shear tests, all three ±32mm cycles were completed without showing excessive strength degradation. Fig. 22 and Fig. 23 show also the suitability of the FE model in predicting the hysteretic behaviour of the X-bracket.

The performed cyclic tests allowed to define main mechanical parameters, by fitting the envelope of the hysteresis curves using the analytical formulation proposed by Foschi and Bonac (1977) and applying proper bi-linearization methods. Table 3 lists results of tests in tension and Table 4 results of tests in shear. As for the first prototype, method (a) of EN 12512 (2006) was chosen for tension tests, whereas the EEEP method (Foliente 1996) was considered suitable for shear tests, due to the different post-elastic behaviour shown. From the obtained bi-linear curves, it was possible to classify the proposed connection into the appropriate ductility class (Low (L), Medium (M) and High (H), according to Eurocode 8 (2013). Characteristic 5^{th} percentile and 95^{th} percentile values were calculated assuming a normal distribution according to EN 1990 (2010) and EN 14358 (2016). The increase of steel strength resulted in an improvement of strength and stiffness with respect to the first prototype.

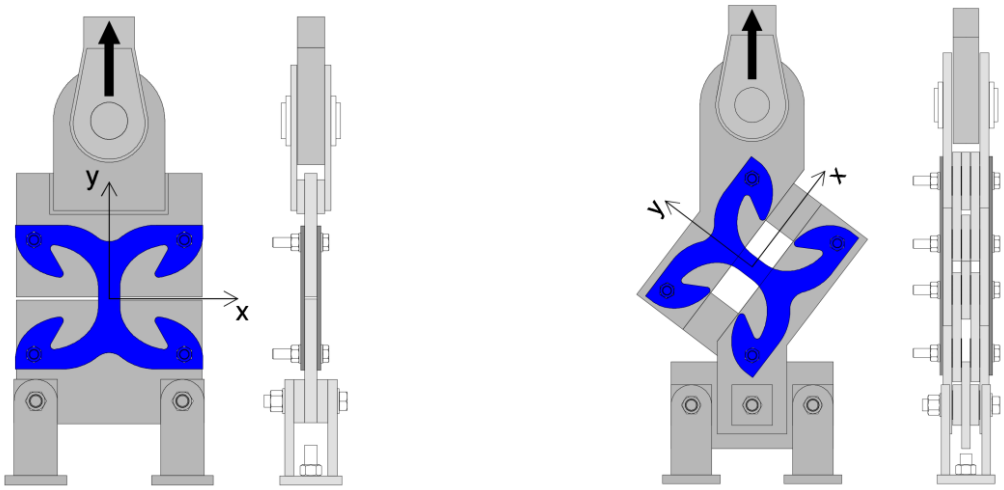

(a) (b)

Fig. 20. Test setup of the X-bracket type 1: (a) Tests in tension; (b) Tests in shear

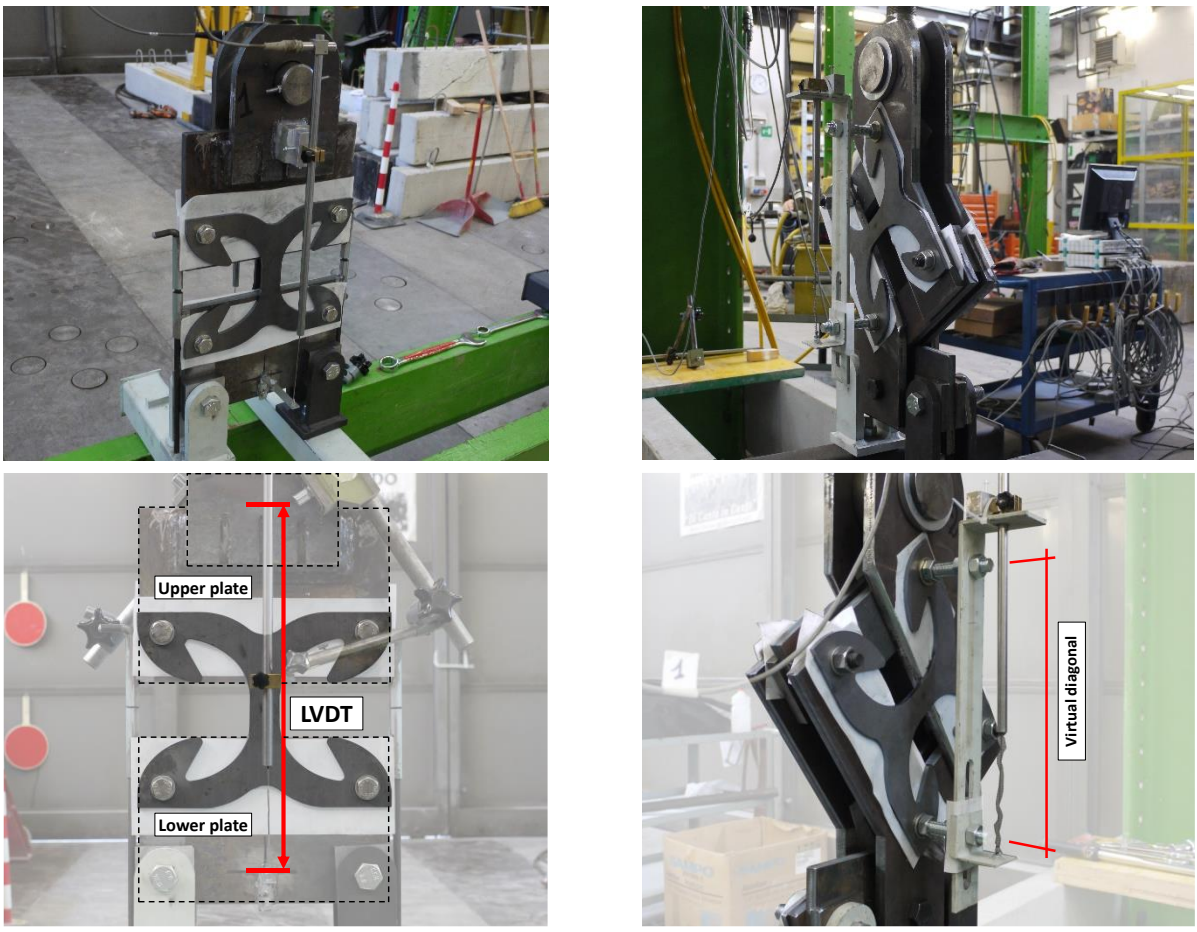

(a) (b)

Fig. 21. Test setup of X-bracket type 1 and positioning of LVDTs: (a) tests in tension; (b) tests in shear

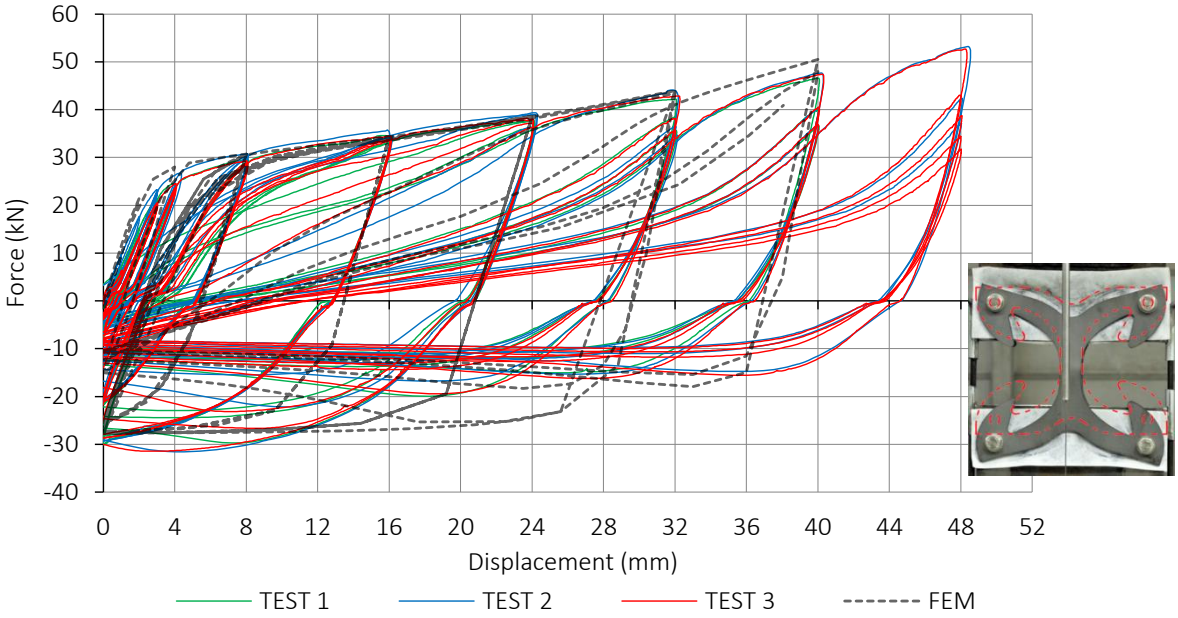

Fig. 22. Force-displacement curves for tests in tension (strength refers to one bracket)

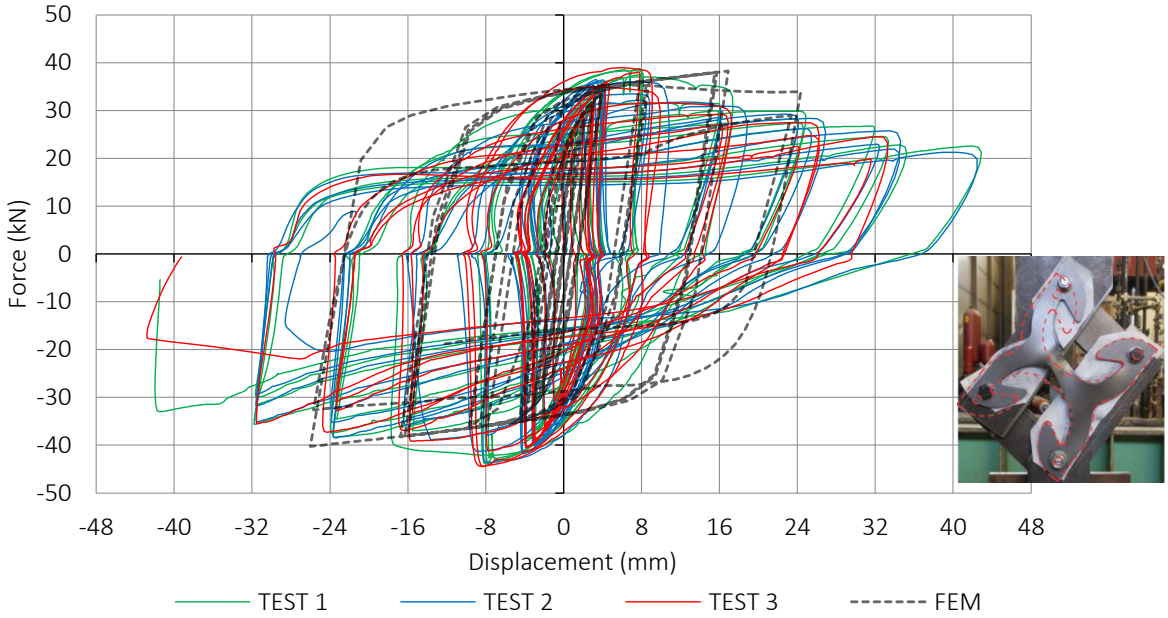

Fig. 23. Force-displacement curves for tests in shear (strength refers to one bracket)

(a)

(b)

Fig. 24. Deformed specimen in tension: (a) Loading; (b) Unloading

Fig. 25. Deformed specimen in shear

Table 3. Tension tests: main mechanical parameters according to EN 12512 (2006) method "a"

Parameter (units)	TEST 1	TEST 2	TEST 3	Mean	SD	COV	EN 1990 (2010)		EN 14358 (2016)	
							k^-	k^+	k^-	k^+
F_y (kN)	28.59	29.51	28.16	28.75	0.62	2.14%	27.41	30.09	25.39	32.11
d_y (mm)	3.26	3.08	3.21	3.18	0.08	2.53%	3.01	3.36	2.81	3.55
F_{max} (kN)	46.60	47.60	47.30	47.17	0.46	0.97%	46.17	48.17	41.65	52.68
d_u (mm)	40.00	40.00	40.00	40.00	-	-	-	-	-	-
k_{el} (kN/mm)	8.78	9.57	8.77	9.04	0.41	4.57%	8.14	9.94	7.98	10.10
k_{pl} (kN/mm)	0.49	0.49	0.52	0.50	0.02	3.12%	0.47	0.53	0.44	0.56
μ (d_u) (-)	12.29	12.98	12.46	12.58	0.32	2.56%	11.87	-	11.10	-
Ductility Class	H	H	H	-	-	-	-	-	-	-

Table 4. Shear tests: main mechanical parameters according to EEEP method (Foliente 1996).

Parameter (units)	TEST 1	TEST 2	TEST 3	Mean	SD	COV	EN 1990 (2010)		EN 14358 (2016)	
							k^-	k^+	k^-	k^+
F_y (kN)	39.15	39.51	39.84	39.50	0.31	0.78%	38.83	40.17	34.88	44.12
d_y (mm)	1.24	1.26	1.25	1.25	0.01	0.97%	1.23	1.28	1.11	1.40
F_{max} (kN)	43.91	43.49	44.45	43.95	0.43	0.98%	43.01	44.89	38.81	49.09
d_u (mm)	32.00	32.00	24.00	-	-	-	-	-	-	-
k_{el} (kN/mm)	31.64	31.25	31.75	31.55	0.23	0.74%	31.03	32.06	27.85	35.24
k_{pl} (kN/mm)	0.00	0.00	0.00	0.00	-	-	-	-	-	-
μ(d_u) (-)	25.86	25.31	19.13	23.43	3.34	14.27%	16.14	-	15.61	-
Ductility Class	H	H	H	-	-	-	-	-	-	-

The tension tests and the bi-linearization method (a) of EN 12512 (2006) returned $F^-_{D,\,y}$ and $F^+_{D,\,peak}$ values of 27.41 kN and 48.17 kN respectively, according to EN 1990 (2010). Therefore, the resulting overstrength factor γ_{Rd} for the X-bracket loaded in tension, according to the conceptual model presented in Section 1.2 and assuming $F^-_{D,\,code} = F^-_{D,\,y}$, is equal to 1.76. In shear loading conditions, γ_{Rd} is equal to 1.15, resulting from $F^-_{D,\,y}$ and $F^+_{D,\,peak}$ values of 38.83 kN and 44.89 kN respectively.

In (Scotta et al. 2017) a comparison of γ_{Rd} evaluated for the X-bracket and for traditional connections, which are characterized by values in the range 2.0÷3.4, is discussed. It can be noted that the use of X-brackets, which localize the ductility and energy dissipation capacity in a steel element, can strongly reduce the scattering of peak force. On the contrary, a steel-to-timber connection with dowel-type fasteners, as traditional connections, has higher statistical dispersion.

According to the calculated values of γ_{Rd}, the anchoring of the X-bracket to a CLT panel subjected to tension loads was designed. The timber element is a 120mm thick CLT panel composed by 5 layers of C24 timber boards. The two 16mm diameter upper fixing points of the X-brackets are supposed to be fastened to the panel with two 16x200mm 8.8-class calibrated bolts, to allow the horizontal arms to rotate and to dissipate energy due to steel plasticization. These two cylindrical restraints are subjected to high concentrated forces,

which would result in predominant wood embedment, compromising the dissipative properties of the connection. A thin steel plate was placed between the bracket and the panel with two 16mm diameter holes in correspondence to the fixing points of the bracket. A rectangular S275JR steel plate with dimensions of 330x200x3mm, was designed and fastened to the panel with fourteen 8x100mm self-tapping partially threaded screws. The characteristic load-bearing capacity of the screws $F_{B,code}^{-}$ was computed according to Eurocode 5 (2014). In detail, a total shear strength $F_{B,code}^{-}$=52.86 kN was obtained for the effective number of screws, evaluating the characteristic embedment strength in the timber member $f_{h,k}$ according to Eurocode 5 formulation (2014), assuming the fastener yield moment $M_{y,Rk}$ and withdrawal capacity $f_{ax,k}$ according to ETA-11/0027 (2016) and a the characteristic value of panel density ρ_k equal to 385 kg/m^3. This value of $F_{B,code}^{-}$ is higher than $\gamma_{Rd} \cdot F_{D,code}^{-}$ = 48.24 kN (assuming again $F_{D,code}^{-} = F_{D,y}^{-}$), thus fulfilling Inequality (1) and complying with the capacity design.

A cyclic-loading test of the complete connection was conducted following the same cyclic-loading procedure and setup adopted for the bracket, in order to obtain a direct comparison between the hysteretic behaviour of the X-bracket and of the complete connection. The experimental test of the complete connection was conducted only in tension. However, by changing the plate dimensions and the position of the screws, it is possible to realize the same over-resistant connection in case of shear loading conditions.

Fig. 26 shows the photos of a non-deformed and a deformed specimen, up to failure. From the superimposition of the results recorded for the X-bracket and the test of the complete connection, a very similar hysteresis behaviour and a negligible decrease of dissipative capacity and strength was evidenced, Fig. 27a. The maximum relative slip of the 3-mm steel plate is 0.4mm, a negligible value with respect to the displacement amplitude of the bracket. The reduction of strength and dissipative capacity (in terms of viscous damping ratio ν_{eq} (EN 12512, 2006) for the complete connection with respect to the mean value from the three tests of the X-bracket can be quantified from a comparison of the orange and the black lines in Fig. 27b-c for all the loading cycles. It can be noted that the recorded viscous damping ratios are substantially higher than traditional hold-downs, having ν_{eq} of about 3 due to marked pinching behaviour (Gavric et al. 2015b).

After the execution of the test of the complete connection, an additional test was performed to the same specimen, replacing only the two X-brackets and the two bolts, whereas the self-tapping screws that fastened the rectangular plate were not replaced. The aim was to give a preliminary evaluation of the possibility of using this bracket as a fuse element, which can be replaced after an earthquake, if accessible. The same loading procedure (EN 12512, 2006) was applied to the specimen. Results show that the device can withstand another cyclic loading procedure without significant degradation in strength and dissipative capacity (Fig. 28, Table 5). It can be noted that the dissipative capacity is almost fully exploited and, neglecting the elastic phase, the mean strength loss ΔF measured for each cycle was about 2.5%.

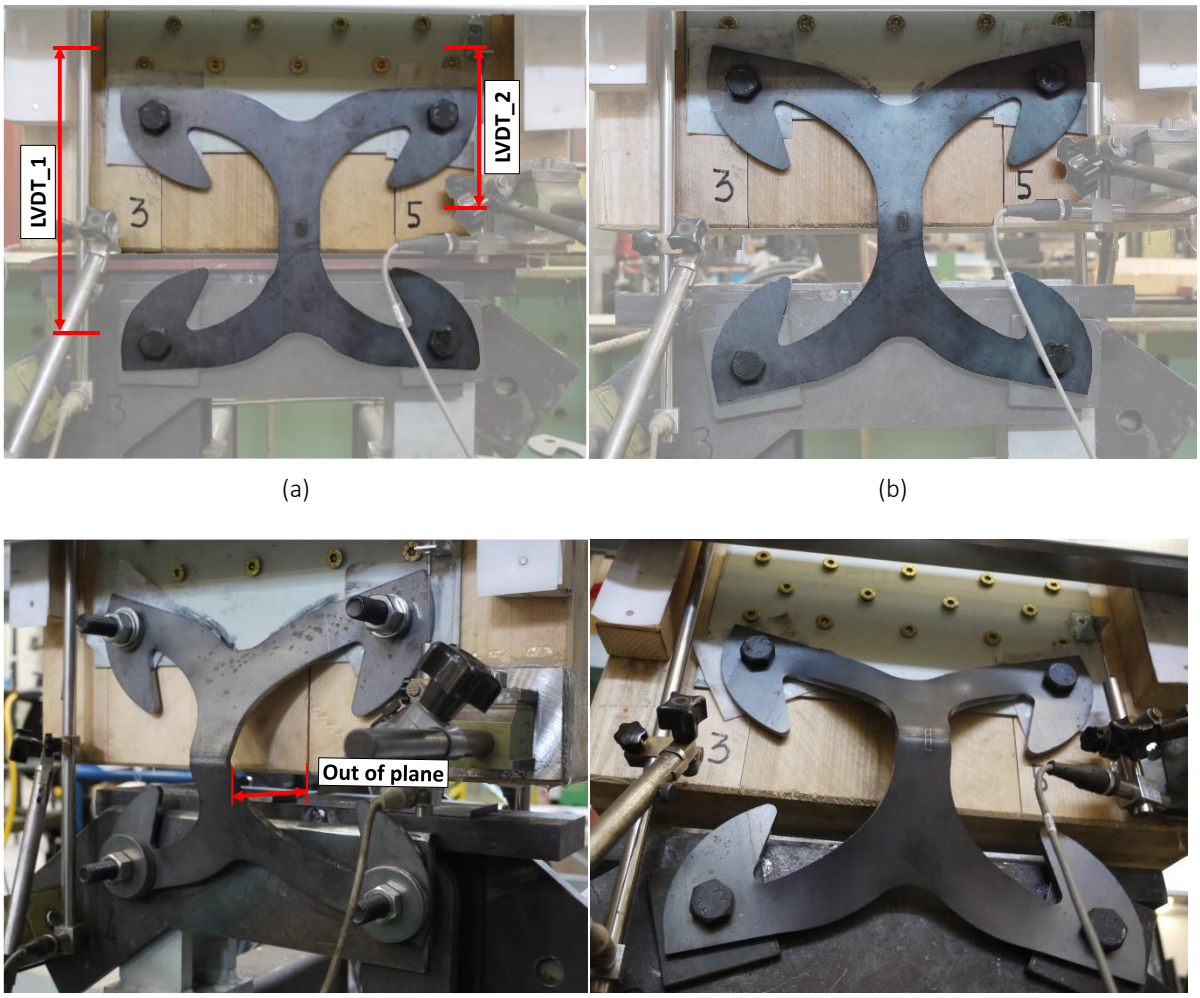

(a) (b)

(c) (d)

Fig. 26. Test of the complete connection: (a) Photo of the non-deformed specimen; (b) Specimen at maximum vertical displacement of 48m; (c,d) Failure in the vertical web

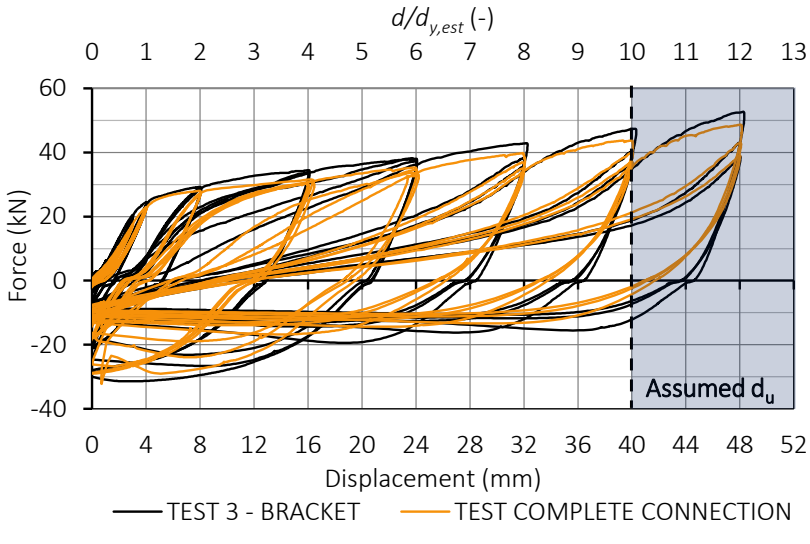

(a)

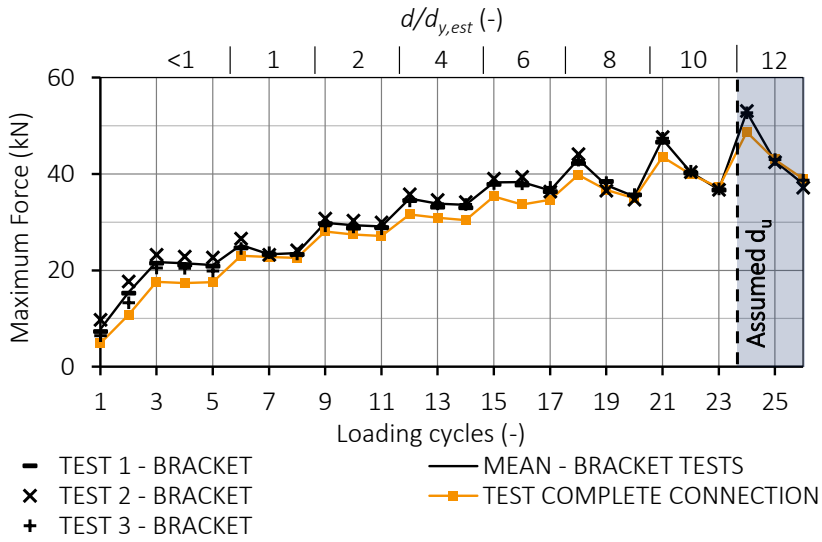

(b)

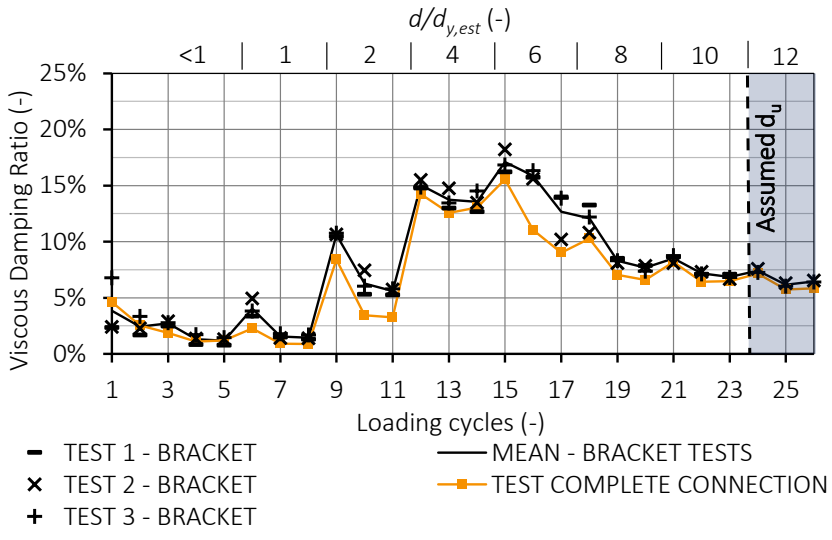

(c)

Fig. 27. Comparison among tests of X-brackets and of the complete connection in tension, $d_{y,est}$ = 4.00 mm: (a) Hysteresis cycles; (b) Maximum force per loading cycle; (c) Equivalent viscous damping. (Scotta et al. 2017)

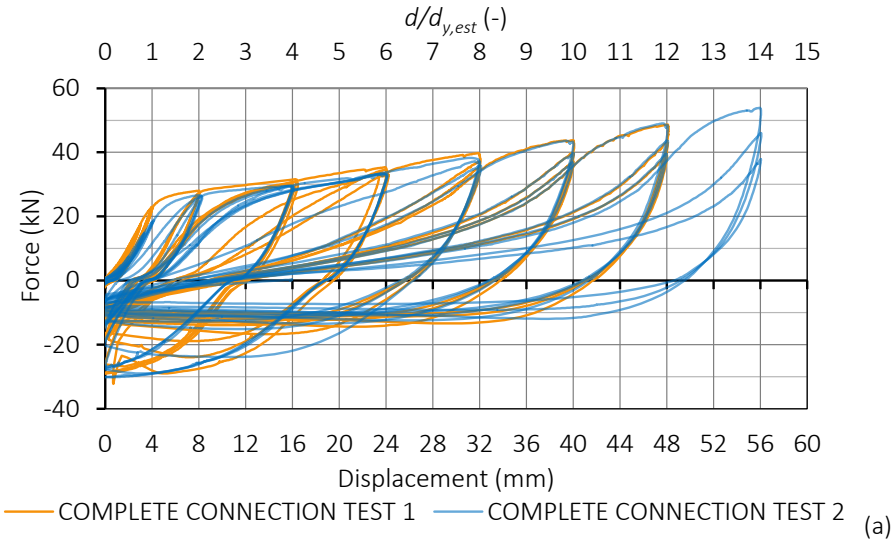

(a)

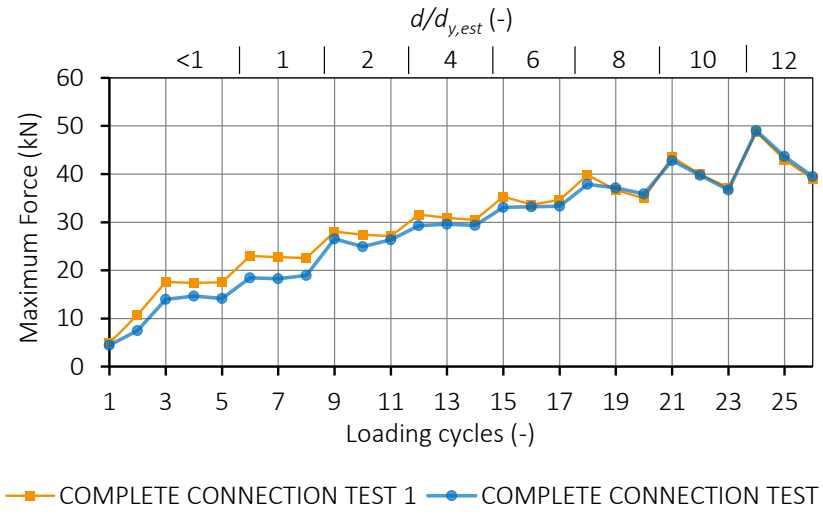

(b)

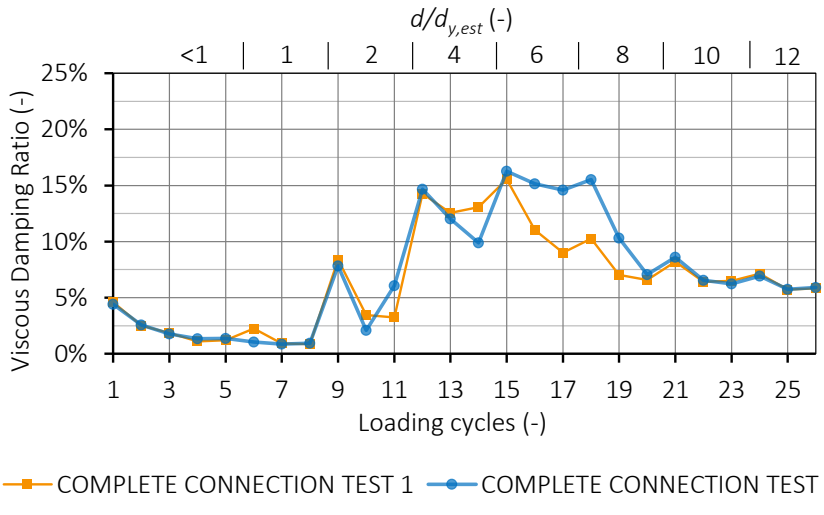

(C)

Fig. 28. Comparison between first and second test of the complete connection in tension, $d_{y,est}$ = 4.00 mm: (a) Hysteresis cycles; (b) Maximum force per loading cycle; (c) Equivalent viscous damping

Table 5. Test results: main mechanical parameters according to EN 12512 (2006) method "a"

Parameter	X-BRACKET MEAN VALUES	COMPLETE CONNECTION TEST 1	COMPLETE CONNECTION TEST 2**
F_y (kN)	28.75	26.17	24.93
d_y (mm)	3.18	4.69	5.77
$F(d_u)$ (kN)	47.17	48.64	53.85
d_u (mm)	40.00*	48.00*	56.00*
k_{el} (kN/mm)	9.04	5.58	4.32
k_{pl} (kN/mm)	0.50	0.57	0.66
μ (d_u) (-)	12.58	10.23	9.70
Ductility Class	H	H	H

* Test stopped before failure

** Same specimen as test 1. Only X-brackets and bolts replaced.

3.3 CONCEALED X-BRACKET TYPE 2

X-bracket type 2 (see Section 2) is the concealed version of the bracket, within a groove in the panel edge. It works with complementary plates obtained directly in the cutting operations (Fig. 6b). In this way, a cylindrical hinge at each fixing point is guaranteed, allowing bending deformation of flanges and rotation around the calibrated bolts. Thickness and curvature radius of the arms were not modified with respect to type 1 bracket. This to maintain unchanged the hysteretic behaviour. Some modifications were applied to the ends of the arms to let them to rotate in contact with the complementary plates. The fastening of this version exploits the same 16mm diameter steel bolts for the main fixings, whereas the complementary plates are to be fastened with self-drilling steel dowels. Position of these dowels was designed with FE simulations in order to find the disposition that better distributes the shear forces among fasteners. Dimensions of the specimens are in Fig. 3b.

3.3.1 Simulations

Numerical FE models were performed to predict the hysteresis behaviour of X-bracket type 2 used as panel-to-panel shear connection or as concealed hold-down. This second option can be obtained using half a bracket welded to a rectangular steel plate, which can be fixed to foundation by means of concrete anchors, see Section 2. Fig. 29 shows the position of the 7mm diameter dowels.

As for type 1, possibility of buckling of the bracket was not neglected in the model, although the CLT panel is supposed to restrain possible out-of-plane deformations. This because, for high amplitude cycles, compression strength perpendicular to the grain of the CLT is not sufficient to avoid partial crushing of the timber boards.

Fig. 30 and Fig. 31 show the numerical predictions of the cyclic behaviour of the X-bracket type 2 used as hold-down. Results for the X-bracket loaded in shear are reported in Fig. 32 and Fig. 33. A comparison with a test of type 1 bracket is also given. It is worth noting that in the model of the X-bracket in tension also a friction

effect (μ = 0.60) in the contact zones between the bracket and the complementary plate was considered, according to the experimental evidence (see Section 3.3.2).

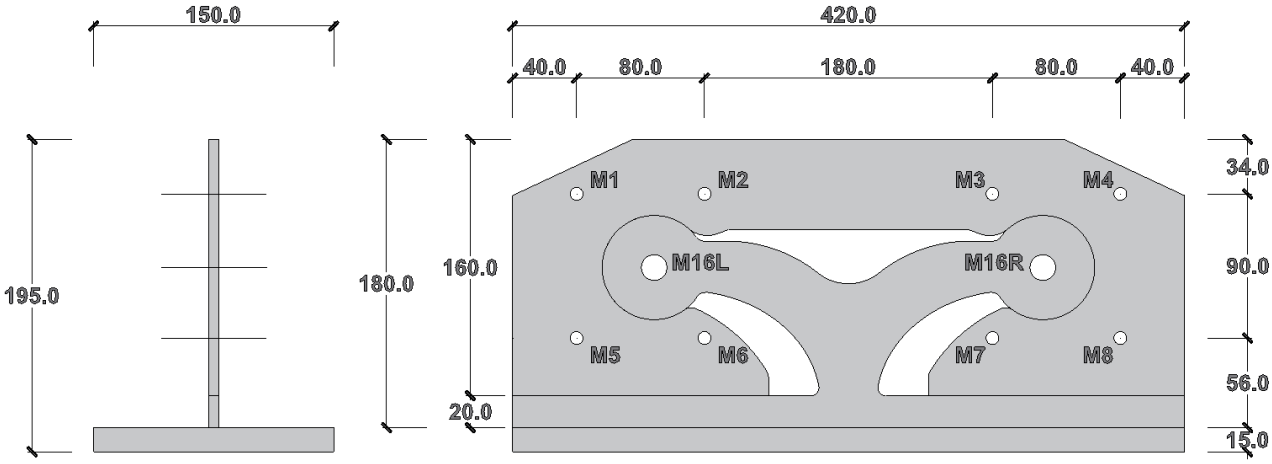

Fig. 29. Dimensions of X-bracket type 2 used as hold-down and position of 7mm diameter self-drilling dowels (M1 to M8) and 16mm diameter dowels

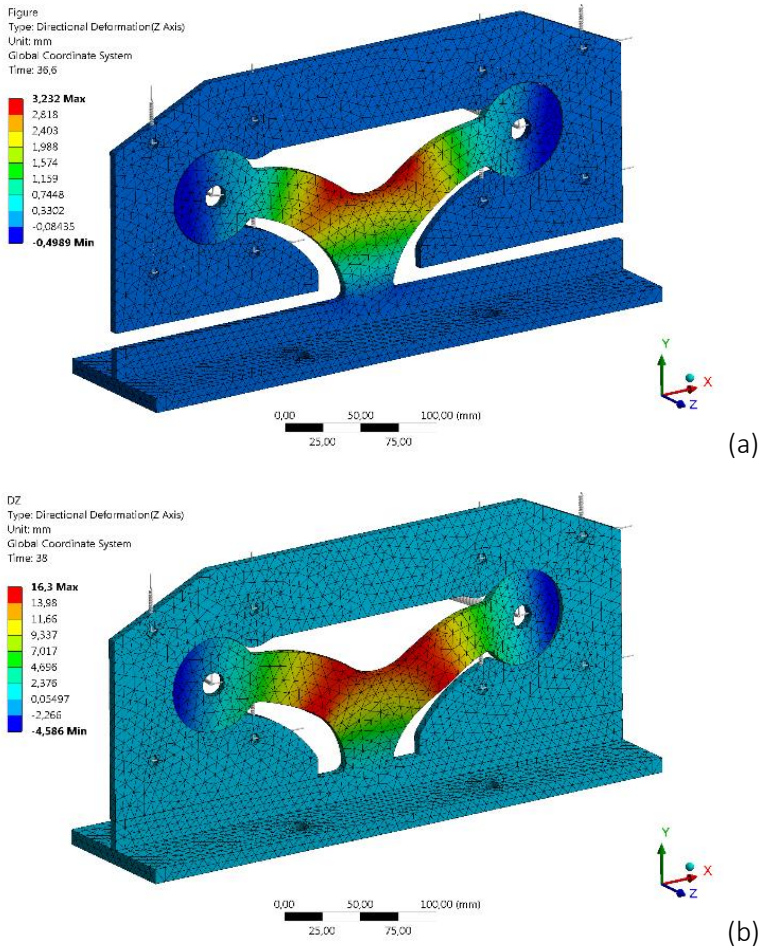

Fig. 30. Out-of-plane deformations of X-bracket type 2 used as hold-downs: (a) At vertical uplift of 20 mm; (b) Residual deformation after the complete cyclic-loading procedure

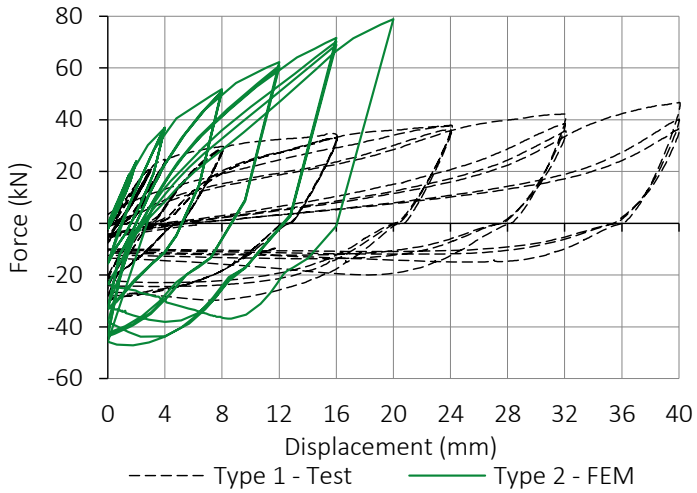

Fig. 31. Results of simulation of X-bracket type 2 in tension as hold-down *vs.* test results of X-bracket type 1 in tension

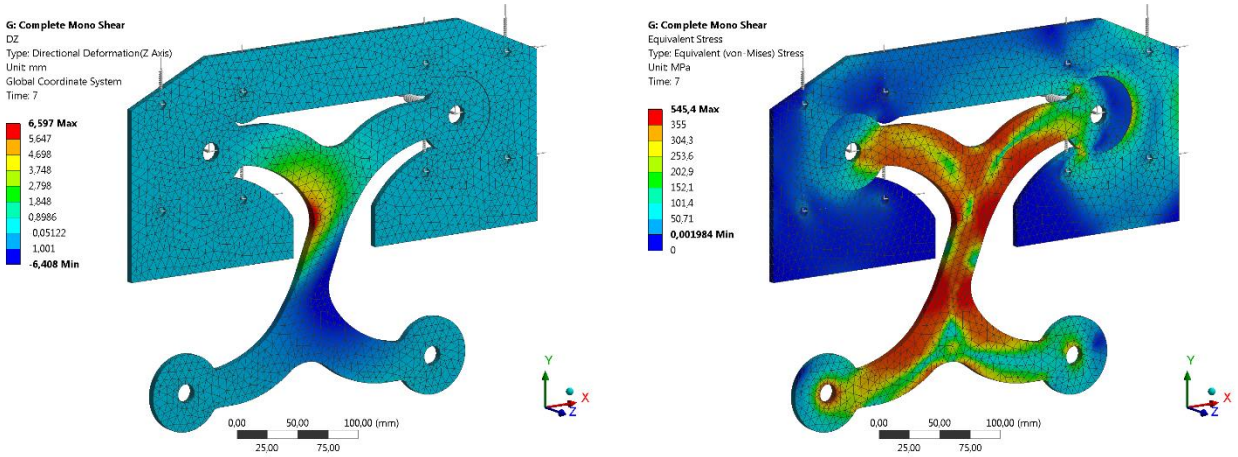

(a) (b)

Fig. 32. Out-of-plane buckling of X-bracket type 2 in shear at 24mm slip: (a) Out-of-plane displacements; (b) Von Mises stress distribution (post-yielding zones in red)

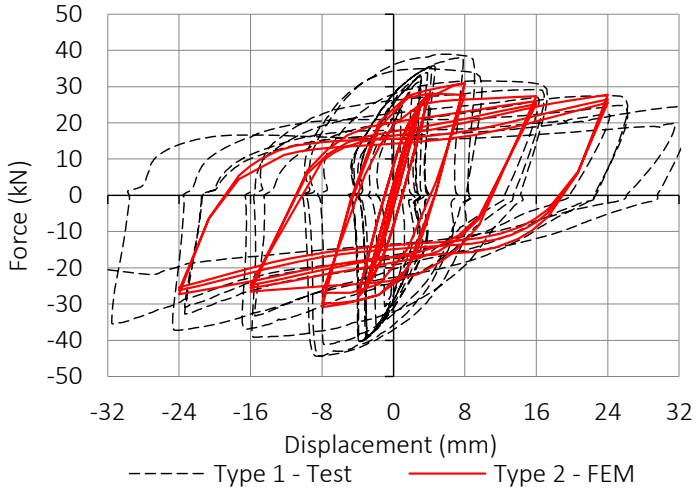

Fig. 33. Results of the numerical simulation of X-bracket type 2 in shear *vs.* test results of X-bracket type 1 in shear

3.3.2 Tests

A special test setup was designed to investigate the behaviour of the X-bracket type 2 as hold-down or shear connection for a panel-to-panel joint (Fig. 34, Fig. 35). In detail:

- For tension tests, a single bracket was anchored to a 5-layer CLT panel with a thickness of 100mm (20-20-20-20-20) and dimensions of 1.0x1.4m. The upper edge of the panel was fixed to a steel beam HEA 140 by means of four 24mm diameter steel rods, welded to an eyebolt mechanism, in order to apply the vertical displacement with a hydraulic actuator. The base plate of the bracket was fixed to the rigid frame with four 16mm diameter steel rods. Two steel profiles with PTFE sheets were placed on each side of the specimen to avoid possible out-of-plane displacements. The vertical uplift of the concealed bracket was monitored with two LVDTs that measured the relative displacement between mid-point of the base steel plate and the CLT panel (see Fig. 36a);
- For shear tests, the same CLT panel used for tension tests was fixed to two CLT rectangular elements, one per side, with one X-bracket type 2 per vertical joint. The lateral panels had the same thickness of the central panel and dimensions of 0.6x1.4m. The same setup of the tension tests was used. The panel-to-panel slip was measured with two LVDTs per bracket, at each side of the panel near the fixing points (see Fig. 36b).

Three tests were performed, two in tension and one in shear. The EN 12512 (2006) cyclic-loading protocol was adopted in all tests imposing a $d_{y,est}$ of 2mm for both shear and tension tests. Fig. 37 shows the obtained force-displacement curves and the comparison with the numerical predictions and Table 6 lists main mechanical parameters. With reference to tension tests (Fig. 37a), the bracket completed successfully all cycles of 20mm amplitude and failed at an uplift of 24 mm due to the accumulated plastic work in the horizontal arms, Fig. 38. No damage was evidenced either in the dowel-type fasteners or in the CLT panel, Fig. 38. Frictional effects were confirmed to be responsible for the higher strength with respect to X-bracket type 1. Moreover, the smaller vertical dimension of the bracket reduced significantly buckling during compression. The shear test (Fig. 37b, Fig. 39) showed a hysteretic response typical of cyclically loaded steel connectors. Failure occurred in the bracket after the 24mm cycles, Fig. 40. An important confinement effect was demonstrated by the CLT panel in limiting to the out-of-plane buckling of the central web.

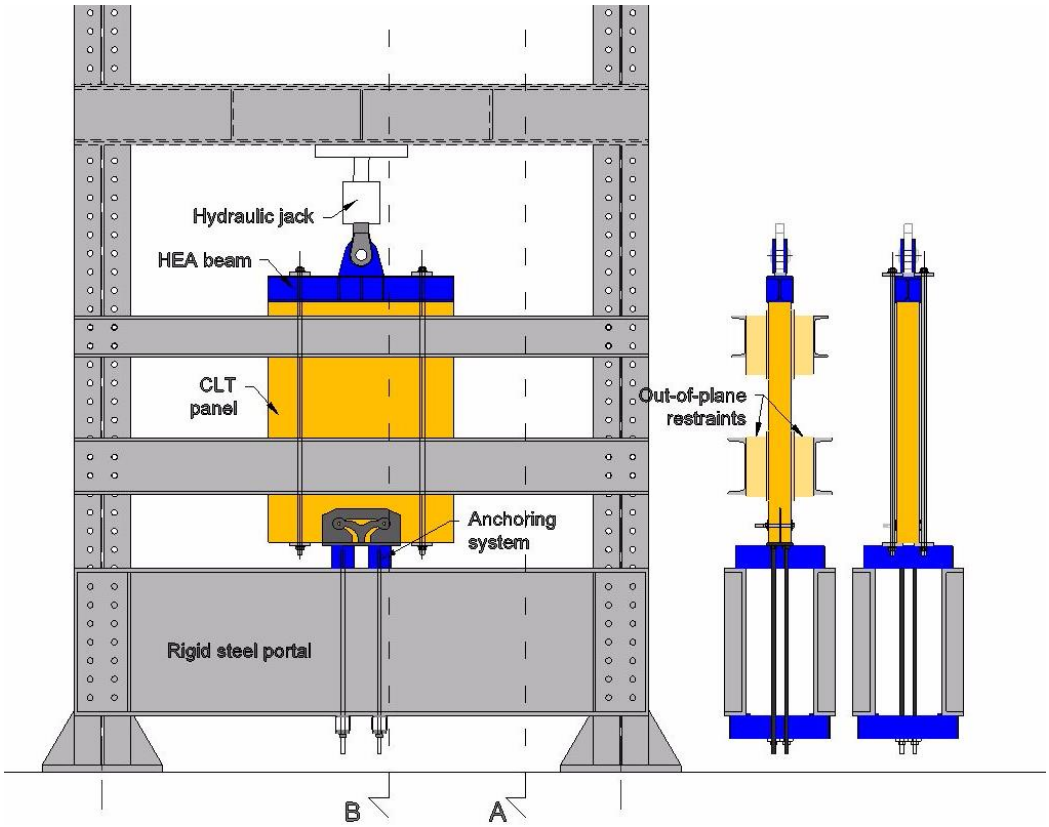

Fig. 34. Test setup for X-bracket type 2 used as hold-down in tension

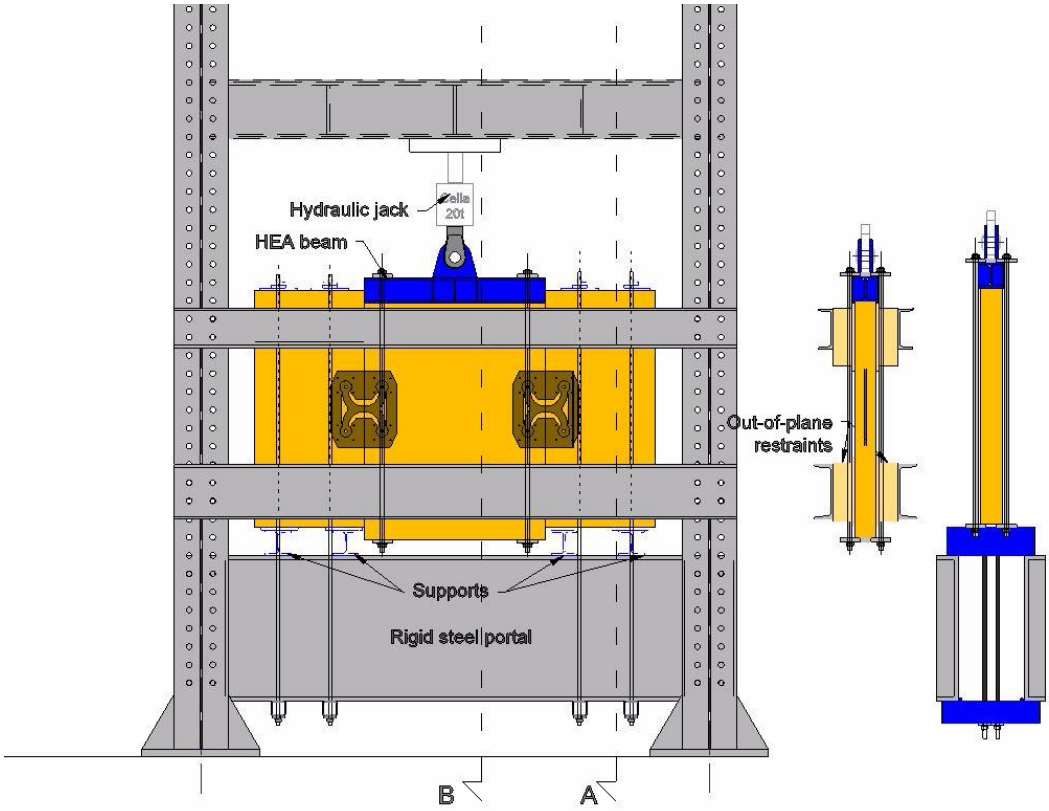

Fig. 35. Test setup for X-bracket type 2 in shear

(a) (b)

Fig. 36. Position of LVDTs: (a) Tension tests; (b) Shear test

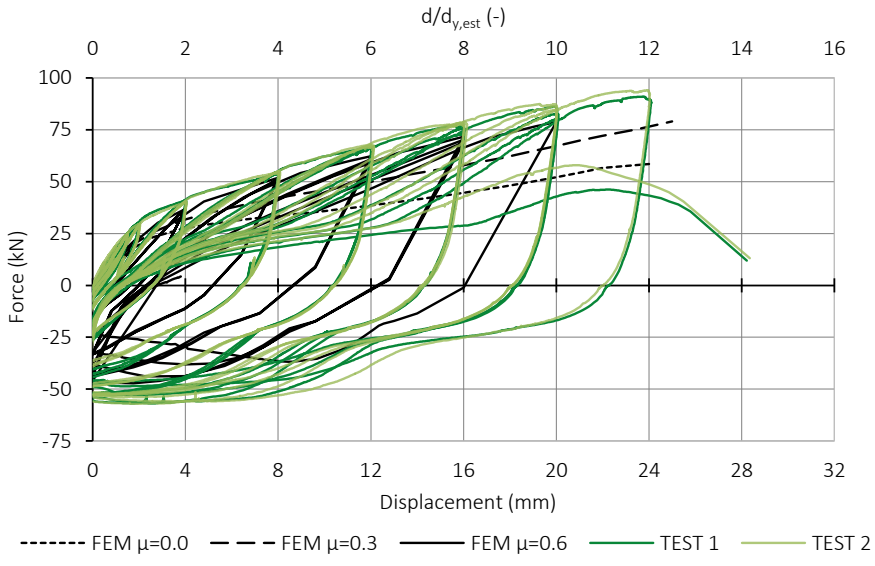

(a)

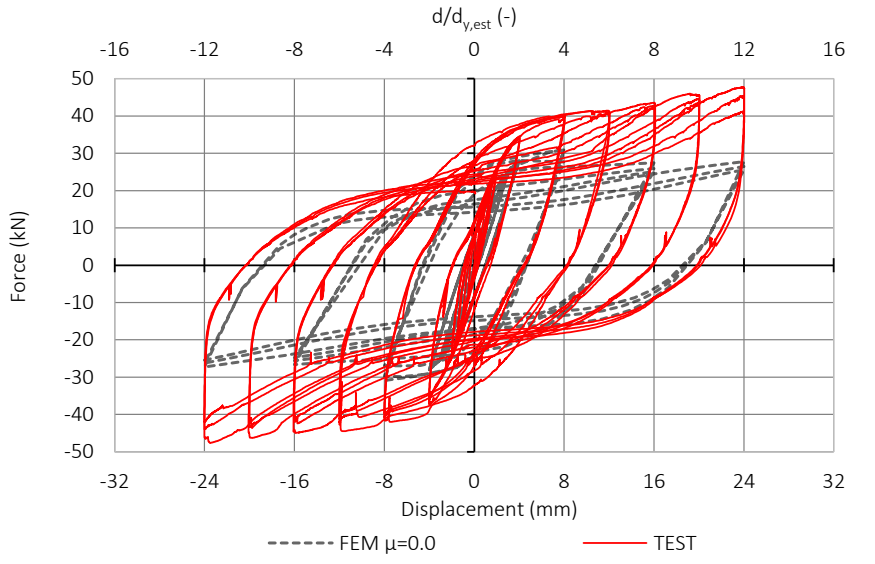

(b)

Fig. 37. Force-displacement curves: (a) Tests in tension; (b) Test in shear

Table 6. Mechanical parameters for X-bracket type 2 according to method "a" of EN12512 (2006)

Parameter	TEST 1 TENSION	TEST 2 TENSION	TEST SHEAR	BILINEAR CURVES
F_y (kN)	37.75	36.64	41.70	
d_y (mm)	1.76	1.71	2.39	
F_{max} (kN)	87.57	88.19	47.50	
d_u (mm)	20.00	20.00	24.00	
k_{el} (kN/mm)	21.43	21.43	17.43	
k_{pl} (kN/mm)	2.22	2.22	0.27	
$\mu(V_u)$ (-)	11.34	11.68	10.03	
Ductility Class	H	H	H	

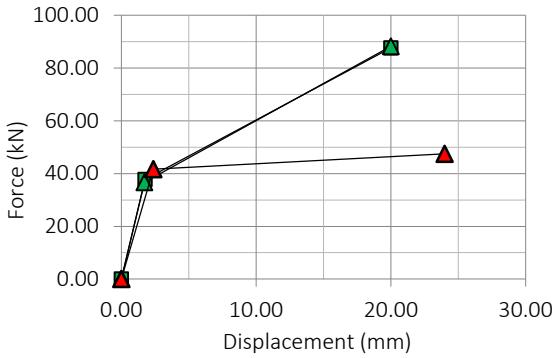

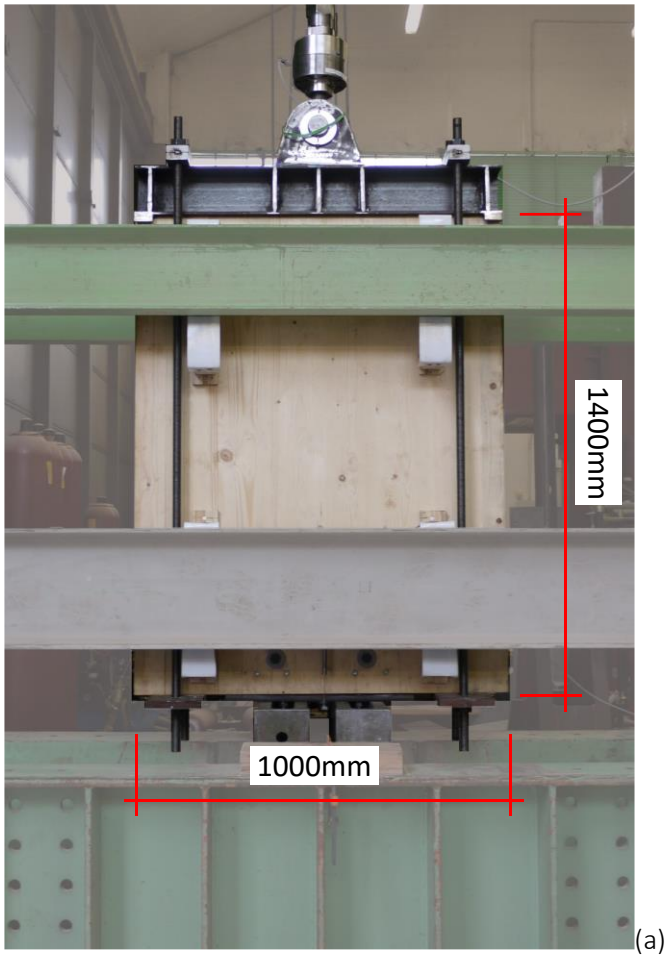

(a)


(b)


(c)


(d)

Fig. 38. Test in tension: (a) Test setup; (b) Specimen at maximum uplift of 24mm; (c) Failure of the X-bracket; (d) Holes in timber panel after test (no evident embedment)

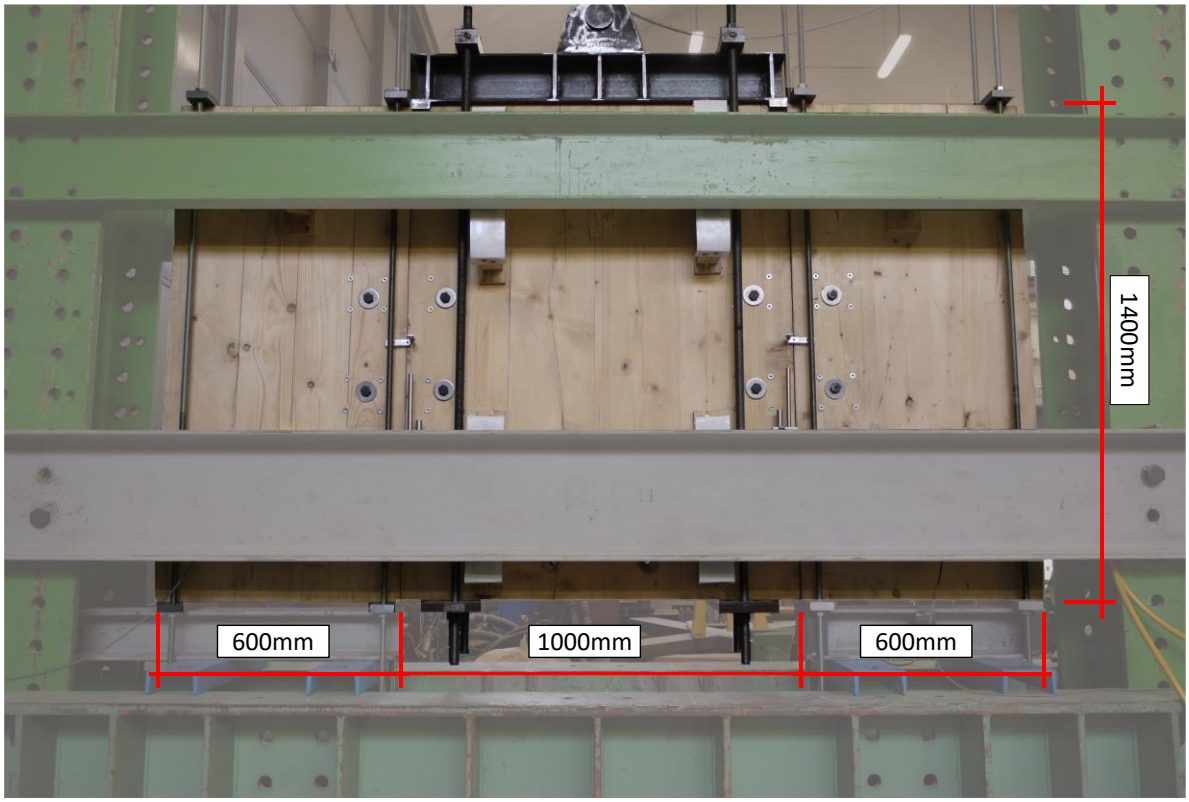

Fig. 39. Setup for test in shear

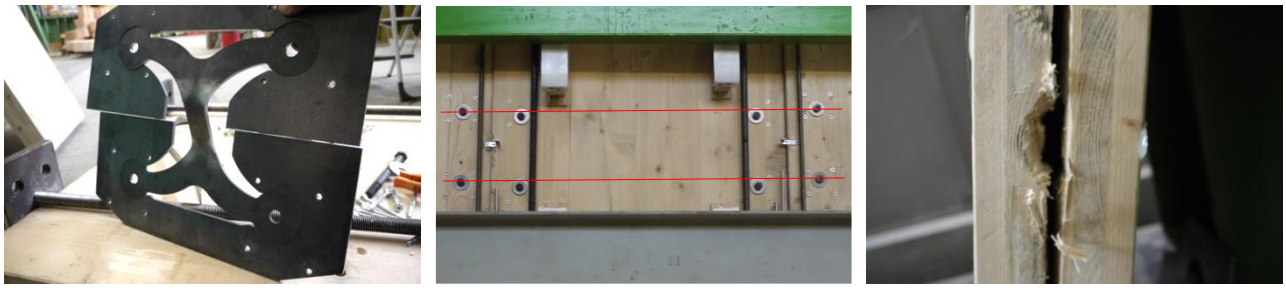

(a) (b) (c)

Fig. 40. Test in shear: (a) Failure of the X-bracket; (b) Specimen at 24mm slip; (c) Damaged inner layers

4. DISCUSSION AND CONCLUSIONS

The experimental and numerical characterization of the X-bracket presented in this Research Report demonstrated many advantages with respect to traditional connections: (1) higher ductility, displacement capacity and dissipative capacity, with equivalent viscous damping ratio approximately double than traditional connections; (2) very low scattering of results and well-defined yielding and failure conditions, resulting in a lower overstrength value and a more reliable application of capacity design; (3) negligible strength degradation and pinching behaviour in its displacement working range.

The two available options of X-bracket demonstrated proper peculiarities:

- *External X-bracket type 1*: does not require any particular woodworking of the CLT panel as it is fixed externally. The buckling of the bracket results in partial pinching phenomenon and consequent reduction of dissipative capacity. However, this phenomenon occurs only for very high displacements. Fire protection has to be addressed as for traditional connections.
- *Concealed X-bracket type 2*: implicitly satisfies the capacity design, using the complementary plates and same fasteners with same position as in tested configurations. Fire protection is guaranteed by the CLT panel. It requires a partial milling of the panel edge.

Other conclusions can be obtained comparing test results (Table 7, Fig. 41, Fig. 42).

The change of steel grade from the first prototype to the type 1 bracket increased the yielding strength for tension loading and shear loading conditions, of about 60% and 40% respectively. With reference to type 2 bracket, although steel was downgraded to an S355 class, the yielding strength in tension increased of an additional 30%, reaching a similar load-bearing capacity of the connection loaded in shear, which on the contrary did not change considerably. This was due to two different effects: 1) the modification of the vertical position of the fixing points with respect to type 1 bracket; 2) the frictional effect between the bracket and the complementary plate produced a considerable strength increment.

The different mechanical response between type 1 and type 2 bracket in terms of equivalent viscous damping ratio υ and the total amount of dissipated energy is shown in Fig. 42.

In Fig. 41a and Fig. 42a,b results of tests in tension are reported in terms of $d/d_{y,est}$ to emphasize better the strength increment obtained with type 2 bracket. For these tests, the calculated equivalent viscous damping at 1st and 3rd cycle is similar up to $d/d_{y,est} = 6$. However, type 2 bracket shows values in the range of 12-15% also for higher displacements ($6 < d/d_{y,est} \leq 10$). Moreover, the reduced pinching phenomenon is confirmed by the reduced losses of viscous damping ratio from the 1st to the 3rd cycle. Typical values of equivalent viscous damping for traditional hold-downs are about 9% (1st cycle) and 3% (third cycle) (Gavric et al. 2015b). Finally, the combination of higher strength and dissipative capacity for type 2 bracket results in an increase of total dissipated energy by the connector of about 54.0%.

With reference to tests in shear, a reduction of the equivalent viscous damping ratio for type 2 bracket was calculated for all the displacement amplitudes, but values are anyway very high if compared to traditional angle brackets (Gavric et al. 2015b, Tomasi and Smith 2015). As for tests in tension, the dissipative capacity of the X-bracket did not vary significantly between the 1st and 3rd cycle.

Table 7. Comparison of the preliminary prototype, type 1 bracket and type 2 bracket (mean values)

	First prototype		Type 1		Type 2*	
Parameter	Tension	Shear	Tension	Shear	Tension**	Shear ***
Steel class	S275JR		S450JR		S355JR	
Dimensions a x b (mm x mm)	303 x 233		303 x 233		308 x 265	
Spacing of fixings (mm x mm)	237 x 180		243 x 185		243 x 200	
F_y (kN)	17.97	28.09	28.75	39.50	37.19	41.70
d_y (mm)	1.96	3.46	3.18	1.25	1.74	2.39
F_{max} (kN)	37.76	29.03	47.17	43.95	87.88	47.50
d_u (mm)	46.20	50.00	40.00	24.00	20.00	24.00
k_{el} (kN/mm)	9.17	8.53	9.04	31.55	21.43	17.43
k_{pl} (kN/mm)	0.45	-	0.50	-	2.22	0.27
μ (d_u) (-)	23.57	14.45	12.58	23.43	11.51	10.03
Ductility Class	H	H	H	H	H	H

* Tests performed including complementary plates; ** Half bracket; *** One test

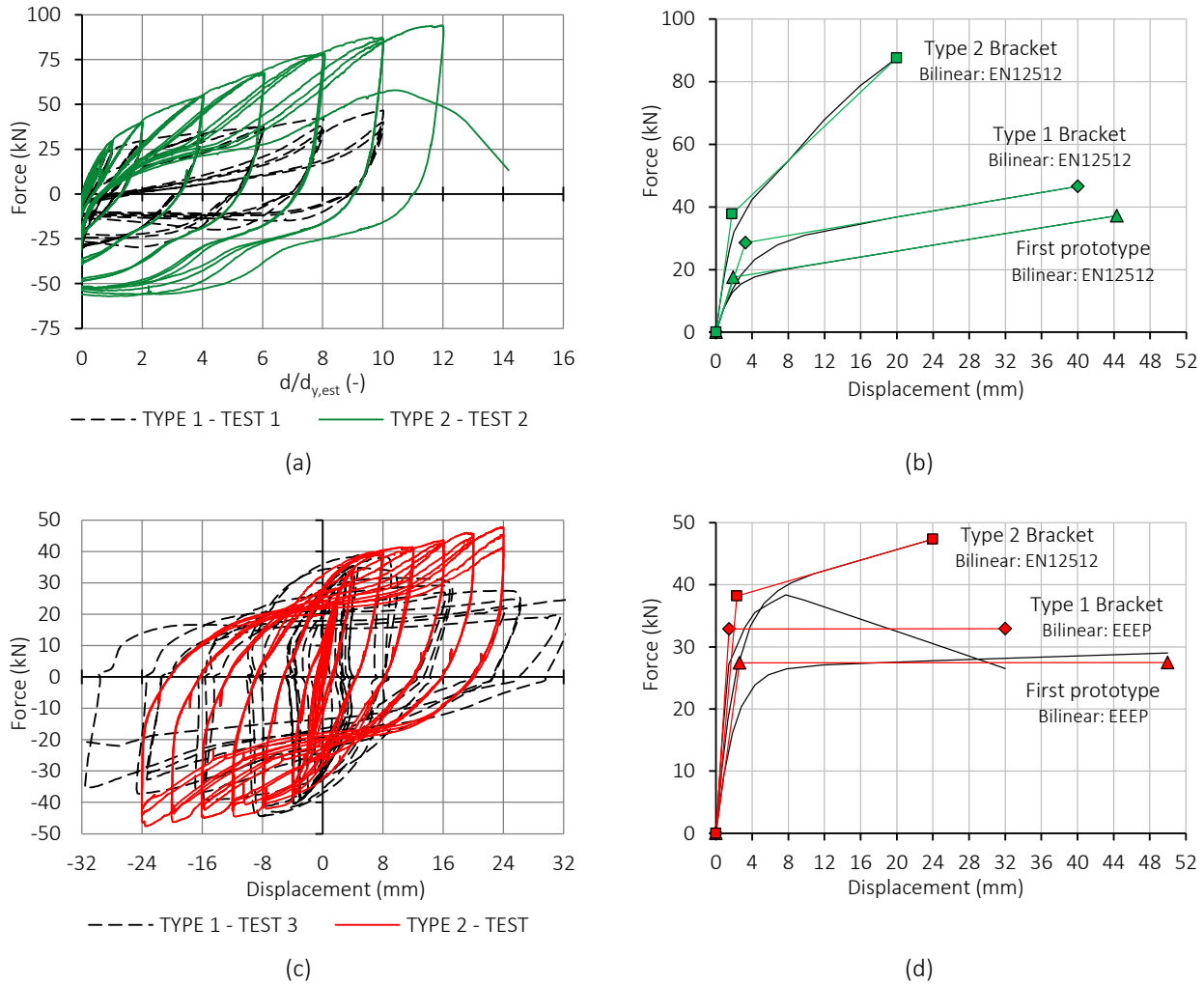

Fig. 41. Comparison of force-displacement cycles, envelope and bilinear curves for tests in tension (a,b) and shear (c,d)

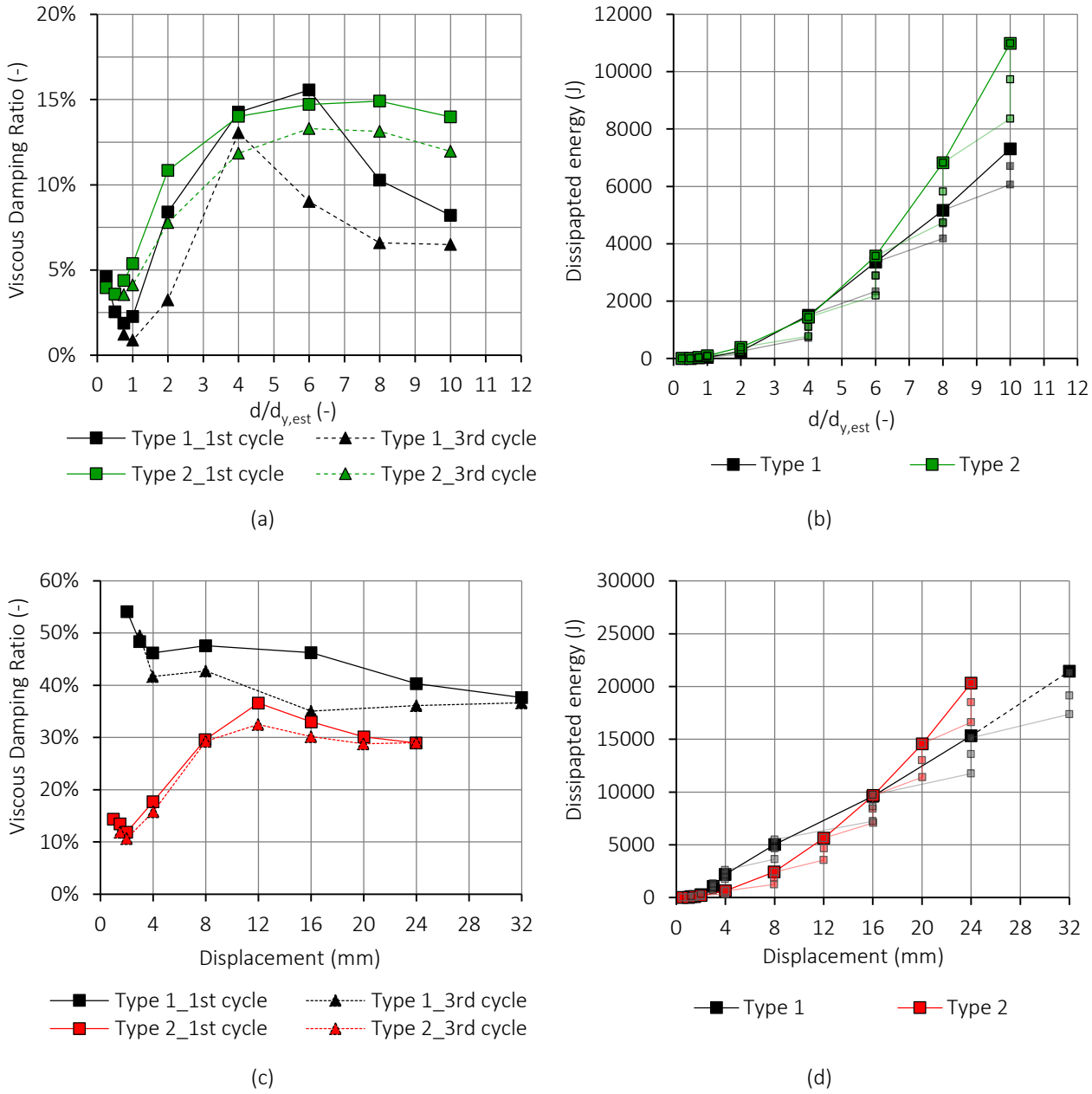

Fig. 42. Viscous damping ratio and dissipated energy for the X-brackets loaded in tension (a,b) and in shear (c,d)

5. ACKNOWLEDGEMENTS

Economical support from “Proof of Concept Network” (PoCN) project, organized and managed by AREA Science Park (Trieste-Italy), financed by MIUR within "Progetti Premiali 2011" action, is acknowledged. Title of the specific project: “foundation system for timber and lightweight structures - ref. UNIPD_03”.

Grateful thanks go to the staff of the Mechanical Testing Laboratory of Department ICEA of the University of Padova for their support during experimentation.

6. REFERENCES

Baird A, Smith T, Palermo A, Pampanin S (2014) Experimental and numerical study of U-shape flexural plate (UFP) dissipators. In New Zealand Society for Earthq Eng Conf, Auckland, New Zealand

Blass HJ, Schmid M, Litze H, Wagner B (2000) Nail plate reinforced joints with dowel-type fasteners. Proceedings of the World Conference on Timber Engineering (WCTE), Whistler, Canada

Ceccotti A (2008) New technologies for construction of medium-rise buildings in seismic regions: the XLAM case. Struct Eng Int 18(2):156-165

Ceccotti A, Sandhaas C, Okabe M, Yasumura M, Minowa C, Kawai N (2013) SOFIE project – 3D shaking table test on a seven-storey full-scale cross-laminated timber building. Earthquake Engng Struct Dyn 42(13):2003-2021

EN 10025-2 (2004) Hot rolled products of structural steels. Technical delivery conditions for non-alloy structural steels. CEN, Brussels

EN 12512 (2006) Timber Structures. Test Methods. Cyclic Testing of Joints Made with Mechanical Fasteners. CEN, Brussels

EN 14358 (2016) Timber structures — Calculation and verification of characteristic values. CEN, Brussels

EN 1990 (2010) Eurocode - Basis of structural design. CEN, Brussels

EN 1993-1-1 (2014) Eurocode 3: Design of steel structures - Part 1-1: General rules and rules for buildings. CEN, Brussels

EN 1995-1-1 (2014) Eurocode 5: Design of timber structures, Part 1-1, General: Common rules and rules for buildings. CEN, Brussels

EN 1998-1 (2013) Eurocode 8: Design of structures for earthquake resistance, Part 1: General rules, seismic actions and rules for buildings. CEN, Brussels

EN ISO 6892-1 (2016) Metallic Materials - Tensile Testing - Part 1: Method of Test at Room Temperature. CEN, Brussels

ETA-11/0027 (2016) Screws for use in timber constructions, ETA-Danmark A/S, Denmark

Flatscher G, Schickhofer G (2015) Shaking-table test of a cross-laminated timber structure. P I Civil Eng Str B 168(11):878-888

Foliente GC (1996) Issues in seismic performance testing and evaluation of timber structural systems. Proceedings of the 1996 International Wood Engineering Conference, New Orleans, USA, 1:29-36

Follesa M, Fragiacomo M, Casagrande D, Tomasi R, Piazza M, Vassallo D, Rossi S (2016) The new version of Chapter 8 of Eurocode 8. Proceedings of the World Conference on Timber Engineering (WCTE), Wien, Austria

Follesa M, Fragiacomo M, Vassallo D, Piazza M, Tomasi R, Rossi S, Casagrande D (2015) A proposal for a new Background Document of Chapter 8 of Eurocode 8. Proceedings of the 2nd International Network on Timber Engineering Research (INTER), Šibenik, Croatia

Foschi RO, Bonac T (1977) Load slip characteristic for connections with common nails. Wood Sci Technol 9:118–123

Fragiacomo M, Dujic B, Sustersic I (2011) Elastic and ductile design of multi-storey crosslam massive wooden buildings under seismic actions. Eng Struct 33(11):3043-3053

Gavric I, Fragiacomo M, Ceccotti A (2013) Capacity seismic design of X-LAM wall systems based on connection mechanical properties. CIB-W18 Meeting 46, Vancouver, Canada

Gavric I, Fragiacomo, M, Ceccotti A (2015a) Cyclic behavior of typical screwed connections for cross-laminated (CLT) structures. Eur J Wood Prod 73(2):179-191

Gavric I, Fragiacomo, M, Ceccotti A (2015b) Cyclic behaviour of typical metal connectors for cross-laminated (CLT) structures. Mat Struct 48:1841-1857

Hashemi A, Zarnani P, Masoudnia R, Quenneville P (2017) Seismic resistant rocking coupled walls with innovative Resilient Slip Friction (RSF) joints. Journal of Constructional Steel Research 129:215-226

Henry RS, Aaleti S, Sritharan S, Ingham JM (2010) Concept and finite-element modeling of new steel shear connectors for self-centering wall systems. Jour Eng Mech 136(2):220-229

Izzi M, Flatscher G, Fragiacomo M, Schickhofer G (2016) Experimental investigations and design provisions of steel-to-timber joints with annular-ringed shank nails for Cross-Laminated Timber structures. Constr Build Mat 122:446-457

Johansen KW (1949) Theory of timber connections. Int Assoc Bridge and Struct Eng 9:249-262

Jorissen A, Fragiacomo M (2011) General notes on ductility in timber structures. Eng Struct 33(11):2987-2997

Kelly JM, Skinner RI, Heine AJ (1972) Mechanisms of energy absorption in special devices for use in earthquake resistant structures. Bull of the New Zealand Society for Earthq Eng 5(3):63-73

Kramer A, Barbosa AR, Sinha A (2016) Performance of steel energy dissipators connected to cross-laminated timber wall panels subjected to tension and cyclic loading. Journal of Structural Engineering 142(4):E4015013

Latour M, Rizzano G (2015) Cyclic Behavior and Modeling of a Dissipative Connector for Cross-Laminated Timber Panel Buildings. J Earthq Eng 19(1):137-171

Loo WY, Kun C, Quenneville P, Chouw N (2014) Experimental testing of a rocking timber shear wall with slip-friction connectors. Earthq Eng Struct Dyn 43(11):1621-1639

Marchi L, Trutalli D, Scotta R, Pozza L, Ceccotti A (2016) A new dissipative connection for CLT buildings. In Structures and Architectures: Beyond their Limits 17:169–177

Marchi L, Trutalli D, Scotta R, Pozza L (2017) Numerical simulation of the coupled tension-shear response of an innovative dissipative connection for CLT buildings. In proceedings of the 6th ECCOMAS Thematic Conference on Computational Methods in Structural Dynamics and Earthquake Engineering (COMPDYN), 15-17 June 2017, Rhodes Island, Greece. DOI: 10.7712/120117

Ottenhaus LM, Li M, Smith T, Quenneville P (2018) Overstrength of dowelled CLT connections under monotonic and cyclic loading. Bull Earthq Eng 16(2):753-773

Palermo A, Pampanin S, Buchanan AH (2006) Experimental investigations on LVL seismic resistant wall and frame subassemblies. Proceedings of the 1st European conference on earthquake engineering and seismology ECEES, Geneva, Switzerland, 3-8 September 2006

Paulay T, Priestley MJN (1992) Seismic design of reinforced concrete and masonry buildings. Wiley, New York

Polastri A, Giongo I, Piazza M (2017) An Innovative Connection System for Cross-Laminated Timber Structures. Structural Engineering International 27(4):502-511

Pozza L, Scotta R (2015) Influence of wall assembly on behaviour of cross-laminated timber buildings. Proceedings of the Institution of Civil Engineers - Structures and Buildings 168(4):275-286. DOI: 10.1680/stbu.13.00081

Pozza L, Scotta R, Trutalli D, Polastri A (2015) Behaviour factor for innovative massive timber shear walls. Bulletin of Earthquake Engineering 13(11):3449-3469. DOI: 10.1007/s10518-015-9765-7

Pozza L, Scotta R, Trutalli D, Polastri A, Smith I (2016) Experimentally based q-factor estimation of cross-laminated timber walls. Proceedings of the Institution of Civil Engineers - Structures and Buildings 169(7):492-507. DOI: 10.1680/jstbu.15.00009

Pozza L, Trutalli D (2017) An analytical formulation of q-factor for mid-rise CLT buildings based on parametric numerical analyses. Bulletin of Earthquake Engineering 15(5):2015–2033. DOI: 10.1007/s10518-016-0047-9

Priestley MJN, Sritharan S, Conley JR, Pampanin S (1999) Preliminary results and conclusions from the PRESSS five-story precast concrete test building. PCI journal 44(6):42-67

Sarti F, Palermo A, Pampanin S (2016) Quasi-static cyclic testing of two-thirds scale unbonded posttensioned rocking dissipative timber walls. Journal of Structural Engineering 142(4),E4015005

Schmidt T, Blass HJ (2017) Dissipative joints for CLT shear walls. Proceedings of the 4th International Network on Timber Engineering Research (INTER), Kyoto, Japan

Scotta R, Pozza L, Trutalli D, Marchi L, Ceccotti A (2015) Dissipative connections for squat or scarcely jointed CLT buildings. Experimental tests and numerical validation. In proceedings of International Network on Timber Engineering Research (INTER), meeting 48, 24-27 August 2015, Šibenik, Croatia

Scotta R, Marchi L, Trutalli D, Pozza L (2016) A dissipative connector for CLT buildings: concept, design and testing. Materials 9(3):139. DOI:10.3390/ma9030139

Scotta R, Trutalli D, Marchi L, Pozza L, Ceccotti A (2017) Capacity design of CLT structures with traditional or innovative seismic-resistant brackets. In proceedings of International Network on Timber Engineering Research (INTER), meeting 50, 28-31 August 2017, Kyoto, Japan

Sustersic I, Fragiacomo M, Dujic B (2011) Influence of connection properties on the ductility and seismic resistance of multi-storey cross-lam buildings. CIB-W18 Meeting 44, Alghero, Italy

Tomasi R, Smith I (2015) Experimental characterization of monotonic and cyclic loading responses of CLT panel-to-foundation angle bracket connections. J Mater Civ Eng 27(6):04014189

Trutalli D, Pozza L (2018) Seismic design of floor–wall joints of multi-storey CLT buildings to comply with regularity in elevation. Bulletin of Earthquake Engineering 16(1):183-201. DOI: 10.1007/s10518-017-0193-8

APPENDIX A: Analysis of results of all performed tests of X-bracket type 1 and 2

X-BRAKET TYPE 1 – TENSION – TEST 1

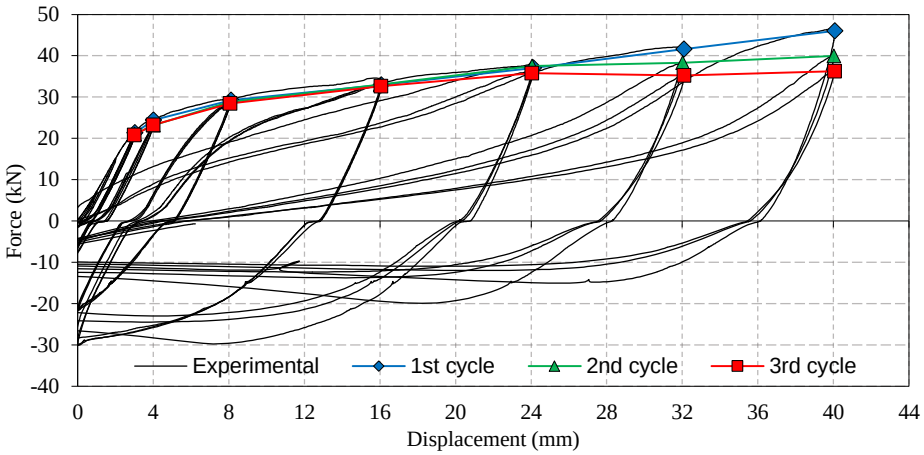

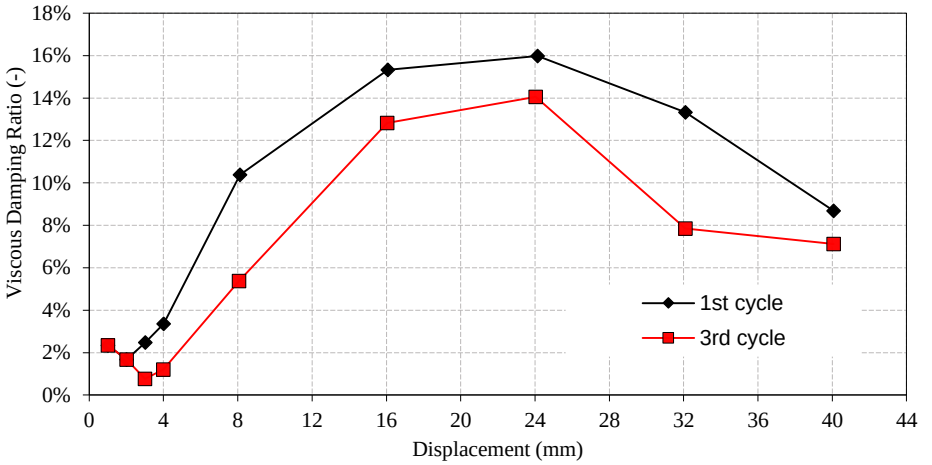

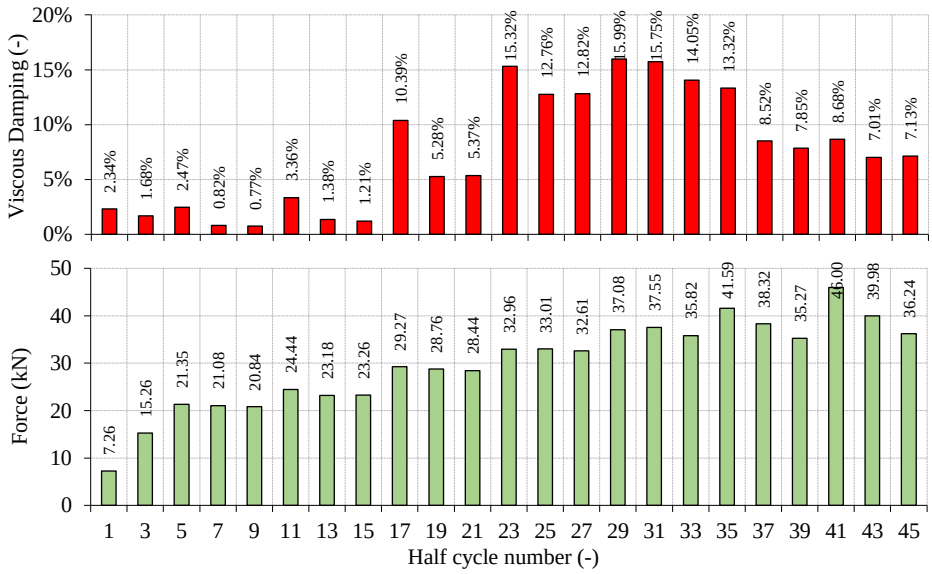

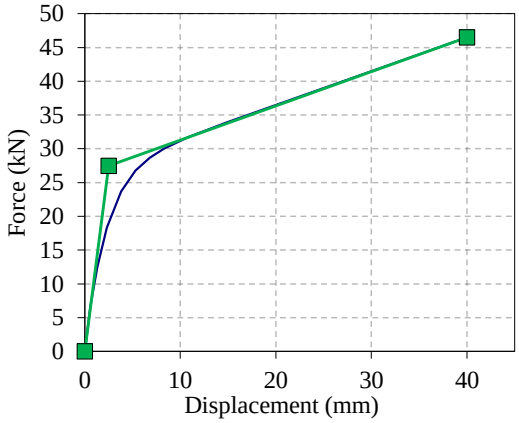

Equivalent bi-linear system according to EN12512 method (a)			
Yielding force	F_y	27.50	(kN)
Yielding displacement	d_y	2.50	(mm)
Ultimate force	F_u	46.50	(kN)
Ultimate displacement	d_u	40.00	(mm)
Maximum Force	F_{max}	46.50	(kN)
Elastic stiffness	k_{el}	11.01	(kN/mm)
Hardening stiffness	k_{pl}	0.51	(kN/mm)
Ductility ratio	μ (d_u)	16.02	-
Ductility	Class	H	-

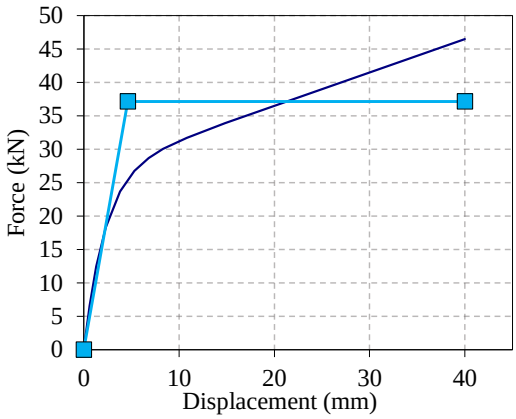

Equivalent bi-linear system according to EEEP method			
Yielding force	F_y	37.11	(kN)
Yielding displacement	d_y	4.59	(mm)
Ultimate force	F_u	46.50	(kN)
Ultimate displacement	d_u	40.00	(mm)
Maximum Force	F_{max}	46.50	(kN)
Elastic stiffness	k_{el}	8.09	(kN/mm)
Hardening stiffness	k_{pl}	0.00	(kN/mm)
Ductility ratio	μ (d_u)	8.72	-
Ductility	Class	H	-

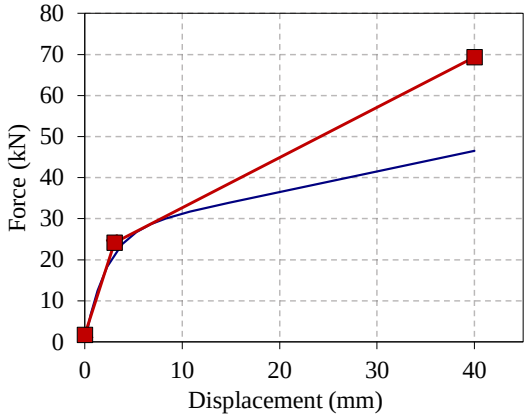

Equivalent bi-linear system according to EN12512 method (b)			
Yielding force	F_y	24.16	(kN)
Yielding displacement	d_y	3.06	(mm)
Ultimate force	F_u	46.50	(kN)
Ultimate displacement	d_u	40.00	(mm)
Maximum Force	F_{max}	46.50	(kN)
Elastic stiffness	k_{el}	7.34	(kN/mm)
Hardening stiffness	k_{pl}	1.22	(kN/mm)
Ductility ratio	μ (d_u)	13.08	-
Ductility	Class	H	-

X-BRAKET TYPE 1 – TENSION – TEST 2

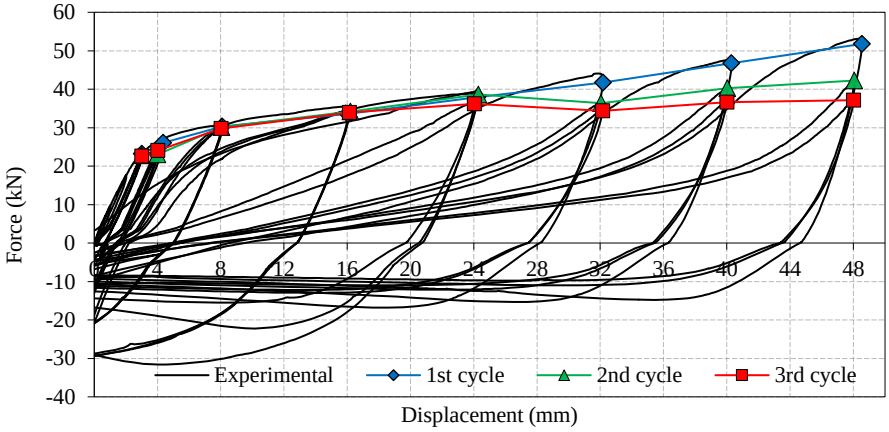

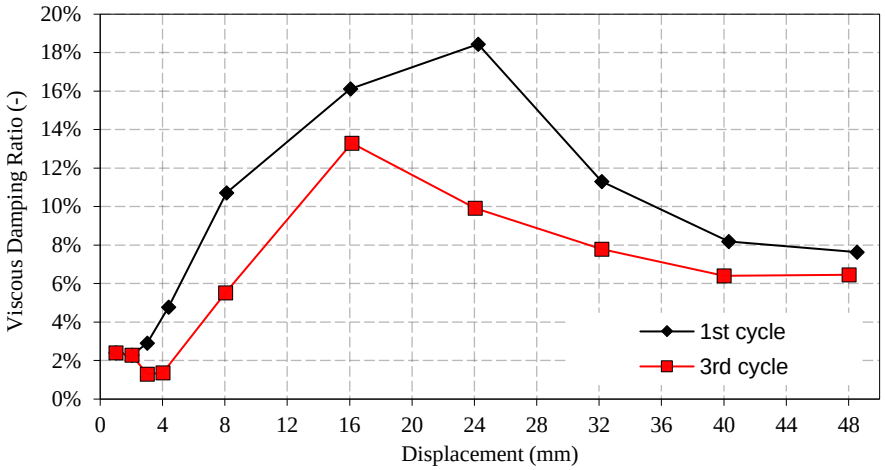

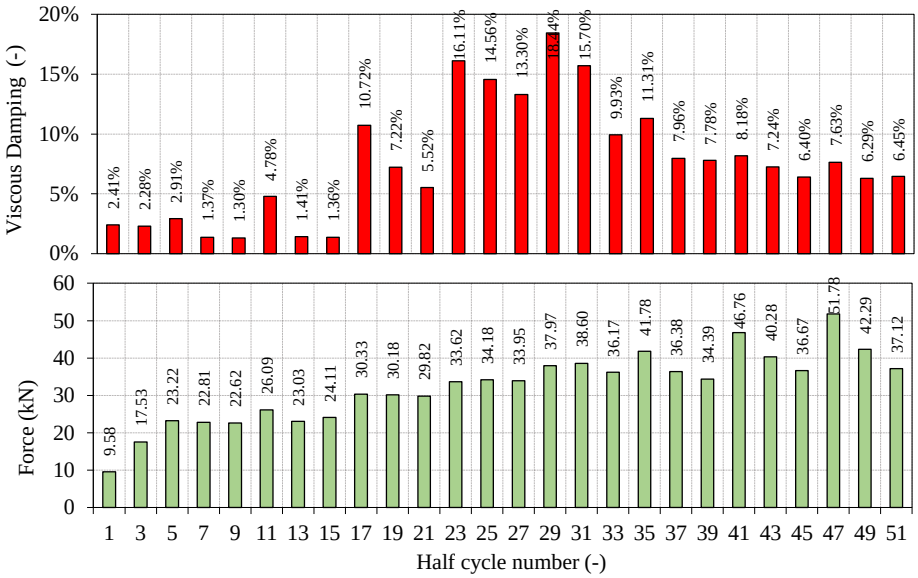

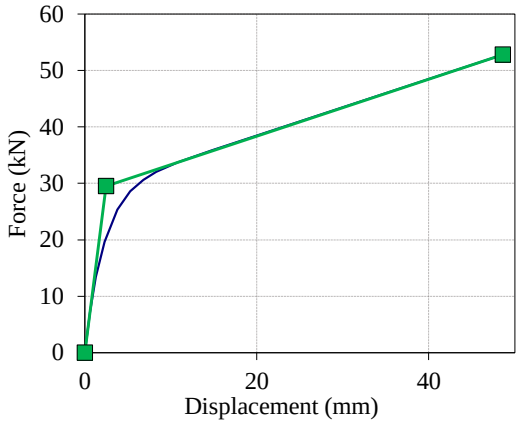

Equivalent bi-linear system according to EN12512 method (a)			
Yielding force	F_y	29.49	(kN)
Yielding displacement	d_y	2.48	(mm)
Ultimate force	F_u	52.80	(kN)
Ultimate displacement	d_u	48.60	(mm)
Maximum Force	F_{max}	52.80	(kN)
Elastic stiffness	k_{el}	11.87	(kN/mm)
Hardening stiffness	k_{pl}	0.51	(kN/mm)
Ductility ratio	μ (d_u)	19.57	-
Ductility	Class	H	-

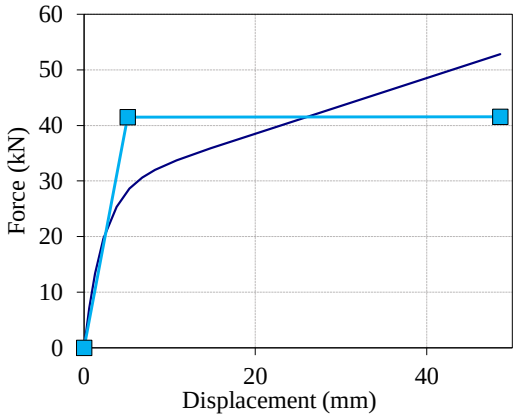

Equivalent bi-linear system according to EEEP method			
Yielding force	F_y	41.49	(kN)
Yielding displacement	d_y	5.11	(mm)
Ultimate force	F_u	52.80	(kN)
Ultimate displacement	d_u	48.60	(mm)
Maximum Force	F_{max}	52.80	(kN)
Elastic stiffness	k_{el}	8.12	(kN/mm)
Hardening stiffness	k_{pl}	0.00	(kN/mm)
Ductility ratio	μ (d_u)	9.51	-
Ductility	Class	H	-

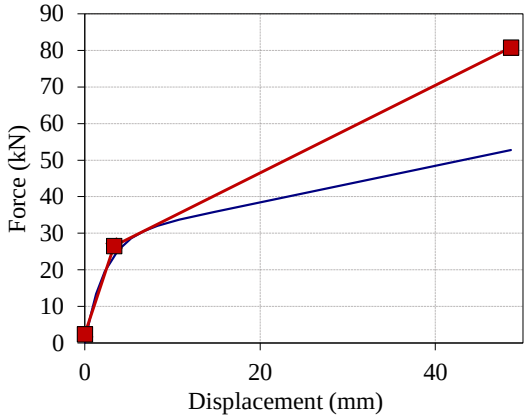

Equivalent bi-linear system according to EN12512 method (b)			
Yielding force	F_y	26.51	(kN)
Yielding displacement	d_y	3.35	(mm)
Ultimate force	F_u	52.80	(kN)
Ultimate displacement	d_u	48.60	(mm)
Maximum Force	F_{max}	52.80	(kN)
Elastic stiffness	k_{el}	7.20	(kN/mm)
Hardening stiffness	k_{pl}	1.20	(kN/mm)
Ductility ratio	μ (d_u)	14.52	-
Ductility	Class	H	-

X-BRAKET TYPE 1 – TENSION – TEST 3

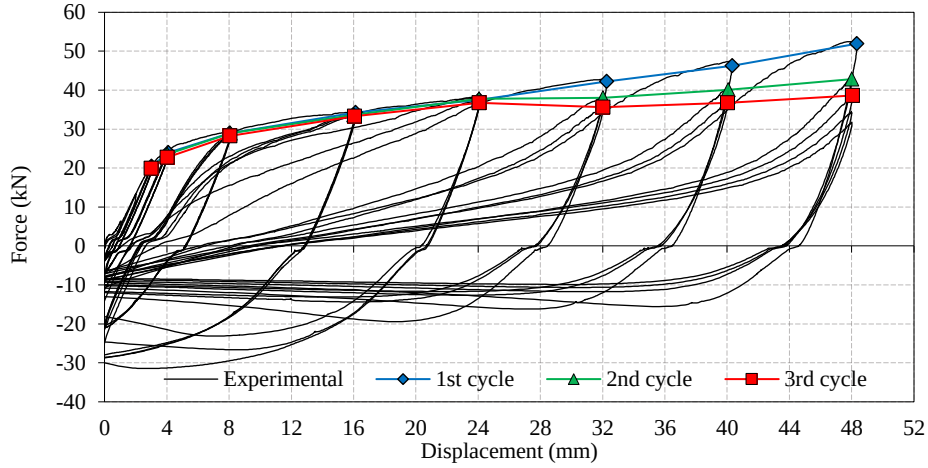

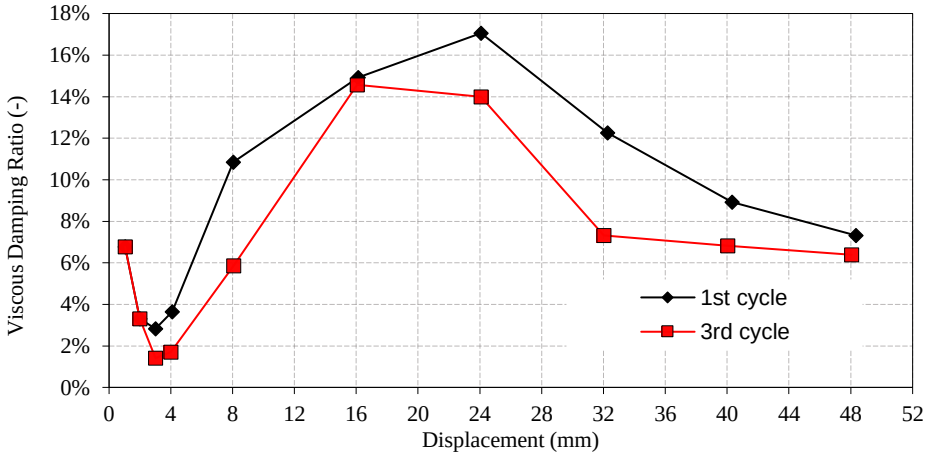

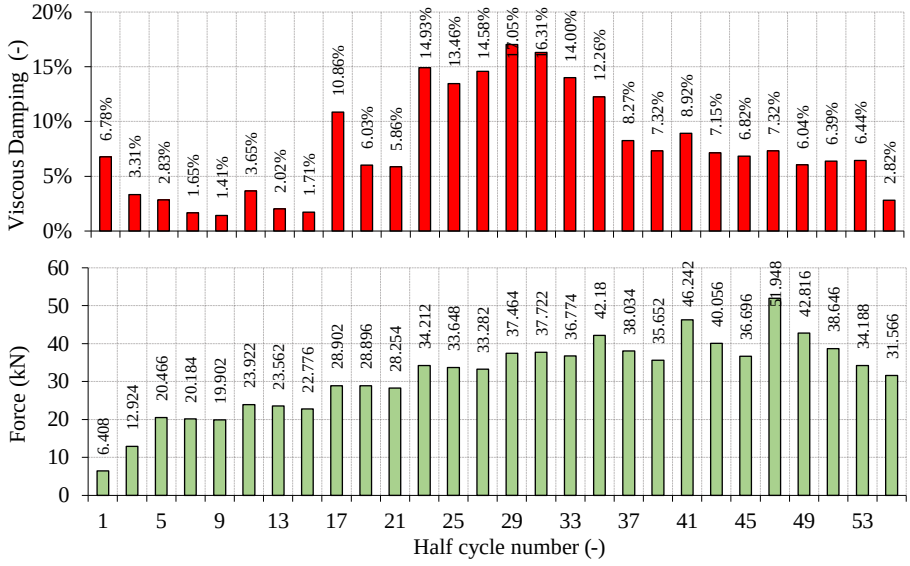

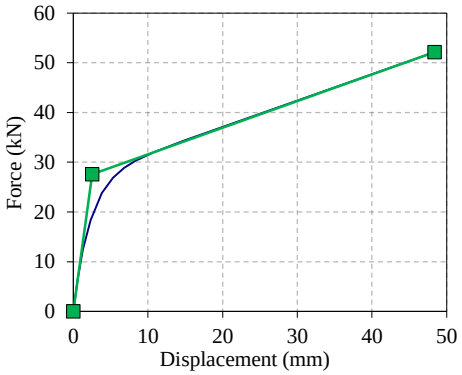

Equivalent bi-linear system according to EN12512 method (a)			
Yielding force	F_y	27.59	(kN)
Yielding displacement	d_y	2.50	(mm)
Ultimate force	F_u	52.15	(kN)
Ultimate displacement	d_u	48.40	(mm)
Maximum Force	F_{max}	52.15	(kN)
Elastic stiffness	k_{el}	11.02	(kN/mm)
Hardening stiffness	k_{pl}	0.54	(kN/mm)
Ductility ratio	μ (d_u)	19.33	-
Ductility	Class	H	-

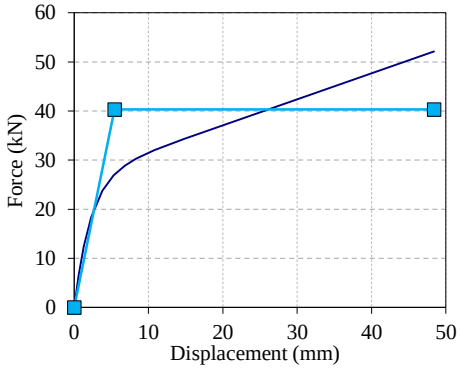

Equivalent bi-linear system according to EEEP method			
Yielding force	F_y	40.32	(kN)
Yielding displacement	d_y	5.41	(mm)
Ultimate force	F_u	52.15	(kN)
Ultimate displacement	d_u	48.40	(mm)
Maximum Force	F_{max}	52.15	(kN)
Elastic stiffness	k_{el}	7.45	(kN/mm)
Hardening stiffness	k_{pl}	0.00	(kN/mm)
Ductility ratio	μ (d_u)	8.94	-
Ductility	Class	H	-

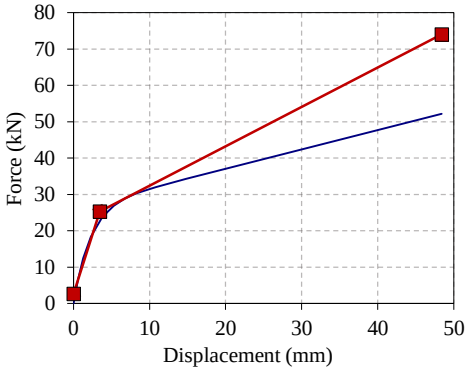

Equivalent bi-linear system according to EN12512 method (b)			
Yielding force	F_y	25.27	(kN)
Yielding displacement	d_y	3.48	(mm)
Ultimate force	F_u	52.15	(kN)
Ultimate displacement	d_u	48.40	(mm)
Maximum Force	F_{max}	52.15	(kN)
Elastic stiffness	k_{el}	6.52	(kN/mm)
Hardening stiffness	k_{pl}	1.09	(kN/mm)
Ductility ratio	μ (d_u)	13.92	-
Ductility	Class	H	-

X-BRAKET TYPE 1 – SHEAR – TEST 1

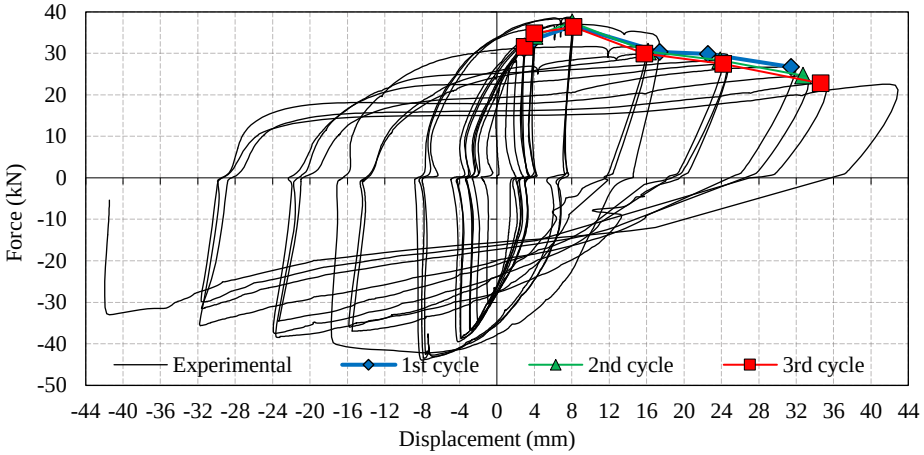

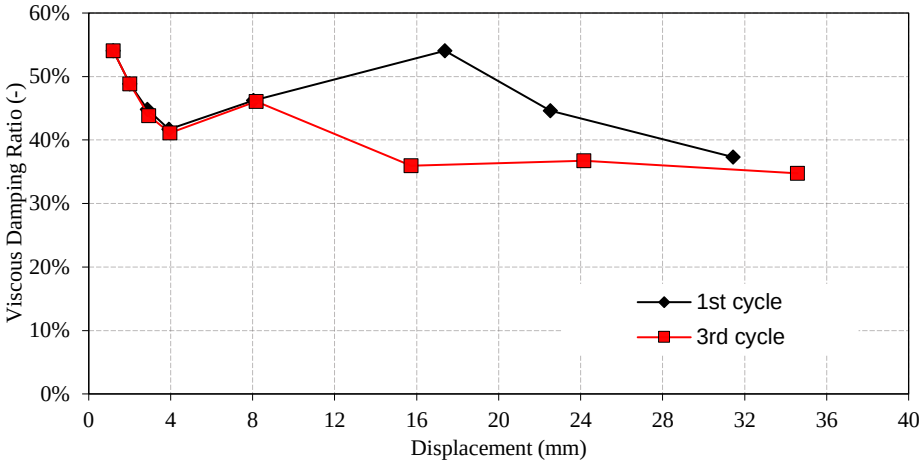

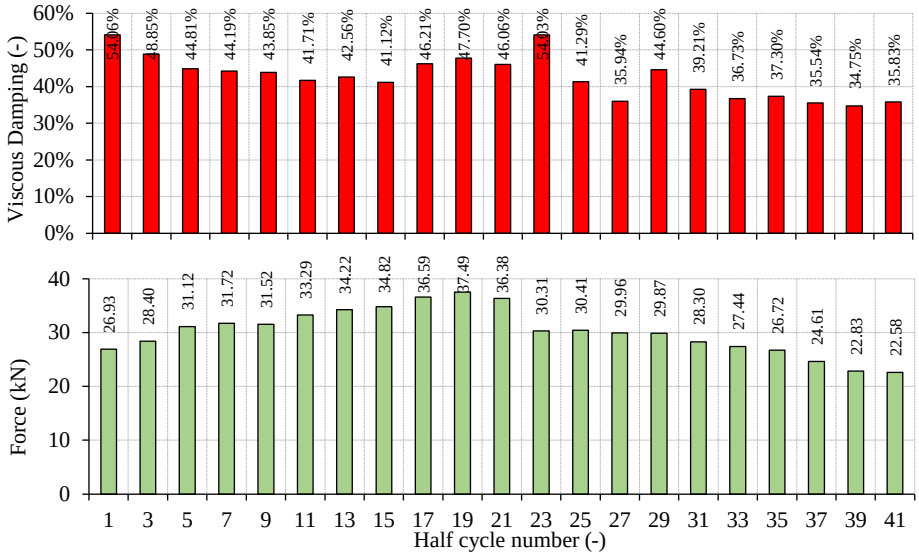

POSITIVE ENVELOPE

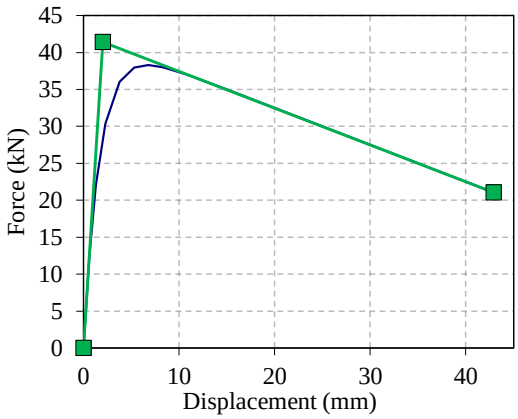

Equivalent bi-linear system according to EN12512 method (a)			
Yielding force	F_y	41.40	(kN)
Yielding displacement	d_y	2.01	(mm)
Ultimate force	F_u	21.05	(kN)
Ultimate displacement	d_u	42.90	(mm)
Maximum Force	F_{max}	38.32	(kN)
Elastic stiffness	k_{el}	20.57	(kN/mm)
Hardening stiffness	k_{pl}	-0.50	(kN/mm)
Ductility ratio	μ (d_u)	21.31	-
Ductility	Class	H	-

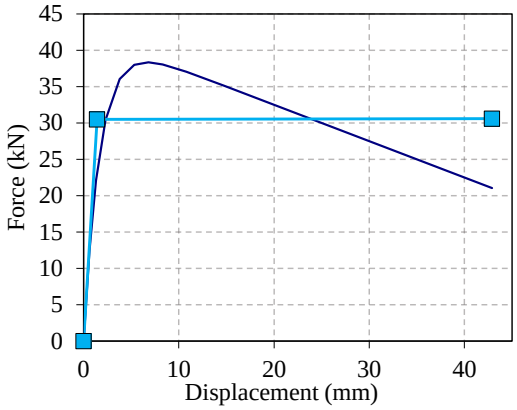

Equivalent bi-linear system according to EEEP method			
Yielding force	F_y	30.49	(kN)
Yielding displacement	d_y	1.39	(mm)
Ultimate force	F_u	21.05	(kN)
Ultimate displacement	d_u	42.90	(mm)
Maximum Force	F_{max}	38.32	(kN)
Elastic stiffness	k_{el}	21.90	(kN/mm)
Hardening stiffness	k_{pl}	0.00	(kN/mm)
Ductility ratio	μ (d_u)	30.81	-
Ductility	Class	H	-

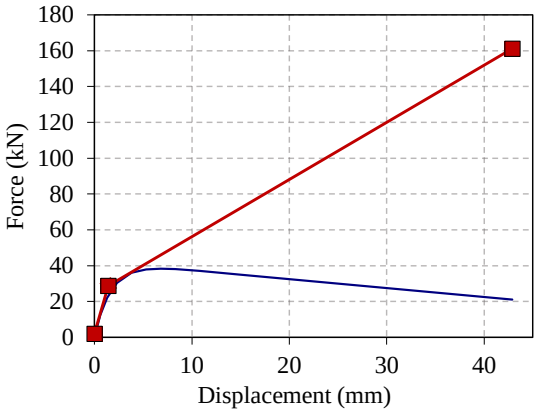

Equivalent bi-linear system according to EN12512 method (b)			
Yielding force	F_y	28.67	(kN)
Yielding displacement	d_y	1.40	(mm)
Ultimate force	F_u	21.05	(kN)
Ultimate displacement	d_u	42.90	(mm)
Maximum Force	F_{max}	38.32	(kN)
Elastic stiffness	k_{el}	19.16	(kN/mm)
Hardening stiffness	k_{pl}	3.19	(kN/mm)
Ductility ratio	μ (d_u)	30.72	-
Ductility	Class	H	-

NEGATIVE ENVELOPE

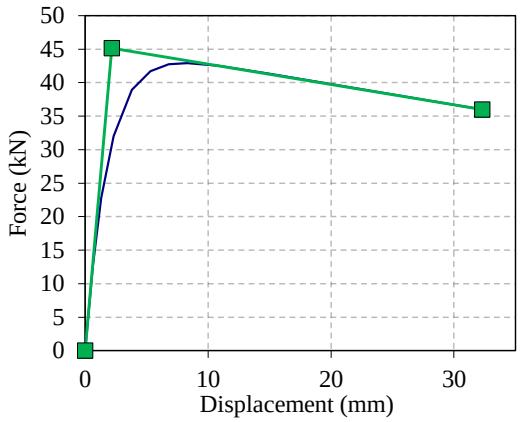

Equivalent bi-linear system according to EN12512 method (a)			
Yielding force	F_y	45.14	(kN)
Yielding displacement	d_y	2.16	(mm)
Ultimate force	F_u	35.99	(kN)
Ultimate displacement	d_u	32.30	(mm)
Maximum Force	F_{max}	42.90	(kN)
Elastic stiffness	k_{el}	20.89	(kN/mm)
Hardening stiffness	k_{pl}	-0.30	(kN/mm)
Ductility ratio	μ (d_u)	14.95	-
Ductility	Class	H	-

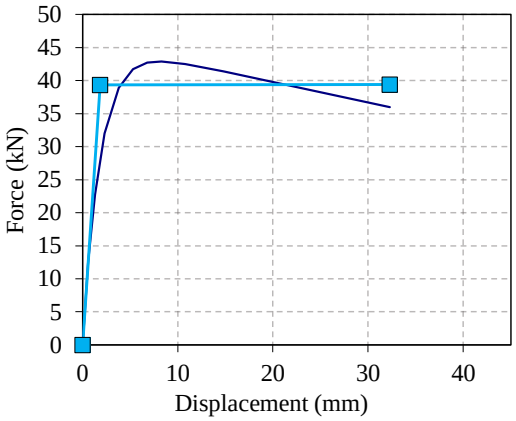

Equivalent bi-linear system according to EEEP method			
Yielding force	F_y	39.37	(kN)
Yielding displacement	d_y	1.84	(mm)
Ultimate force	F_u	35.99	(kN)
Ultimate displacement	d_u	32.30	(mm)
Maximum Force	F_{max}	42.90	(kN)
Elastic stiffness	k_{el}	21.45	(kN/mm)
Hardening stiffness	k_{pl}	0.00	(kN/mm)
Ductility ratio	μ (d_u)	17.60	-
Ductility	Class	H	-

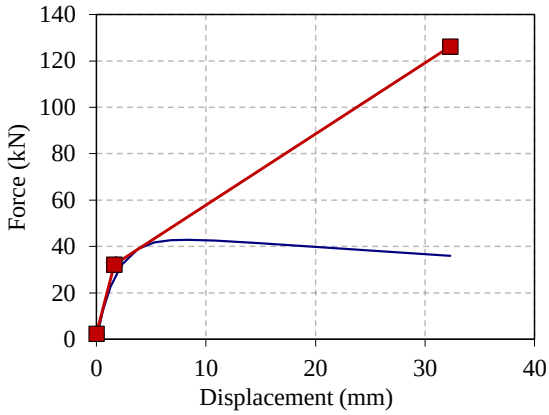

Equivalent bi-linear system according to EN12512 method (b)			
Yielding force	F_y	32.21	(kN)
Yielding displacement	d_y	1.62	(mm)
Ultimate force	F_u	35.99	(kN)
Ultimate displacement	d_u	32.30	(mm)
Maximum Force	F_{max}	42.90	(kN)
Elastic stiffness	k_{el}	18.39	(kN/mm)
Hardening stiffness	k_{pl}	3.06	(kN/mm)
Ductility ratio	μ (d_u)	19.96	-
Ductility	Class	H	-

X-BRAKET TYPE 1 – SHEAR – TEST 2

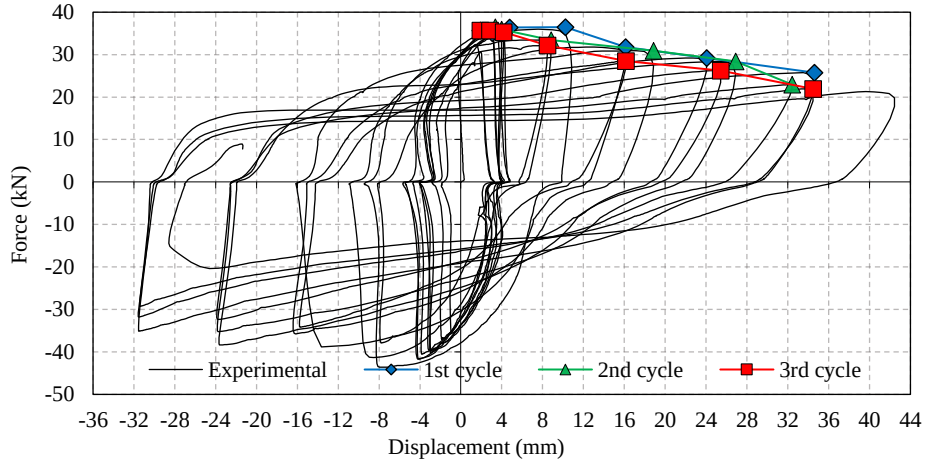

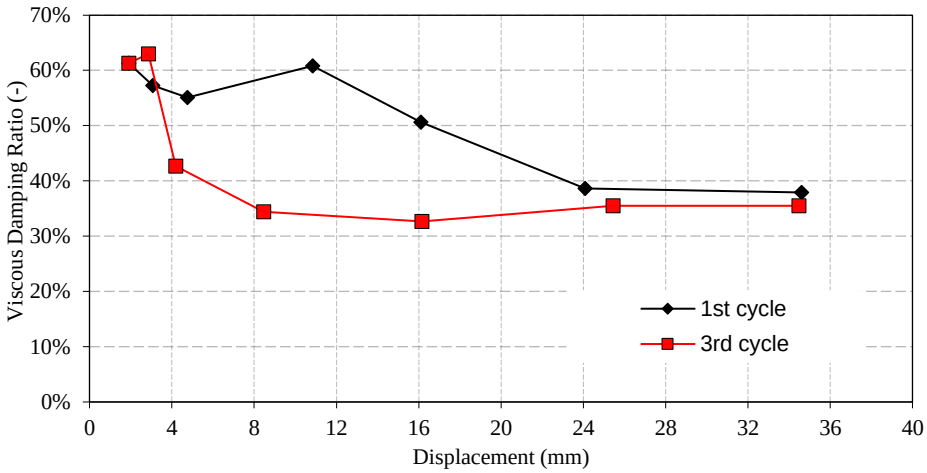

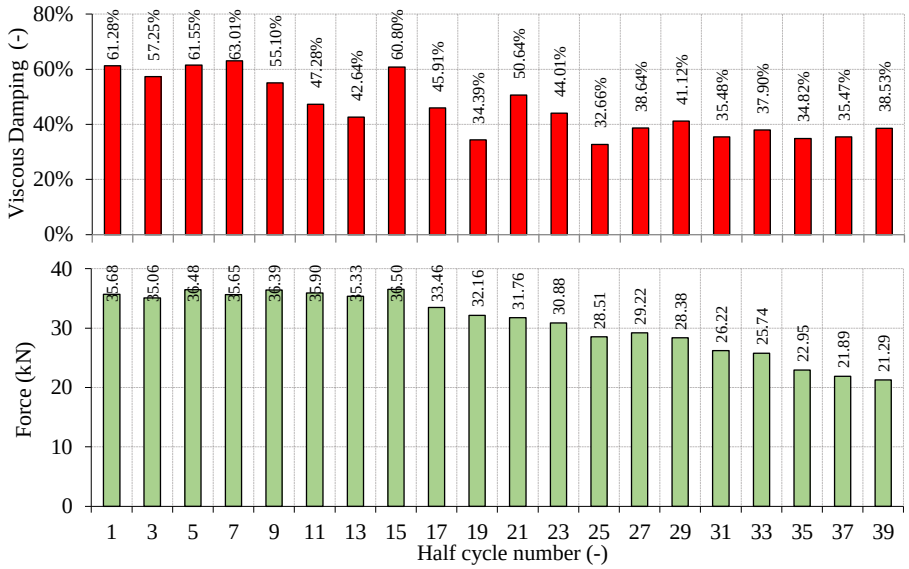

POSITIVE ENVELOPE

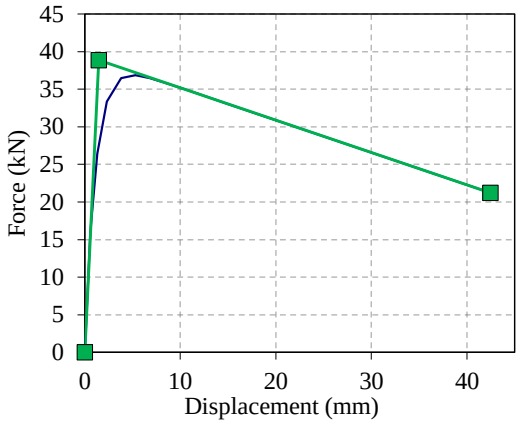

Equivalent bi-linear system according to EN12512 method (a)			
Yielding force	F_y	38.87	(kN)
Yielding displacement	d_y	1.46	(mm)
Ultimate force	F_u	21.24	(kN)
Ultimate displacement	d_u	42.47	(mm)
Maximum Force	F_{max}	36.86	(kN)
Elastic stiffness	k_{el}	26.68	(kN/mm)
Hardening stiffness	k_{pl}	-0.43	(kN/mm)
Ductility ratio	μ (d_u)	29.15	-
Ductility	Class	H	-

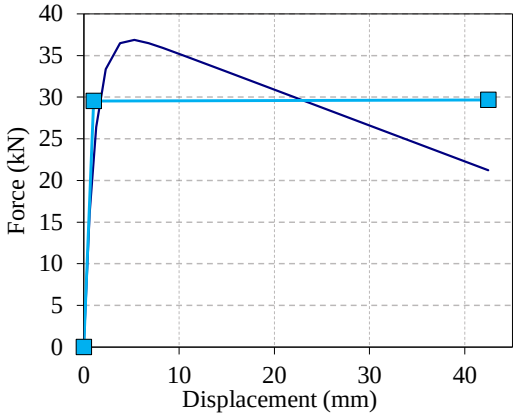

Equivalent bi-linear system according to EEEP method			
Yielding force	F_y	29.55	(kN)
Yielding displacement	d_y	1.00	(mm)
Ultimate force	F_u	21.24	(kN)
Ultimate displacement	d_u	42.47	(mm)
Maximum Force	F_{max}	36.86	(kN)
Elastic stiffness	k_{el}	29.49	(kN/mm)
Hardening stiffness	k_{pl}	0.00	(kN/mm)
Ductility ratio	μ (d_u)	42.37	-
Ductility	Class	H	-

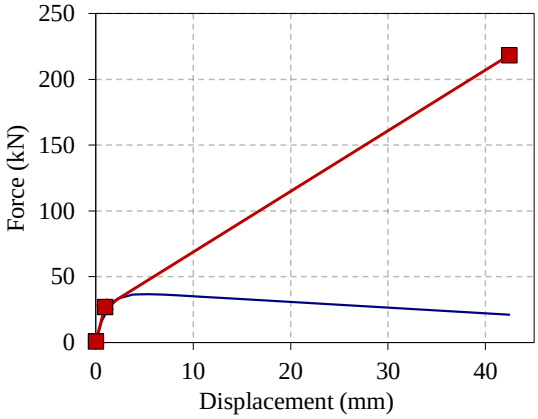

Equivalent bi-linear system according to EN12512 method (b)			
Yielding force	F_y	27.12	(kN)
Yielding displacement	d_y	0.95	(mm)
Ultimate force	F_u	21.24	(kN)
Ultimate displacement	d_u	42.47	(mm)
Maximum Force	F_{max}	36.86	(kN)
Elastic stiffness	k_{el}	27.64	(kN/mm)
Hardening stiffness	k_{pl}	4.61	(kN/mm)
Ductility ratio	μ (d_u)	44.81	-
Ductility	Class	H	-

NEGATIVE ENVELOPE

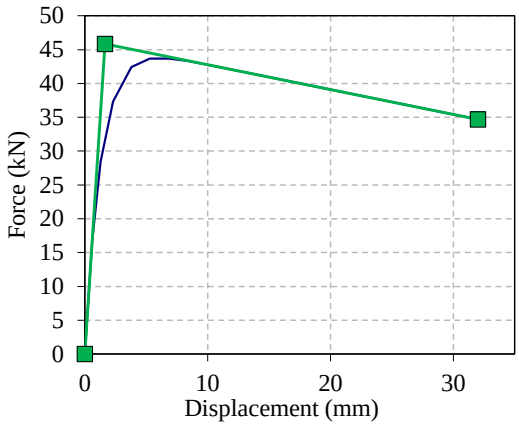

Equivalent bi-linear system according to EN12512 method (a)			
Yielding force	F_y	45.87	(kN)
Yielding displacement	d_y	1.66	(mm)
Ultimate force	F_u	34.66	(kN)
Ultimate displacement	d_u	32.00	(mm)
Maximum Force	F_{max}	43.70	(kN)
Elastic stiffness	k_{el}	27.71	(kN/mm)
Hardening stiffness	k_{pl}	-0.37	(kN/mm)
Ductility ratio	μ (d_u)	19.33	-
Ductility	Class	H	-

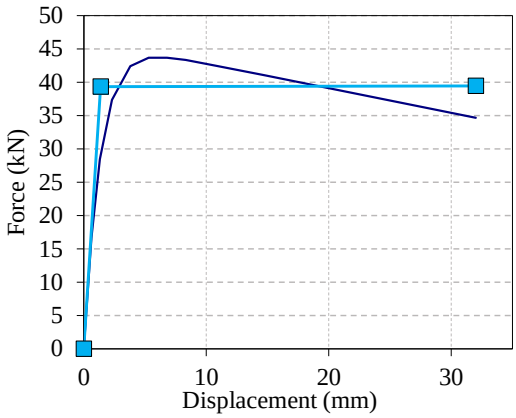

Equivalent bi-linear system according to EEEP method			
Yielding force	F_y	39.35	(kN)
Yielding displacement	d_y	1.35	(mm)
Ultimate force	F_u	34.66	(kN)
Ultimate displacement	d_u	32.00	(mm)
Maximum Force	F_{max}	43.70	(kN)
Elastic stiffness	k_{el}	29.13	(kN/mm)
Hardening stiffness	k_{pl}	0.00	(kN/mm)
Ductility ratio	μ (d_u)	23.69	-
Ductility	Class	H	-

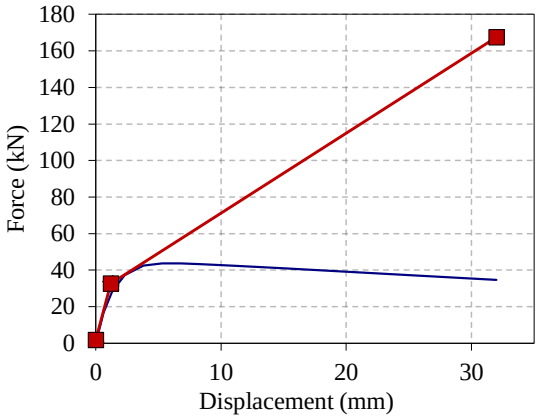

Equivalent bi-linear system according to EN12512 method (b)			
Yielding force	F_y	32.72	(kN)
Yielding displacement	d_y	1.18	(mm)
Ultimate force	F_u	34.66	(kN)
Ultimate displacement	d_u	32.00	(mm)
Maximum Force	F_{max}	43.70	(kN)
Elastic stiffness	k_{el}	26.22	(kN/mm)
Hardening stiffness	k_{pl}	4.37	(kN/mm)
Ductility ratio	μ (d_u)	27.09	-
Ductility	Class	H	-

X-BRAKET TYPE 1 – SHEAR – TEST 3

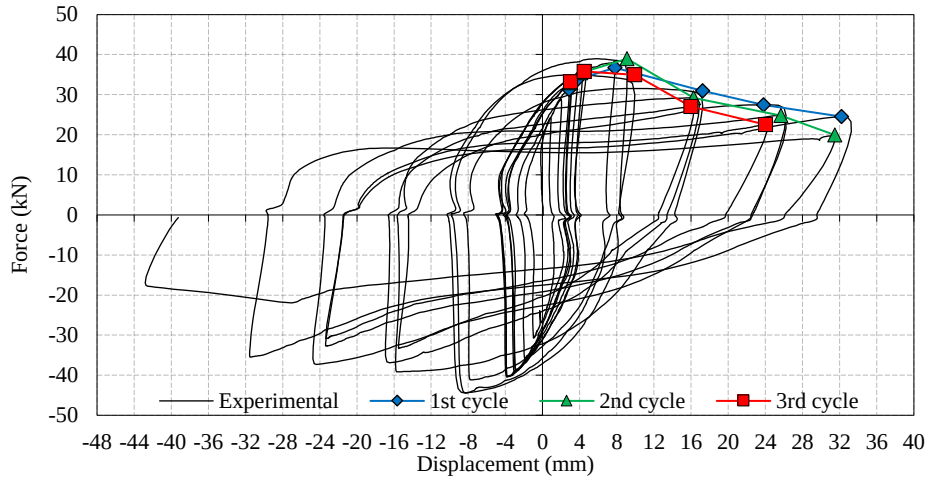

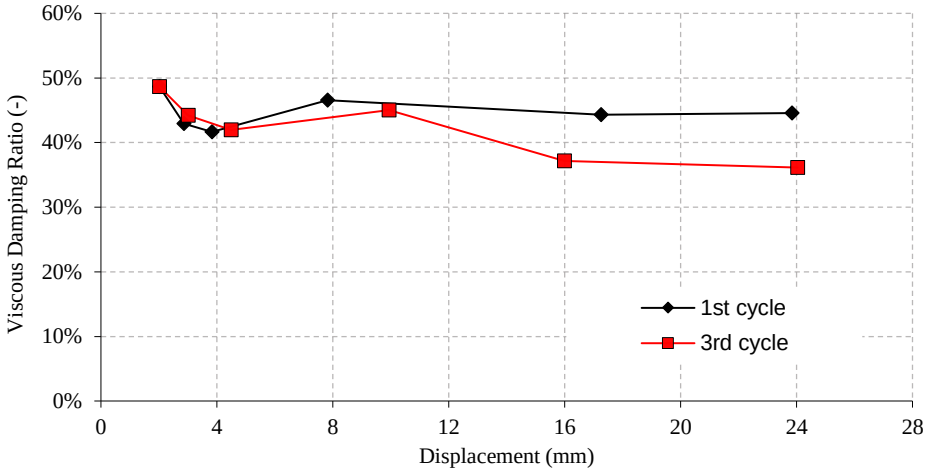

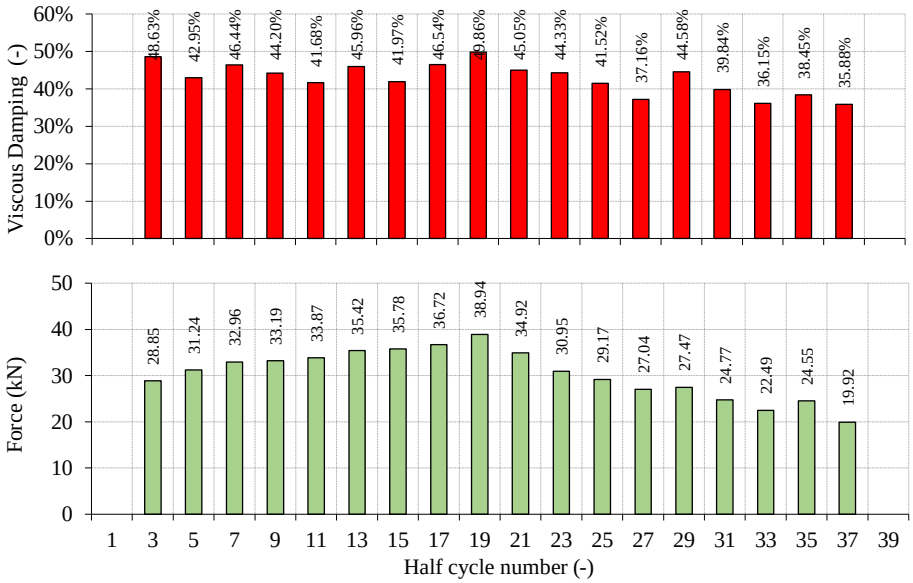

POSITIVE ENVELOPE

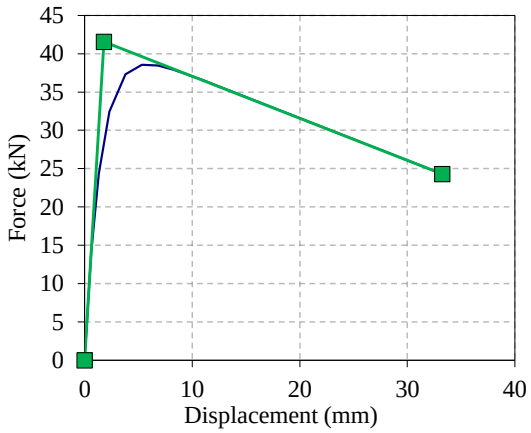

Equivalent bi-linear system according to EN12512 method (a)			
Yielding force	F_y	41.58	(kN)
Yielding displacement	d_y	1.79	(mm)
Ultimate force	F_u	24.31	(kN)
Ultimate displacement	d_u	33.26	(mm)
Maximum Force	F_{max}	38.54	(kN)
Elastic stiffness	k_{el}	23.29	(kN/mm)
Hardening stiffness	k_{pl}	-0.55	(kN/mm)
Ductility ratio	μ (d_u)	18.63	-
Ductility	Class	H	-

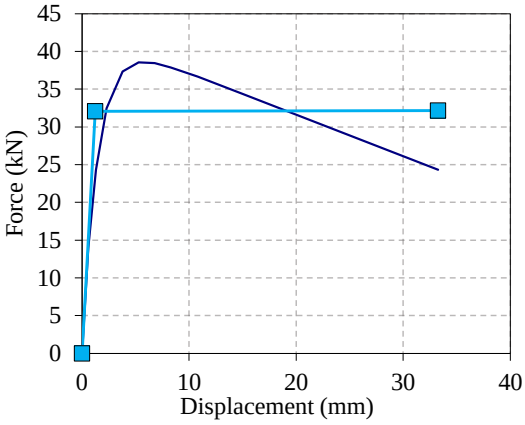

Equivalent bi-linear system according to EEEP method			
Yielding force	F_y	32.07	(kN)
Yielding displacement	d_y	1.25	(mm)
Ultimate force	F_u	24.31	(kN)
Ultimate displacement	d_u	33.26	(mm)
Maximum Force	F_{max}	38.54	(kN)
Elastic stiffness	k_{el}	25.69	(kN/mm)
Hardening stiffness	k_{pl}	0.00	(kN/mm)
Ductility ratio	μ (d_u)	26.65	-
Ductility	Class	H	-

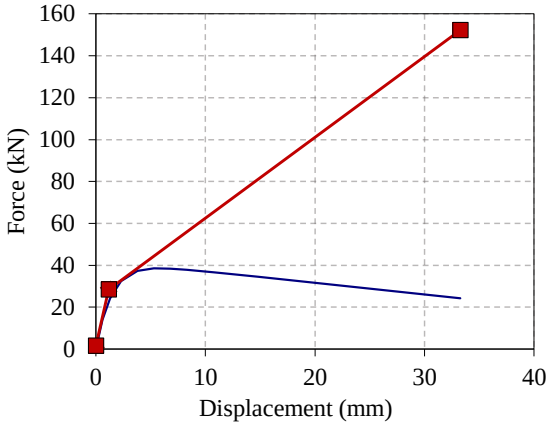

Equivalent bi-linear system according to EN12512 method (b)			
Yielding force	F_y	28.44	(kN)
Yielding displacement	d_y	1.16	(mm)
Ultimate force	F_u	24.31	(kN)
Ultimate displacement	d_u	33.26	(mm)
Maximum Force	F_{max}	38.54	(kN)
Elastic stiffness	k_{el}	23.12	(kN/mm)
Hardening stiffness	k_{pl}	3.85	(kN/mm)
Ductility ratio	μ (d_u)	28.59	-
Ductility	Class	H	-

NEGATIVE ENVELOPE

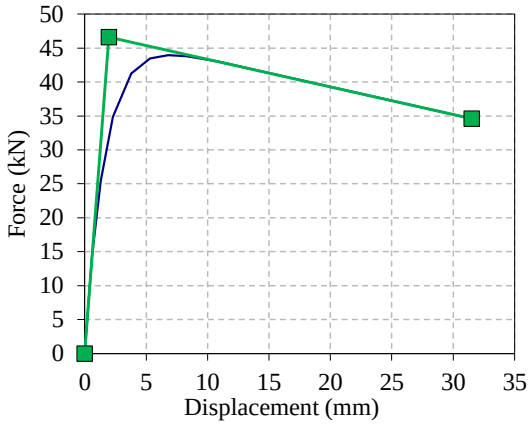

Equivalent bi-linear system according to EN12512 method (a)			
Yielding force	F_y	46.60	(kN)
Yielding displacement	d_y	1.96	(mm)
Ultimate force	F_u	34.58	(kN)
Ultimate displacement	d_u	31.50	(mm)
Maximum Force	F_{max}	43.96	(kN)
Elastic stiffness	k_{el}	23.81	(kN/mm)
Hardening stiffness	k_{pl}	-0.41	(kN/mm)
Ductility ratio	μ (d_u)	16.09	-
Ductility	Class	H	-

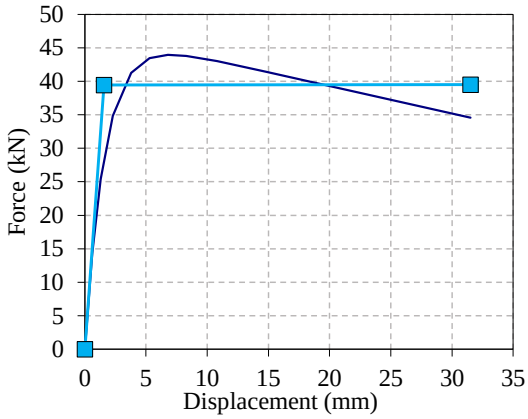

Equivalent bi-linear system according to EEEP method			
Yielding force	F_y	39.43	(kN)
Yielding displacement	d_y	1.57	(mm)
Ultimate force	F_u	34.58	(kN)
Ultimate displacement	d_u	31.50	(mm)
Maximum Force	F_{max}	43.96	(kN)
Elastic stiffness	k_{el}	25.12	(kN/mm)
Hardening stiffness	k_{pl}	0.00	(kN/mm)
Ductility ratio	μ (d_u)	20.06	-
Ductility	Class	H	-

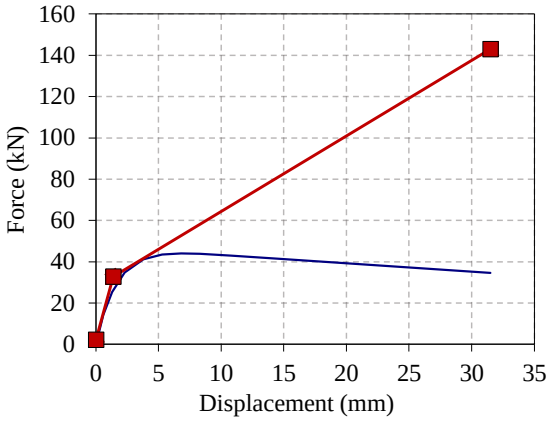

Equivalent bi-linear system according to EN12512 method (b)			
Yielding force	F_y	32.77	(kN)
Yielding displacement	d_y	1.39	(mm)
Ultimate force	F_u	34.58	(kN)
Ultimate displacement	d_u	31.50	(mm)
Maximum Force	F_{max}	43.96	(kN)
Elastic stiffness	k_{el}	21.98	(kN/mm)
Hardening stiffness	k_{pl}	3.66	(kN/mm)
Ductility ratio	μ (d_u)	22.64	-
Ductility	Class	H	-

X-BRAKET TYPE 1 – TEST COMPLETE CONNECTION – TENSION – TEST 1

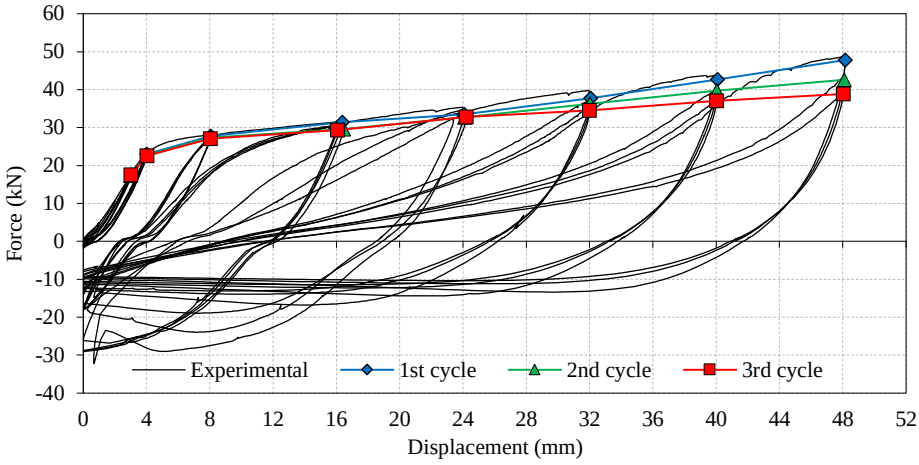

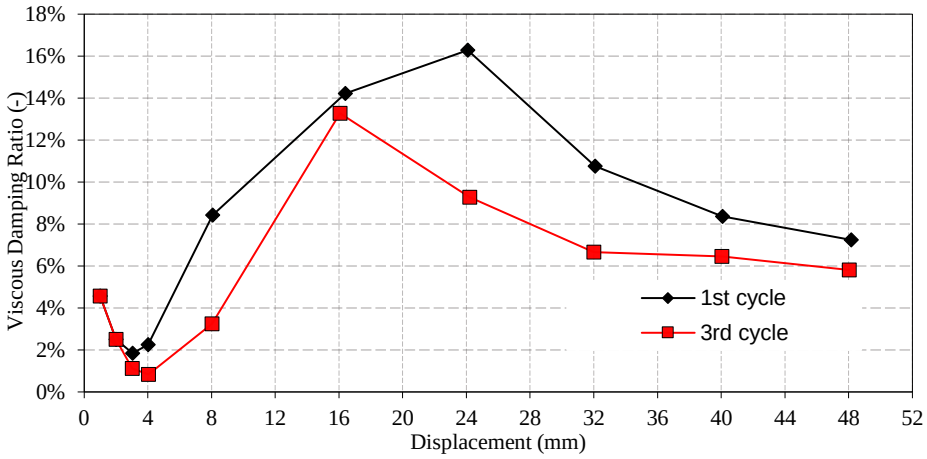

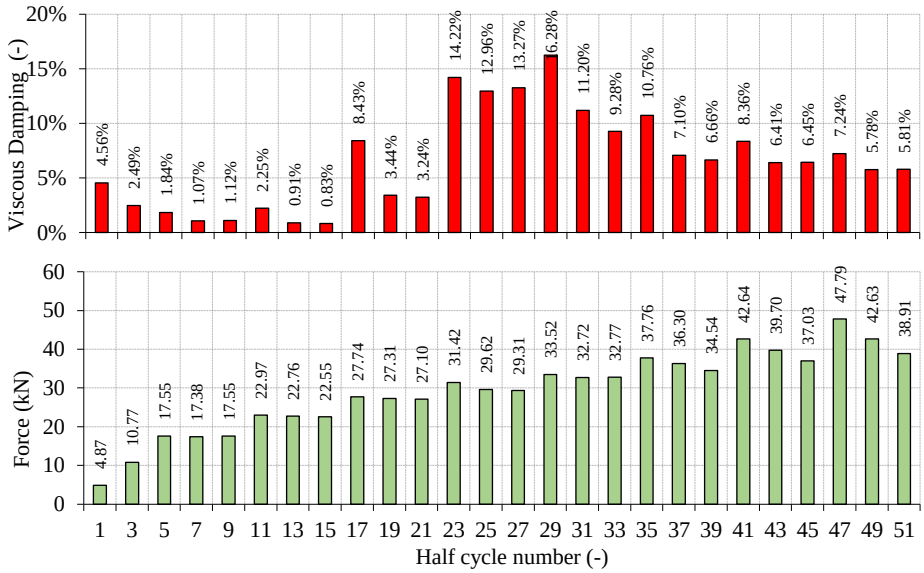

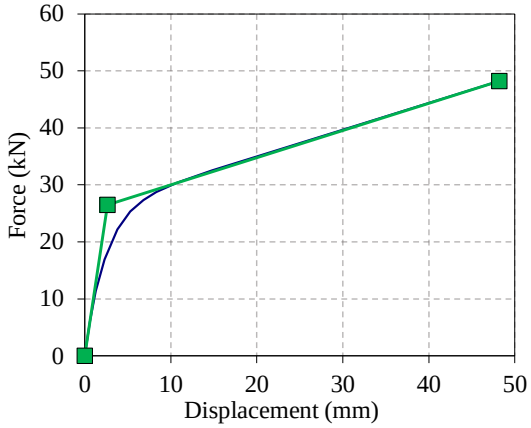

Equivalent bi-linear system according to EN12512 method (a)			
Yielding force	F_y	26.52	(kN)
Yielding displacement	d_y	2.66	(mm)
Ultimate force	F_u	48.25	(kN)
Ultimate displacement	d_u	48.20	(mm)
Maximum Force	F_{max}	48.25	(kN)
Elastic stiffness	k_{el}	9.96	(kN/mm)
Hardening stiffness	k_{pl}	0.48	(kN/mm)
Ductility ratio	μ (d_u)	18.10	-
Ductility	Class	H	-

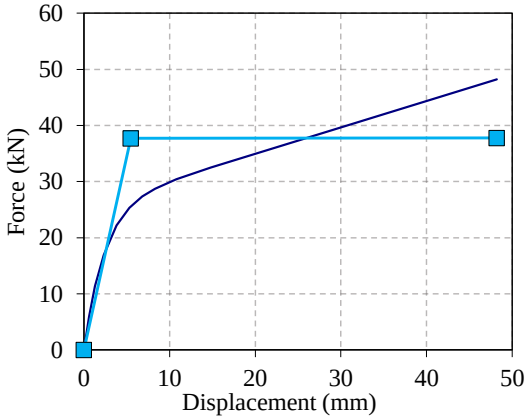

Equivalent bi-linear system according to EEEP method			
Yielding force	F_y	37.75	(kN)
Yielding displacement	d_y	5.48	(mm)
Ultimate force	F_u	48.25	(kN)
Ultimate displacement	d_u	48.20	(mm)
Maximum Force	F_{max}	48.25	(kN)
Elastic stiffness	k_{el}	6.89	(kN/mm)
Hardening stiffness	k_{pl}	0.00	(kN/mm)
Ductility ratio	μ (d_u)	8.80	-
Ductility	Class	H	-

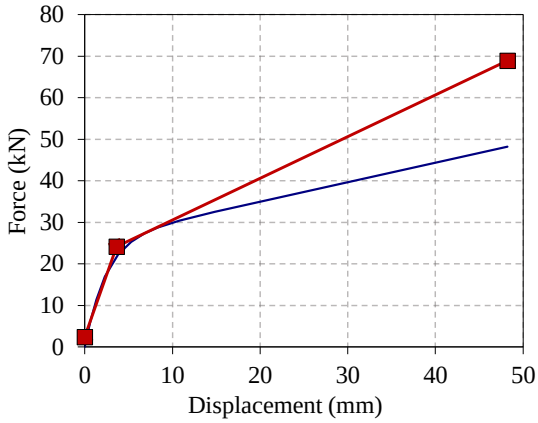

Equivalent bi-linear system according to EN12512 method (b)			
Yielding force	F_y	24.12	(kN)
Yielding displacement	d_y	3.60	(mm)
Ultimate force	F_u	48.25	(kN)
Ultimate displacement	d_u	48.20	(mm)
Maximum Force	F_{max}	48.25	(kN)
Elastic stiffness	k_{el}	6.03	(kN/mm)
Hardening stiffness	k_{pl}	1.01	(kN/mm)
Ductility ratio	μ (d_u)	13.39	-
Ductility	Class	H	-

X-BRAKET TYPE 1 – TEST COMPLETE CONNECTION – TENSION – REPLICATION OF TEST 1 WITH REPLACEMNT OF BRAKETS

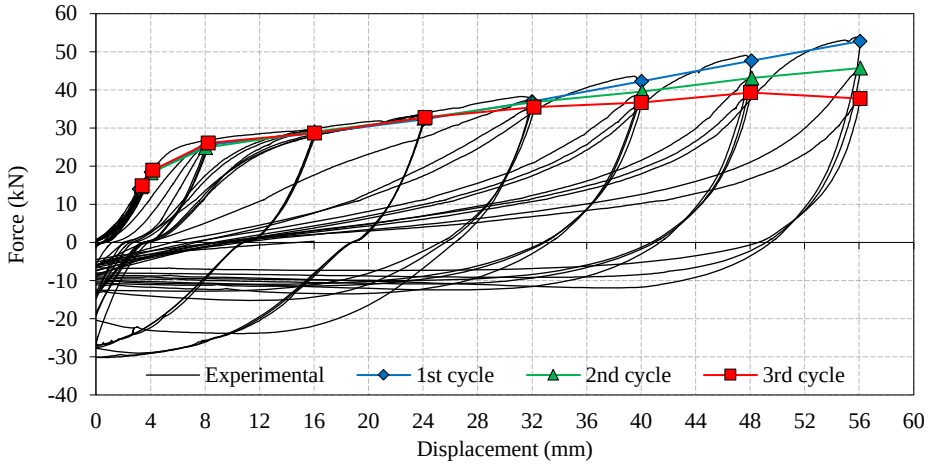

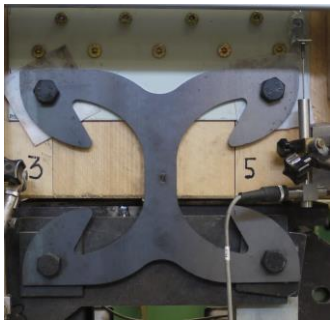

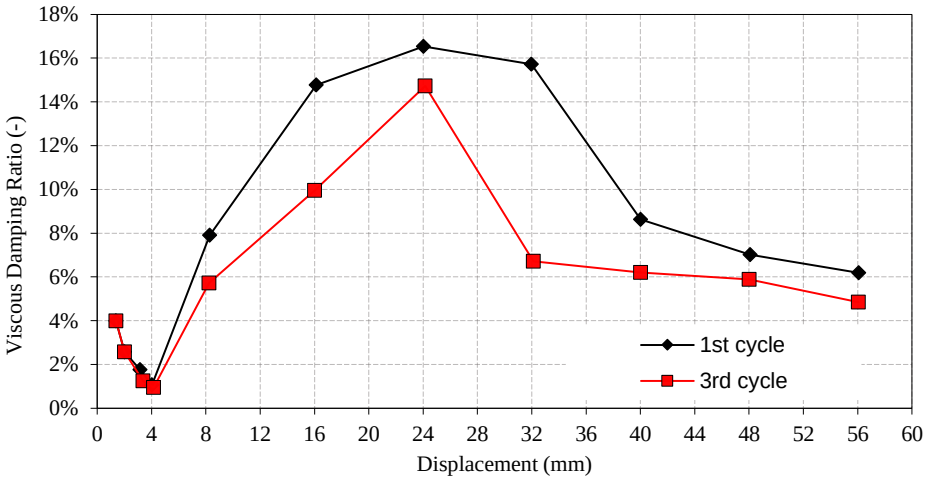

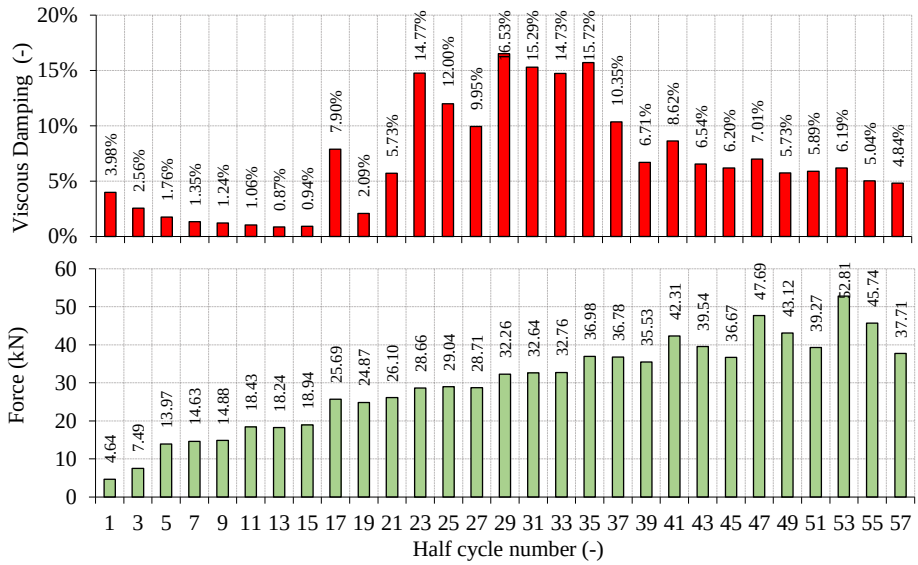

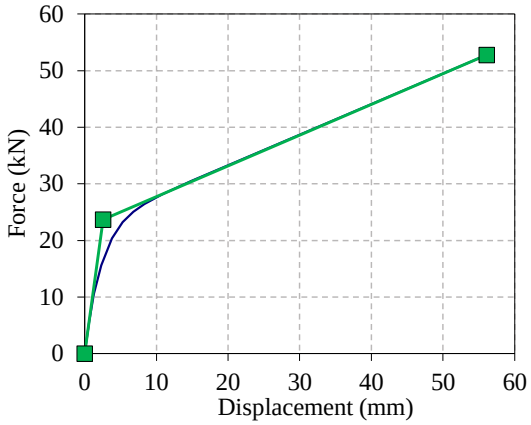

Equivalent bi-linear system according to EN12512 method (a)			
Yielding force	F_y	23.66	(kN)
Yielding displacement	d_y	2.55	(mm)
Ultimate force	F_u	52.79	(kN)
Ultimate displacement	d_u	56.10	(mm)
Maximum Force	F_{max}	52.79	(kN)
Elastic stiffness	k_{el}	9.29	(kN/mm)
Hardening stiffness	k_{pl}	0.54	(kN/mm)
Ductility ratio	μ (d_u)	22.03	-
Ductility	Class	H	-

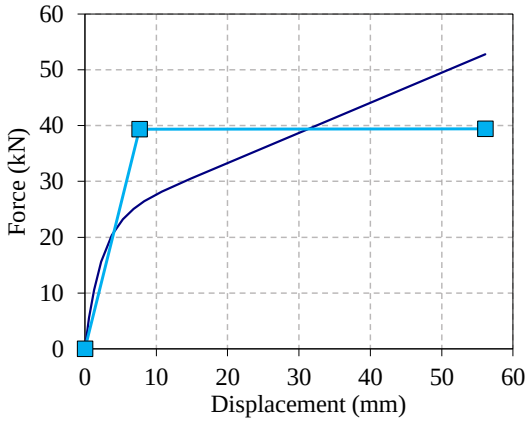

Equivalent bi-linear system according to EEEP method			
Yielding force	F_y	39.39	(kN)
Yielding displacement	d_y	7.65	(mm)
Ultimate force	F_u	52.79	(kN)
Ultimate displacement	d_u	56.10	(mm)
Maximum Force	F_{max}	52.79	(kN)
Elastic stiffness	k_{el}	5.15	(kN/mm)
Hardening stiffness	k_{pl}	0.00	(kN/mm)
Ductility ratio	μ (d_u)	7.34	-
Ductility	Class	H	-

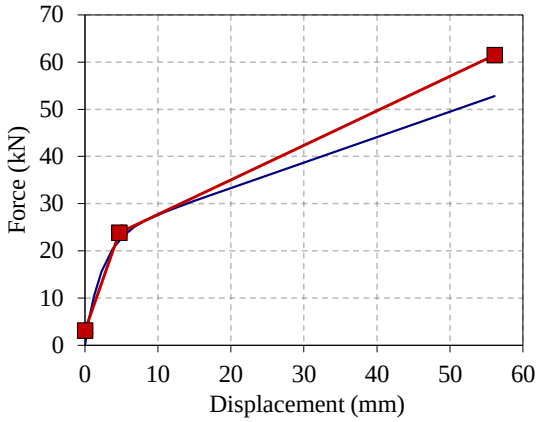

Equivalent bi-linear system according to EN12512 method (b)			
Yielding force	F_y	23.80	(kN)
Yielding displacement	d_y	4.71	(mm)
Ultimate force	F_u	52.79	(kN)
Ultimate displacement	d_u	56.10	(mm)
Maximum Force	F_{max}	52.79	(kN)
Elastic stiffness	k_{el}	4.40	(kN/mm)
Hardening stiffness	k_{pl}	0.73	(kN/mm)
Ductility ratio	μ (d_u)	11.91	-
Ductility	Class	H	-

X-BRAKET TYPE 2 – TEST COMPLETE CONNECTION – TENSION – TEST 1

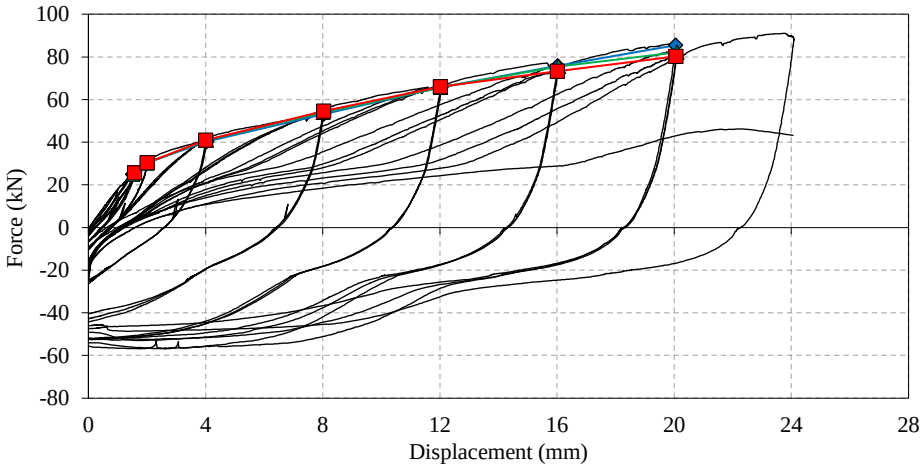

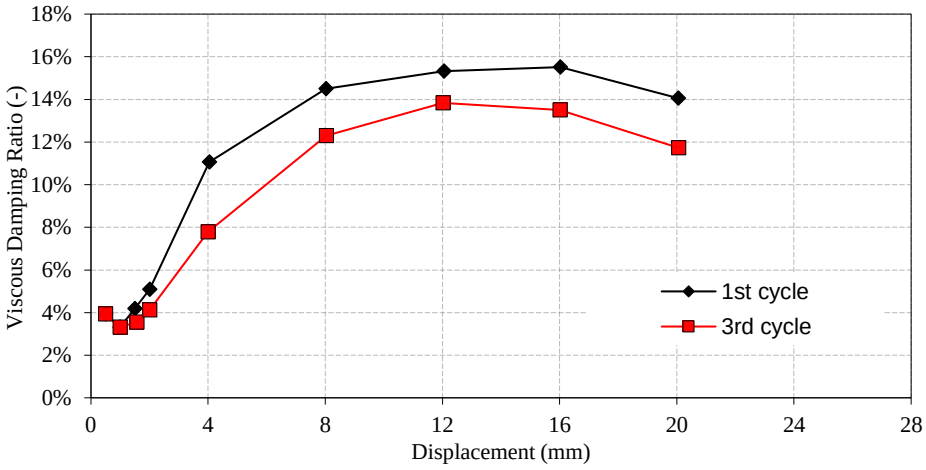

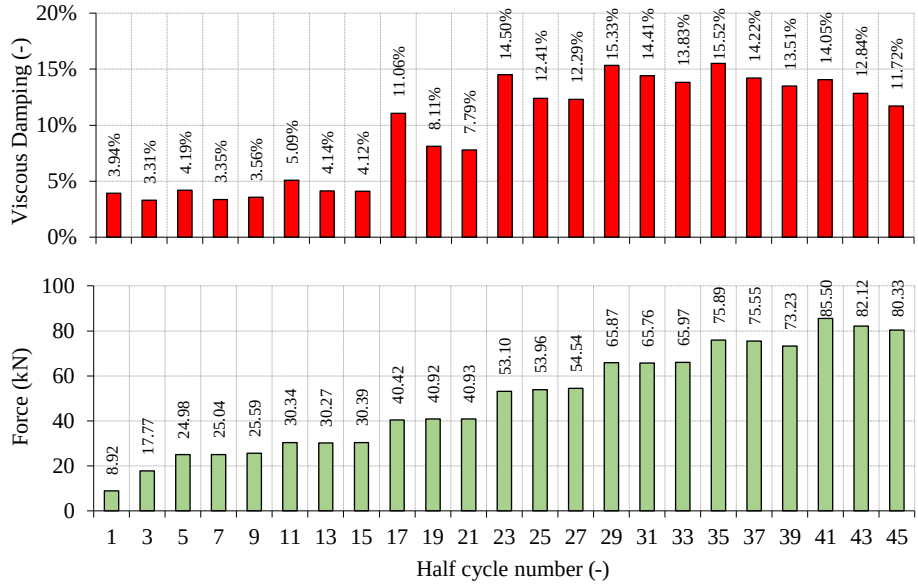

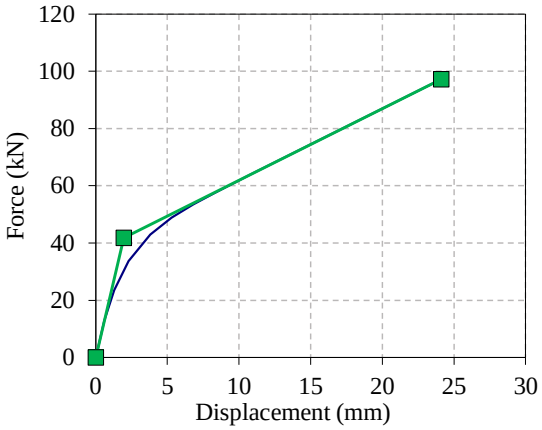

Equivalent bi-linear system according to EN12512 method (a)			
Yielding force	F_y	41.82	(kN)
Yielding displacement	d_y	1.96	(mm)
Ultimate force	F_u	97.25	(kN)
Ultimate displacement	d_u	24.10	(mm)
Maximum Force	F_{max}	97.25	(kN)
Elastic stiffness	k_{el}	21.39	(kN/mm)
Hardening stiffness	k_{pl}	2.50	(kN/mm)
Ductility ratio	μ (d_u)	12.33	-
Ductility	Class	H	-

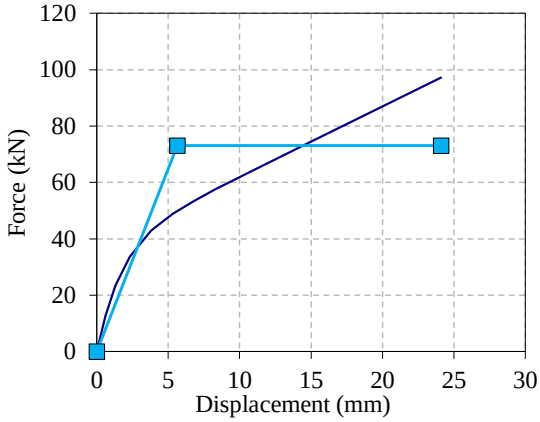

Equivalent bi-linear system according to EEEP method			
Yielding force	F_y	73.08	(kN)
Yielding displacement	d_y	5.64	(mm)
Ultimate force	F_u	97.25	(kN)
Ultimate displacement	d_u	24.10	(mm)
Maximum Force	F_{max}	97.25	(kN)
Elastic stiffness	k_{el}	12.97	(kN/mm)
Hardening stiffness	k_{pl}	0.00	(kN/mm)
Ductility ratio	μ (d_u)	4.28	-
Ductility	Class	M	-

X-BRAKET TYPE 2 – TEST COMPLETE CONNECTION – TENSION – TEST 2

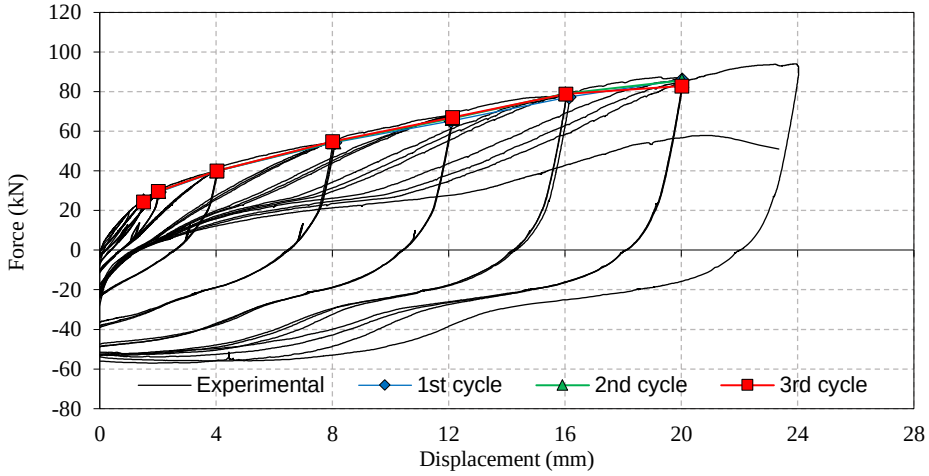

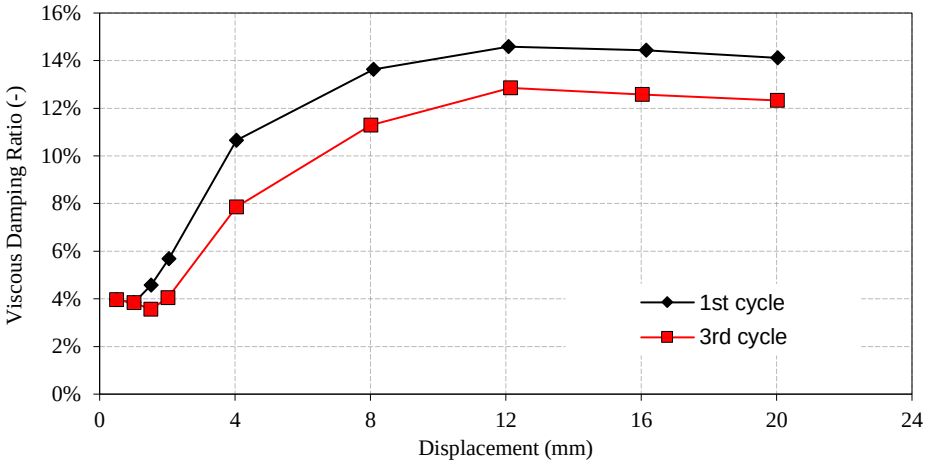

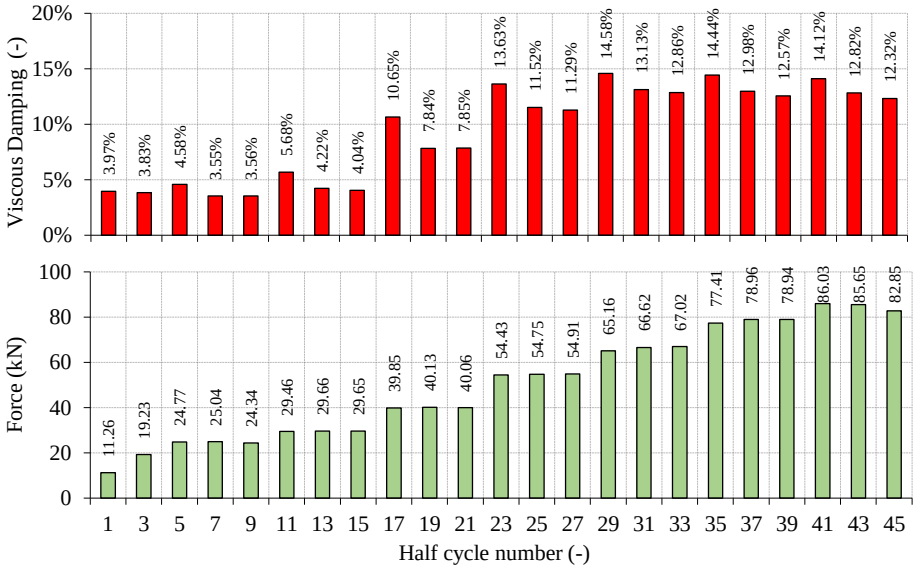

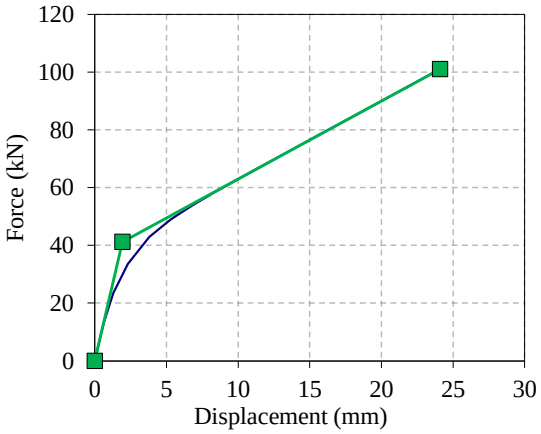

Equivalent bi-linear system according to EN12512 method (a)			
Yielding force	F_y	41.14	(kN)
Yielding displacement	d_y	1.93	(mm)
Ultimate force	F_u	101.07	(kN)
Ultimate displacement	d_u	24.10	(mm)
Maximum Force	F_{max}	101.07	(kN)
Elastic stiffness	k_{el}	21.37	(kN/mm)
Hardening stiffness	k_{pl}	2.70	(kN/mm)
Ductility ratio	μ (d_u)	12.52	-
Ductility	Class	H	-

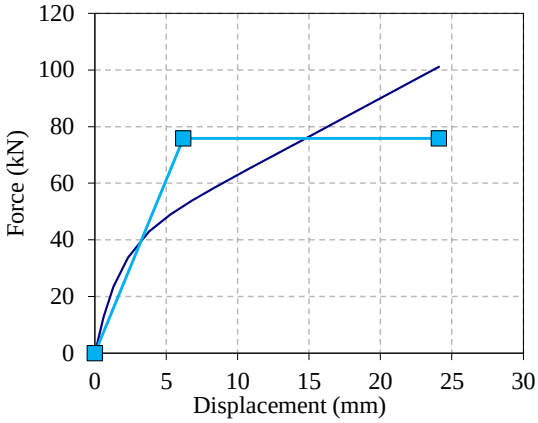

Equivalent bi-linear system according to EEEP method			
Yielding force	F_y	75.80	(kN)
Yielding displacement	d_y	6.19	(mm)
Ultimate force	F_u	101.07	(kN)
Ultimate displacement	d_u	24.10	(mm)
Maximum Force	F_{max}	101.07	(kN)
Elastic stiffness	k_{el}	12.25	(kN/mm)
Hardening stiffness	k_{pl}	0.00	(kN/mm)
Ductility ratio	μ (d_u)	3.90	-
Ductility	Class	L	-

X-BRAKET TYPE 2 – TEST COMPLETE CONNECTION – SHEAR

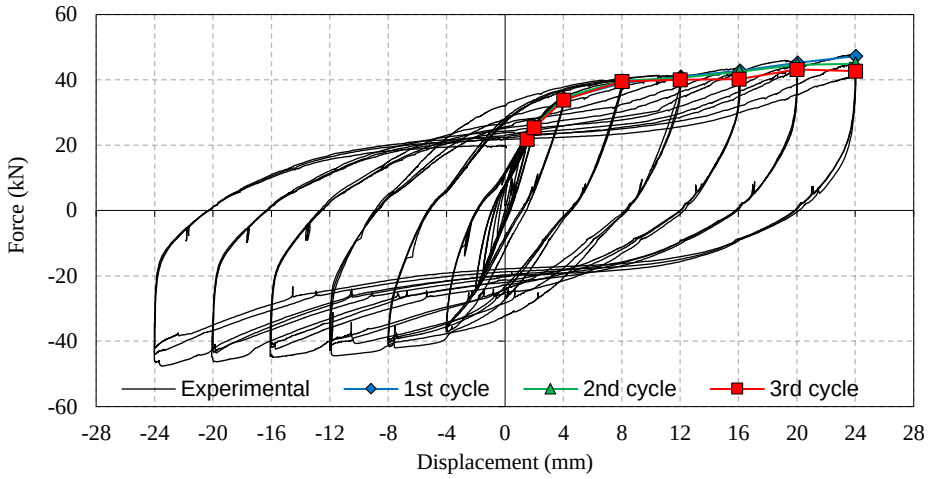

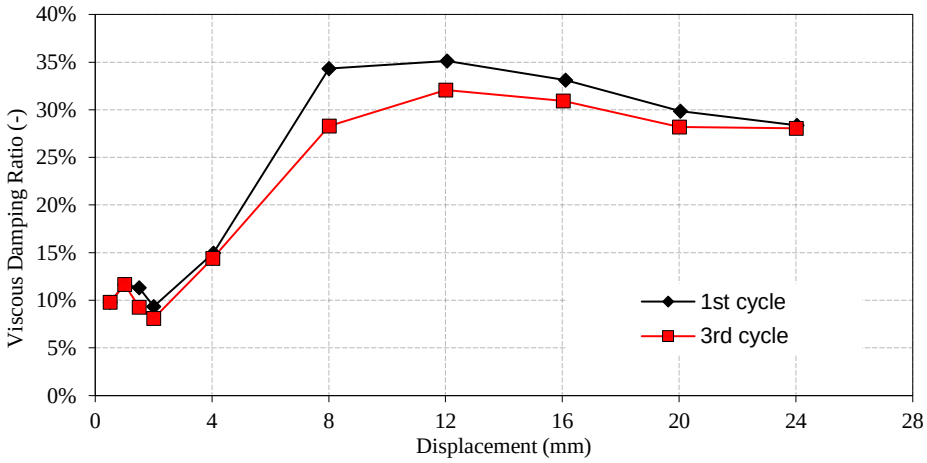

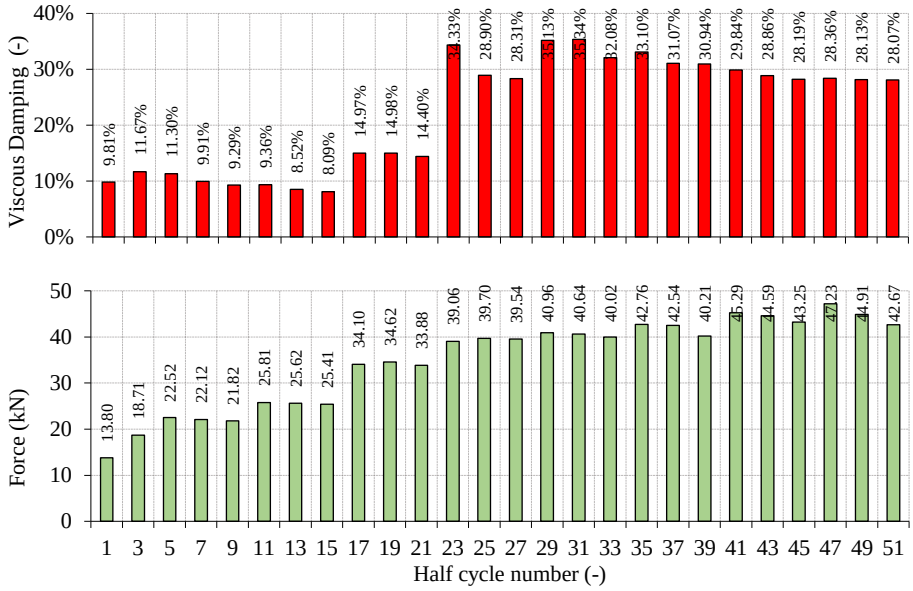

POSITIVE ENVELOPE

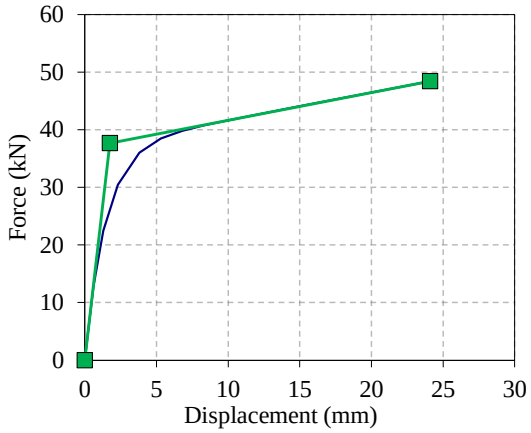

Equivalent bi-linear system according to EN12512 method (a)			
Yielding force	F_y	37.71	(kN)
Yielding displacement	d_y	1.76	(mm)
Ultimate force	F_u	48.47	(kN)
Ultimate displacement	d_u	24.10	(mm)
Maximum Force	F_{max}	48.47	(kN)
Elastic stiffness	k_{el}	21.37	(kN/mm)
Hardening stiffness	k_{pl}	0.48	(kN/mm)
Ductility ratio	μ (d_u)	13.66	-
Ductility	Class	H	-

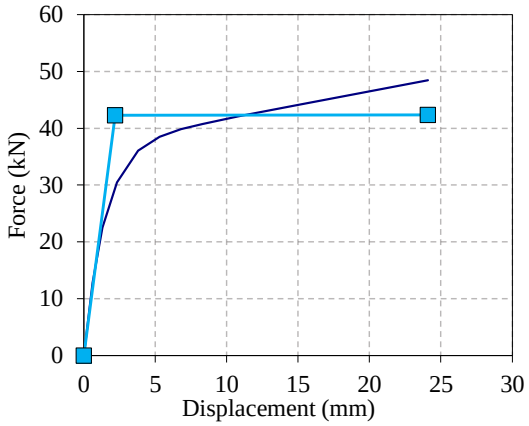

Equivalent bi-linear system according to EEEP method			
Yielding force	F_y	42.28	(kN)
Yielding displacement	d_y	2.18	(mm)
Ultimate force	F_u	48.47	(kN)
Ultimate displacement	d_u	24.10	(mm)
Maximum Force	F_{max}	48.47	(kN)
Elastic stiffness	k_{el}	19.39	(kN/mm)
Hardening stiffness	k_{pl}	0.00	(kN/mm)
Ductility ratio	μ (d_u)	11.05	-
Ductility	Class	H	-

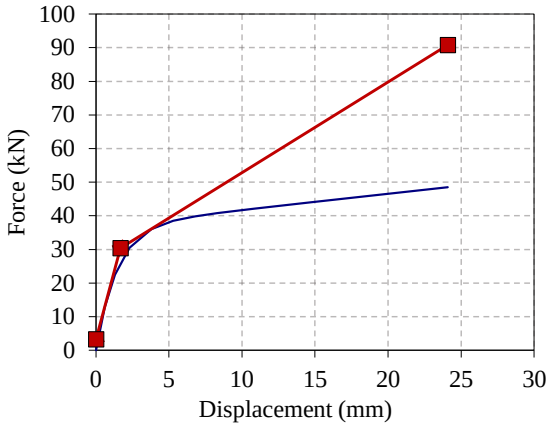

Equivalent bi-linear system according to EN12512 method (b)			
Yielding force	F_y	30.39	(kN)
Yielding displacement	d_y	1.68	(mm)
Ultimate force	F_u	48.47	(kN)
Ultimate displacement	d_u	24.10	(mm)
Maximum Force	F_{max}	48.47	(kN)
Elastic stiffness	k_{el}	16.16	(kN/mm)
Hardening stiffness	k_{pl}	2.69	(kN/mm)
Ductility ratio	μ (d_u)	14.33	-
Ductility	Class	H	-

NEGATIVE ENVELOPE

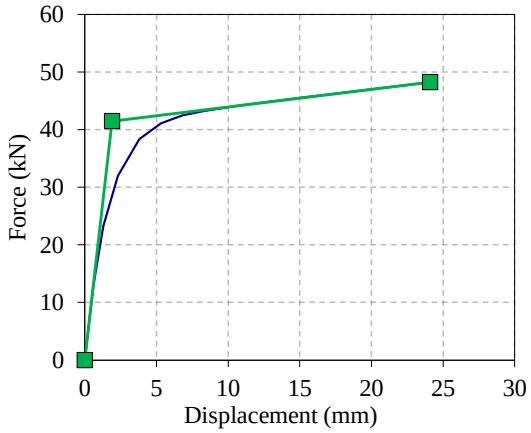

Equivalent bi-linear system according to EN12512 method (a)			
Yielding force	F_y	41.49	(kN)
Yielding displacement	d_y	1.91	(mm)
Ultimate force	F_u	48.23	(kN)
Ultimate displacement	d_u	24.10	(mm)
Maximum Force	F_{max}	48.23	(kN)
Elastic stiffness	k_{el}	21.72	(kN/mm)
Hardening stiffness	k_{pl}	0.30	(kN/mm)
Ductility ratio	μ (d_u)	12.62	-
Ductility	Class	H	-

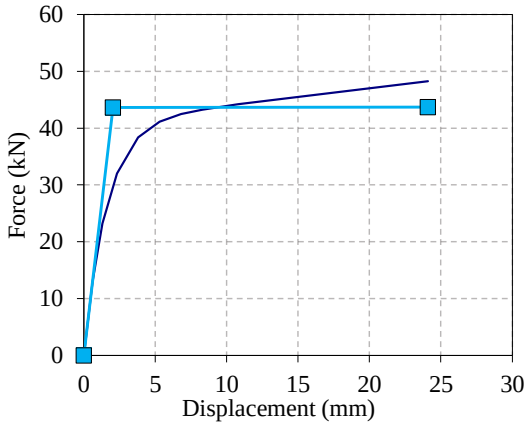

Equivalent bi-linear system according to EEEP method			
Yielding force	F_y	43.63	(kN)
Yielding displacement	d_y	2.04	(mm)
Ultimate force	F_u	48.23	(kN)
Ultimate displacement	d_u	24.10	(mm)
Maximum Force	F_{max}	48.23	(kN)
Elastic stiffness	k_{el}	21.44	(kN/mm)
Hardening stiffness	k_{pl}	0.00	(kN/mm)
Ductility ratio	μ (d_u)	11.84	-
Ductility	Class	H	-

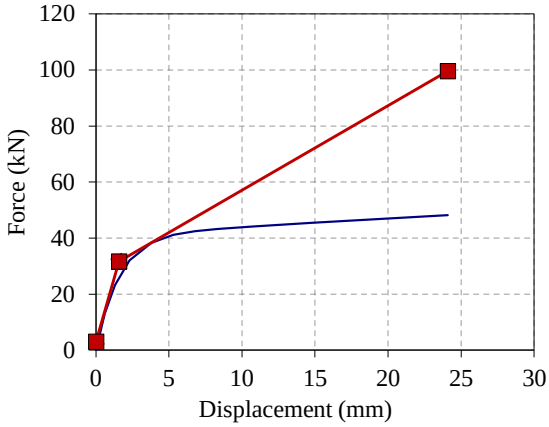

Equivalent bi-linear system according to EN12512 method (b)			
Yielding force	F_y	31.71	(kN)
Yielding displacement	d_y	1.59	(mm)
Ultimate force	F_u	48.23	(kN)
Ultimate displacement	d_u	24.10	(mm)
Maximum Force	F_{max}	48.23	(kN)
Elastic stiffness	k_{el}	18.09	(kN/mm)
Hardening stiffness	k_{pl}	3.01	(kN/mm)
Ductility ratio	μ (d_u)	15.19	-
Ductility	Class	H	-

X-BRAKET TYPE 2, SPECIAL USAGE AS EXTERNAL BRACKET – TEST COMPLETE CONNECTION WITH SPECIAL ELEMENTS TO INCREASE WOOD EMBEDMENT STRENGTH – TENSION

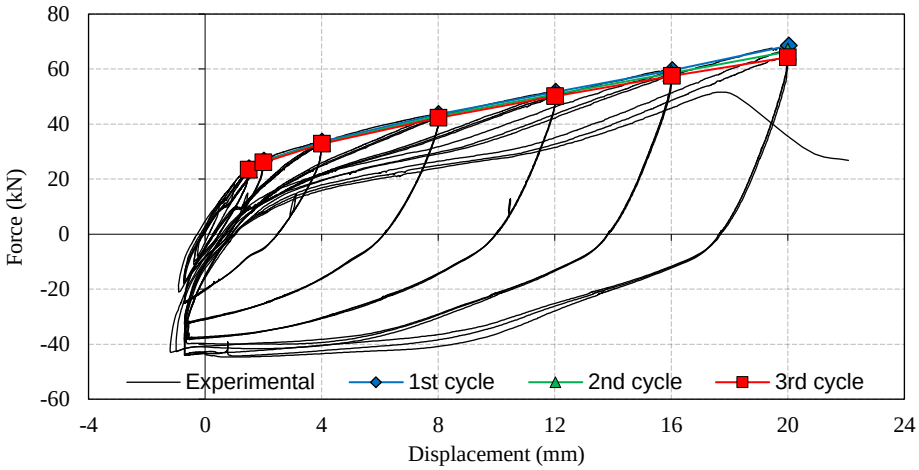

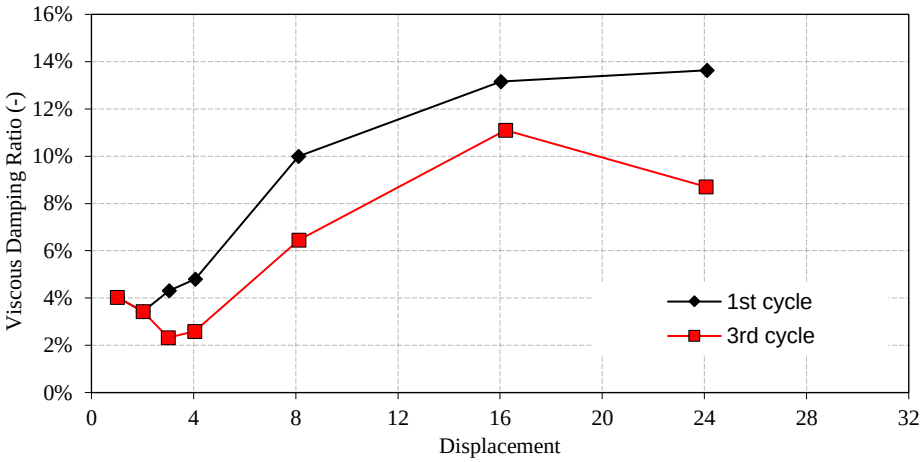

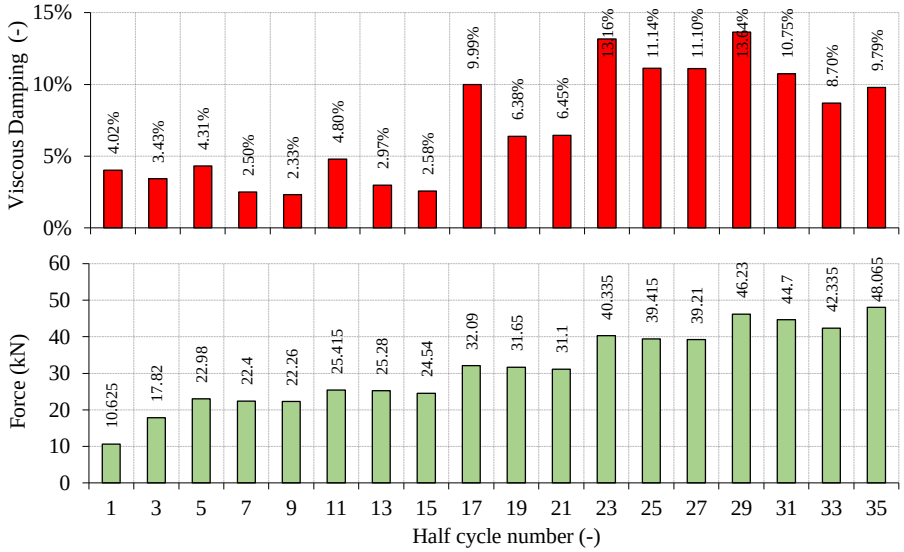

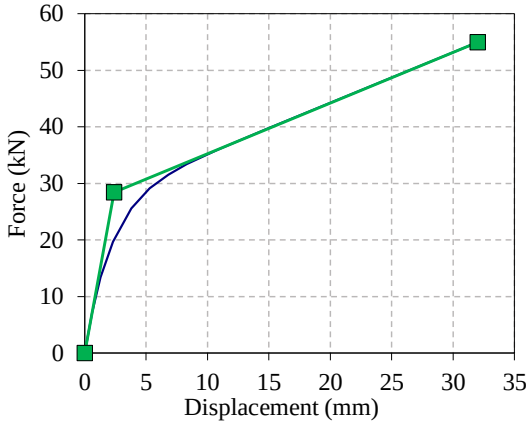

Equivalent bi-linear system according to EN12512 method (a)			
Yielding force	F_y	28.43	(kN)
Yielding displacement	d_y	2.40	(mm)
Ultimate force	F_u	54.98	(kN)
Ultimate displacement	d_u	32.00	(mm)
Maximum Force	F_{max}	54.98	(kN)
Elastic stiffness	k_{el}	11.87	(kN/mm)
Hardening stiffness	k_{pl}	0.90	(kN/mm)
Ductility ratio	μ (d_u)	13.36	-
Ductility	Class	H	-

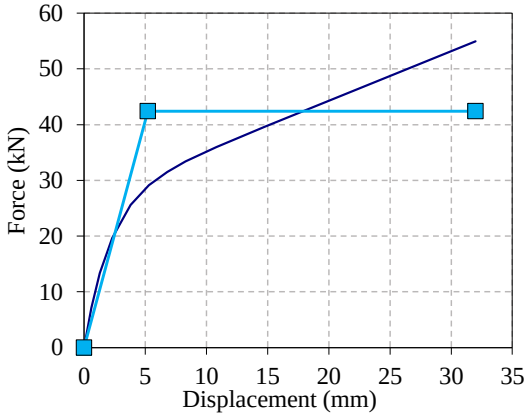

Equivalent bi-linear system according to EEEP method			
Yielding force	F_y	42.40	(kN)
Yielding displacement	d_y	5.21	(mm)
Ultimate force	F_u	54.98	(kN)
Ultimate displacement	d_u	32.00	(mm)
Maximum Force	F_{max}	54.98	(kN)
Elastic stiffness	k_{el}	8.15	(kN/mm)
Hardening stiffness	k_{pl}	0.00	(kN/mm)
Ductility ratio	μ (d_u)	6.15	-
Ductility	Class	H	-

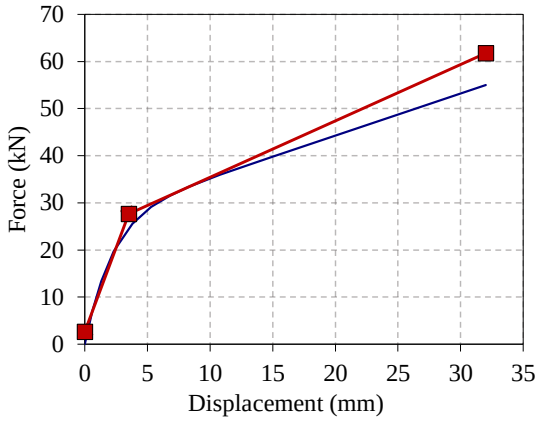

Equivalent bi-linear system according to EN12512 method (b)			
Yielding force	F_y	27.66	(kN)
Yielding displacement	d_y	3.49	(mm)
Ultimate force	F_u	54.98	(kN)
Ultimate displacement	d_u	32.00	(mm)
Maximum Force	F_{max}	54.98	(kN)
Elastic stiffness	k_{el}	7.17	(kN/mm)
Hardening stiffness	k_{pl}	1.20	(kN/mm)
Ductility ratio	μ (d_u)	9.17	-
Ductility	Class	H	-

X-BRAKET TYPE 2 – TEST COMPLETE CONNECTION WITH SPECIAL ELEMENTS TO INCREASE WOOD EMBEDMENT STRENGTH – TENSION

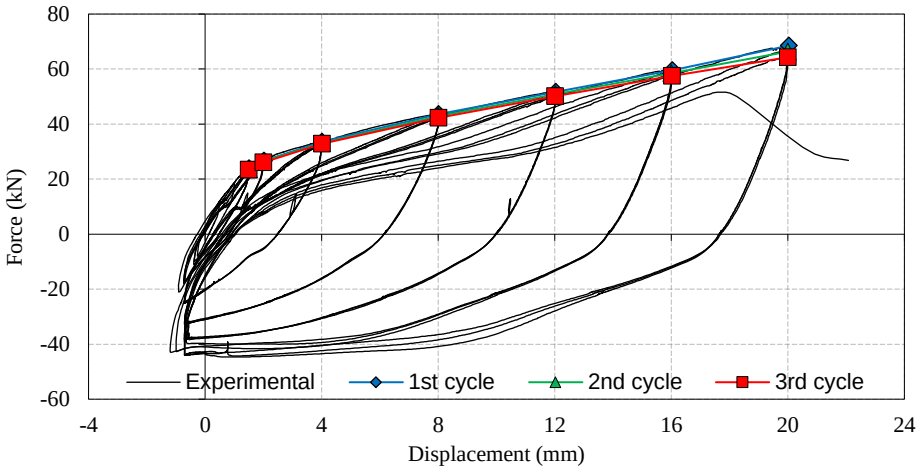

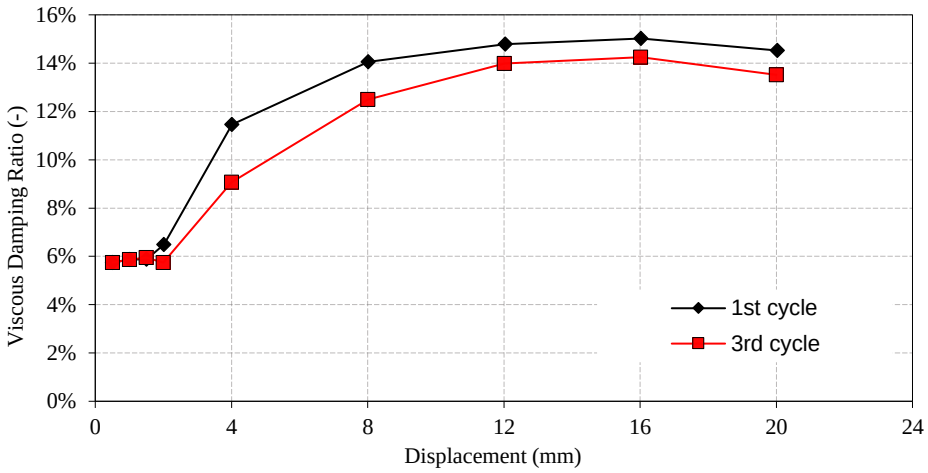

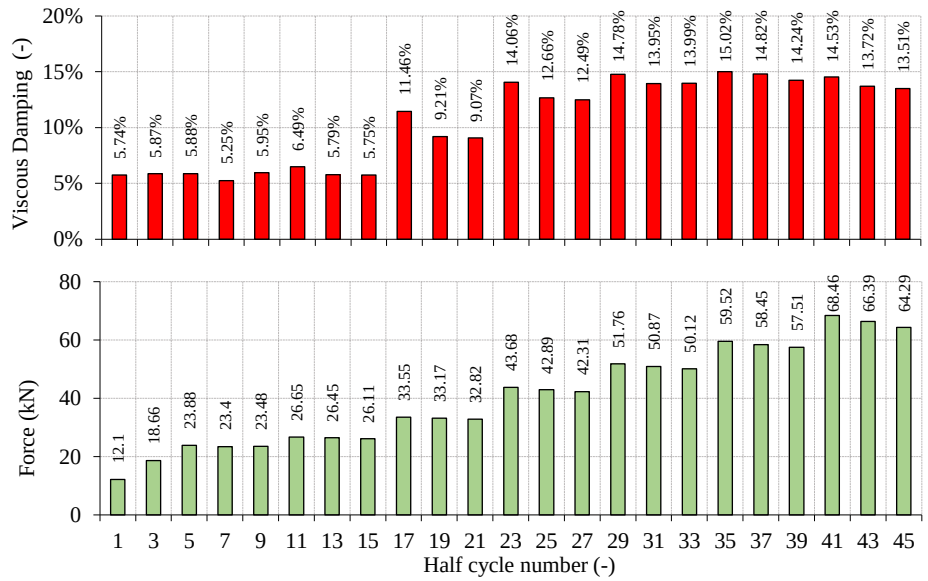

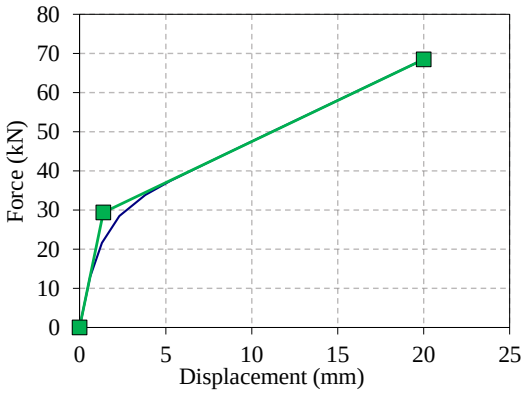

Equivalent bi-linear system according to EN12512 method (a)			
Yielding force	F_y	29.38	(kN)
Yielding displacement	d_y	1.37	(mm)
Ultimate force	F_u	68.50	(kN)
Ultimate displacement	d_u	20.00	(mm)
Maximum Force	F_{max}	68.50	(kN)
Elastic stiffness	k_{el}	21.44	(kN/mm)
Hardening stiffness	k_{pl}	2.10	(kN/mm)
Ductility ratio	μ (d_u)	14.60	-
Ductility	Class	H	-

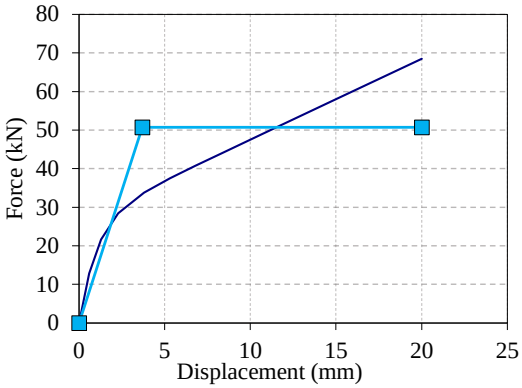

Equivalent bi-linear system according to EEEP method			
Yielding force	F_y	50.74	(kN)
Yielding displacement	d_y	3.70	(mm)
Ultimate force	F_u	68.50	(kN)
Ultimate displacement	d_u	20.00	(mm)
Maximum Force	F_{max}	68.50	(kN)
Elastic stiffness	k_{el}	13.70	(kN/mm)
Hardening stiffness	k_{pl}	0.00	(kN/mm)
Ductility ratio	μ (d_u)	5.40	-
Ductility	Class	M	-